The Role of the R-domain in Regulated Trafficking of the Cystic Fibrosis Transmembrane Conductance Regulator.

by

Christopher Michael Lewarchik

B.S. Microbiology, Duquesne University, 1996

Submitted to the Graduate Faculty of

The Department of Cell Biology & Physiology in partial fulfillment

of the requirements for the degree of

Doctor of Philosophy

University of Pittsburgh

2008

UNIVERSITY OF PITTSBURGH

School of Medicine

This dissertation was presented

by

Christopher M. Lewarchik

It was defended on

August 18, 2008

and approved by

Daniel C. Devor Ph.D., Associate Professor, Cell Biology and Physiology

Thomas R. Kleyman M.D., Professor and Chief, Renal-Electrolyte Division.

Barry London M.D., Ph.D., Professor and Chief, Division of Cardiology

Joseph M. Pliewski M.D. Associate Professor, Pulmonary, Allergy and Critical Care Medicine

Dissertation Advisor: Raymond A. Frizzell Ph.D., Professor and Chair, Cell Biology and Physiology

The Role of the R-domain in Regulated Trafficking of the Cystic Fibrosis Transmembrane Conductance Regulator.

Christopher M. Lewarchik, PhD

University of Pittsburgh, 2008

The cystic fibrosis transmembrane conductance regulator (CFTR) is a phosphorylation-regulated chloride channel that is a member of the ATP-binding cassette (ABC) transporter family [1]. It is involved in the movement of chloride ions across epithelial membranes in the airways, sweat glands, intestine and pancreas [2]. Mutations in CFTR that result in a loss of channel function result in the disease cystic fibrosis, affecting nearly 1 in 2500 people in northern Europe and the United States [3]. As a member of the ABC transporter family, CFTR shares the structural features of these proteins. Unique to CFTR is the presence of a cytoplasmic R-domain, that contains multiple phosphorylation sites. Phosphorylation of the R domain is required for CFTR channel gating, and cAMP/PKA simulation can also elicit insertion of CFTR into the plasma membrane from intracellular compartments [4]. We evaluated the structural basis of regulated CFTR trafficking by determining agonist-evoked increases in plasma membrane capacitance (C_m) of *Xenopus* oocytes expressing CFTR deletion mutants. Expression of CFTR as a split construct that omitted the R-domain (Δaa 635-834) produced a channel with elevated basal current (I_m) and no ΔI_m or trafficking response (ΔC_m) upon cAMP/PKA stimulation, indicating that the structure(s) required for regulated CFTR trafficking are contained within the R domain. Additional deletions

showed that removal of amino acids 817-838 produced a channel with regulated gating that lacked the agonist-induced increase in CFTR trafficking. This 22aa region exhibits helical structure, bears a net negative charge of -9, is highly conserved among species, and has been termed NEG2 [5, 6]. Injection of NEG2 peptide into oocytes expressing split ΔNEG2 CFTR prior to stimulation restored the agonist-evoked ΔC_m, consistent with the concept that this sequence mediates regulated CFTR trafficking. Further modifications of NEG2 suggest that the trafficking phenotype depends primarily on its helical structure. These observations suggest that the NEG2 region at the C-terminus of the R domain allows CFTR to enter a regulated intracellular compartment from which it traffics to the plasma membrane in response to cAMP/PKA-stimulation.

TABLE OF CONTENTS

LIST OF TABLES

LIST OF FIGURES

PREFACE

At this time I would like to thank my Ph.D advisor Raymond A. Frizzell for all of his guidance, encouragement and patience while this work was being completed. I would also like to thank the other members of my committee, especially Dr. Dan Devor. Without your help it would have been impossible for me to complete this project.

I also feel is it approporiate for me to extend my sincerest thanks to those who have encouraged my scientific career from the beginning. Specifically, I am referring to Dr. John F. Stolz and Dr. John Doctor at Duquesne University. During my undergraduate studies at Duquesne, they played a pivitol role in sparking a strong interest in scientific exploration in me. Their influence opened my eyes to the world of science eventually leading to my decision to pursue a career in science.

Another group that I feel reqires acknlwledgement is my family. The encouragement of my parents from childhood throught the completion of my Ph.D gave me the strength and determination to make it through the tough times. Last, but without a doubt, not least, I would like to thank my fiencee Anna Marie White. Words cannot describe how much her encouragement and belief in me aided me during the completion of this work.

1.0 INTRODUCTION

1.1 THE CELL MEMBRANE:

In 1855, Carl Wilhelm von Nägeli and Hugo von Mohl ushered in the science of membrane biology. In their studies, they suggested the presence of a biological membrane based on their microscopic observations of plant cells [7]. German physiologist Wilhelm Pfeffer refined the definition of biological membranes in 1875 when he suggested that membranes were discrete structures that could serve as selective barriers [8]. "Pfeffer's Postulate" served to establish the paradigm that cells contained some type of membrane structure which functioned to separate the inner cytosolic domain from the extracellular luminal environment. Additional studies by Gorter, & Grendel *et al*., and Danielli & Davson *et al.,* [9, 10] were required to fully develop our current view of the plasma membrane as a bilayer composed of two opposing layers of lipid molecules arranged so that their hydrocarbon tails face one another to form an oily core, while their charged heads face the aqueous solutions on either side of the membrane.

The previous decades of research have led to several generally accepted characteristics of biological membranes. The first is that biological membranes are made up of a mixture of lipids and proteins, an idea that was initially proposed by Davson &

Danielli in 1935 [10]. The second generally accepted membrane characteristic is that the cell membrane consists of three classes of amphipathic lipids: phospholipids, glycolipids, and cholesterol which spontaneously arrange so that the hydrophobic "tail" regions are shielded from the surrounding polar fluid, causing the more hydrophilic "head" regions to associate with the cytosolic and extracellular faces of the resulting bilayer. These observations culminated in the proposal of the fluid-mosaic model of biological membranes by Singer & Nickelson in 1972 [11].

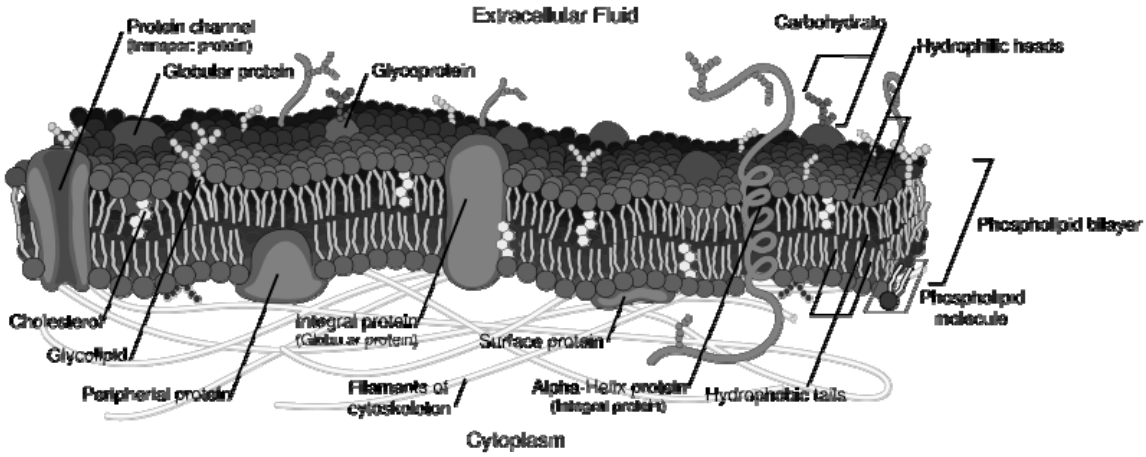

Figure 1-1: Fluid Mosaic Model of Plasma Membrane [11].

This model proposes that the biological membrane can be considered as a two-dimensional liquid where all lipid and protein molecules diffuse more or less freely. In contrast to previous static representations of the biological membrane, the fluid mosaic model is dynamic and possesses the structural features that allow for communication between the extracellular environment and the cytosolic (intracellular) compartment via signal transduction and selective transport of solutes [7].

1.2 TRANSPORT ACROSS PLASMA MEMBRANE:

Because of the oily core, a pure lipid bilayer is permeable to only small hydrophobic solutes and the permeability of polar inorganic compounds and ions is very low. This suggests that the cell membrane can only distinguish between solutes based on a few limited characteristics (e.g. size or number of hydrogen bonding groups). However, for the cell to allow easy access for specific metabolites from the environment and to facilitate easy removal of waste products, it must have greater flexibility of response than a simple lipid bilayer membrane can give. This was demonstrated by the work of Overton *et al*., [12], and later by Collander *et al.,* [13], where they examined the permeability of various solutes and found that small water-soluble molecules appeared to permeate the membrane more rapidly than could be accounted for on the basis of their lipid solubility alone. Additionally, Davson and Danielli *et al*.,[14] showed that glycerol penetrates an erythrocyte membrane 100 times faster than predicted. These observations led them to propose that membranes contain "active patches" which allow increased permeability of certain substrates across the membrane.

This work was not limited to the movement of non-charged molecules across the membrane. Throughout the 19th century, several groups were examining the electro-chemical mechanism underlying nerve and muscle function. The first group to suggest that ions move into and out of cells came from Carlo Matteucci when he suggested that tetanus toxin was somehow influencing the flow of ions into and out of muscle cells [15]. Despite his observations, a sound mathematical explanation of this phenomenon remained elusive. Further progress was made during the late 1880's when Walter Nernst published his equations which allow for the calculation of the electrical potential of

selective biological membranes [16], followed by Wilhelm Ostwald's suggestion that the electrical potential across artificial semi-permeable membranes was due to selective permeability of ions [17]. These observations culminated with the development of the "membrane theory" proposed by Julius Bernstein in 1902 [18]. In his landmark publication he proposed that 1.) Living cells are composed of an electrolytic interior surrounded by a thin membrane that is selectively permeable to ions. 2.) At rest, there is a pre-existing electrical difference (potential) across the membrane 3.) During activity, the ion permeability of the membrane increases, which reduces the potential to a comparatively low value [18].

1.3 IDENTIFICATION OF ION CHANNELS:

Another significant advance in the study of ion transport came in 1940 when Webb & Young began studying ion currents in the squid giant axon [19]. The use of the squid giant axon as a model system for examination of ion transport resulted in Hodgkin & Katz concluding that the action potential was the result of the entry of sodium ions followed by an efflux of potassium ions from the cell [20]. However, the exact mechanism of how sodium passes through the cell membrane was not known. The elucidation of this mechanism was greatly aided by the invention of the glass microelectrode [21] and the voltage clamp technique [22-24]. Using these methods, Hodgkin & Huxley were able to explain the action potentials in terms of movement of specific ions (K^+, Na^+, Cl^-) through pores in axonal membranes, as well as demonstrate

that ion channels were fundamental to neuronal signaling [23]. These observations, and the use of radioactive tracer ions to track movement of ions across the plasma membrane, led to the commonly accepted idea that the ions were passing single file through a "narrow pore" or channel [23, 25].

In 1976, the development of the patch clamp method by Neher & Sakmann revolutionized the ability of physiologists to examine ion channels and how they function in cells [26]. Until then, researchers had only been able to study ion channels in neurons collectively (i.e. macroscopic currents). The invention of patch clamping permitted the analysis of individual channels leading to characterization of different types of channels as well as deduction of some of their structural features.

1.4 CURRENT VIEW OF ION CHANNELS:

The work of the researchers highlighted above as well as countless others, has led to the current view of ion channels as integral membrane proteins, or more typically, an assembly of several proteins that respond to a particular stimulus [3]. The common stimuli which activate ion channels include a change in membrane potential, a neurotransmitter (ligand binding), mechanical deformation or a second messenger such as cyclic adenosine monophosphate (cAMP).

In general, ion channels contain several membrane-spanning domains which form a conduction pathway called "the pore". When a channel is open, the movement of a particular ion through the channel is influenced by two criteria. The first is the

electrochemical gradient. The electrochemical gradient across the membrane actually consists of two gradients, the concentration gradient and membrane potential. The concentration gradient is the difference between ion concentrations on both sides of the membrane and the membrane potential refers to the electrical potential difference (voltage) across the membrane. An example of ion movement through a selective barrier in response to the electrochemical gradient is shown in figure 1-2. According to this model, ions will move down their concentration gradient from high to low. Since ions are charged, their movement will be influenced by the concentration gradient as well as the electric field across the membrane (i.e. positive charge will be attracted to a negative charge and repelled by negative charges). Thus, the total force on an ions movement will be determined by the combined effects of the electrical and chemical gradients. From this model, it can be assumed that there will be some electrochemical potential at which the electrical force on the ion exactly balances the opposing force of the ion which is given by the Nernst equation.

$$E=(RT/zF)*\ln([out]/[in])$$

Where E is the equilibrium potential in volts, R is the gas constant (8.31 J K^{-1} mol^{-1}), T is the temperature in degrees Kelvin, z is the charge of the ion and F is Faraday's constant ($9.64x10^4$ C mol^{-1}). [in] & [out] are the internal and external concentrations of the ion respectively.

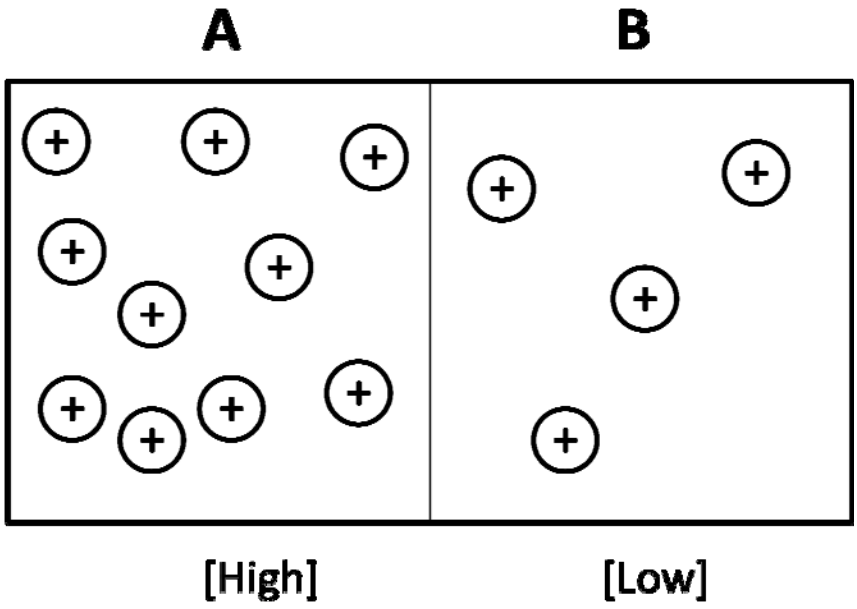

Figure 1-2: Model of Electrochemical Gradient [3]

In this model compartments A & B contain [High] and [Low] concentrations of positive ions. If the barrier (membrane) separating A & B is made permeable to the positive ion, they will move down their concentration gradient from A to B. The will result in an increase in the positive charge in B which will tend to oppose the movement of more positive ions. Movement of ions from A to B will continue until the system reaches the equilibrium potential where the electrical gradient exactly balances the chemical gradient.

The second criterion that influences an ion's movement is the relative permeability of the channel to a particular ion. In most cases, ion channels do not act as pores that allow free diffusion of all ions; instead they function like molecular sieves showing considerable discrimination in the kinds of ions each channel allows to pass [3]. This can be appricated from the permeability ratio equation:

$$E_{rev}=(RT)/F*\ln(P_K[K]_o + P_{Na}[Na]_o + P_{Cl}[Cl]_i)\div(P_K[K]_i + P_{Na}[Na]_i + P_{Cl}[Cl]_o)$$

Using this equation is it possible to calculate the permeability ratios between different ions from measurements of reversal potentials, but not absolute permeabilities if ionic concentrations are known. Where E_{rev} is the reversal potential, R is the gas constant, T is the temperature in degrees Kelvin, F is Faraday's constant, P_x is the permeability of an ion, $[X]_o$ is the concentration of an ion outside of the cell and $[X]_i$ is the concentration of an ion inside of the cell.

In addition to the general structural characteristics of ion channels, many channel properties have been deduced by recording single channel activity using the patch clamp technique. A typical single channel current recording is shown in figure 1-3. The data obtained from these recordings show that a typical stimulated channel opens for a short interval and then closes and opens again after a variable amount of time [27]. The process of transition from the open to the closed state (and vice versa) is known as gating. The amount of time that each channel remains open or closed is highly variable and is quantified as the open probability (P_o). The open probability is defined as the fraction of time the channel spends in the open state which can be calculated by dividing the sum of all the open times by the duration of the recording [3]. These characteristics have led to

the identification and classification of a large quantity of ion channels located in every cell type.

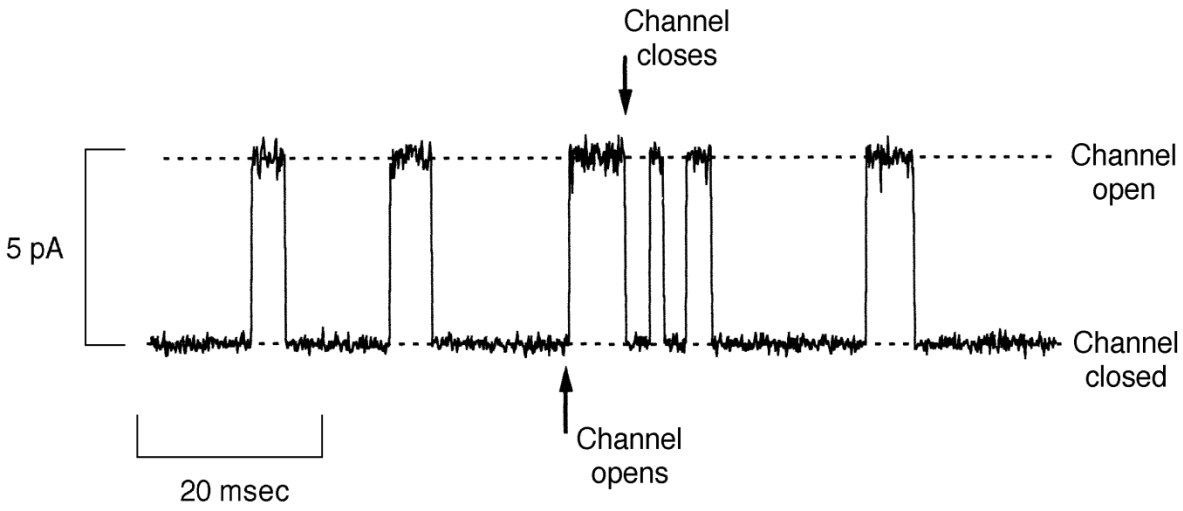

Figure 1-3: Single Channel Currents Recorded using Patch Clamp. [3]

When the channel opens ions move through it creating a tiny current shown as an upward deflection of the trace. As shown here, a fixed membrane potential the amplitude of the single channel current is constant but the length of the time the channel remains open is variable.

1.5 ION CONDUCTANCE IN SECRETORY EPITHELIA:

1.5.1 The Two Membrane Model.

As the volume of ion channel research increased, it became evident that ion channels are present and function in many cell types, not just those cells deemed "excitable" cells such as neurons. For example, studies on frog skin by Ussing and colleagues revealed that it would absorb sodium ions against a 100-fold concentration difference on the interstitial side [28]. This movement of sodium across the frog skin was shown to be dependent on the presence of sodium on the pond side and the presence of potassium on the interstitial side [28, 29]. These studies led to the proposal of the two-membrane model for epithelial sodium uptake or the Koefoed-Johnsen-Ussing (KJU) model in 1958 [figure 1-4] [30]. In this model, the sodium uptake by an epithelium can be understood in the context of two membranes acting in series. The outer membrane is permeable to H_20 and sodium and the inner membrane is permeable to potassium and is where the pump, which exchanges cellular sodium for interstitial potassium, resides. In the KJU model, the action of the pump limits the increase in intracellular sodium concentration achieving a steady state in which the cells will continue to import sodium as long as it can be supplied with Adenosine 5'-triphosphate (ATP) [30].

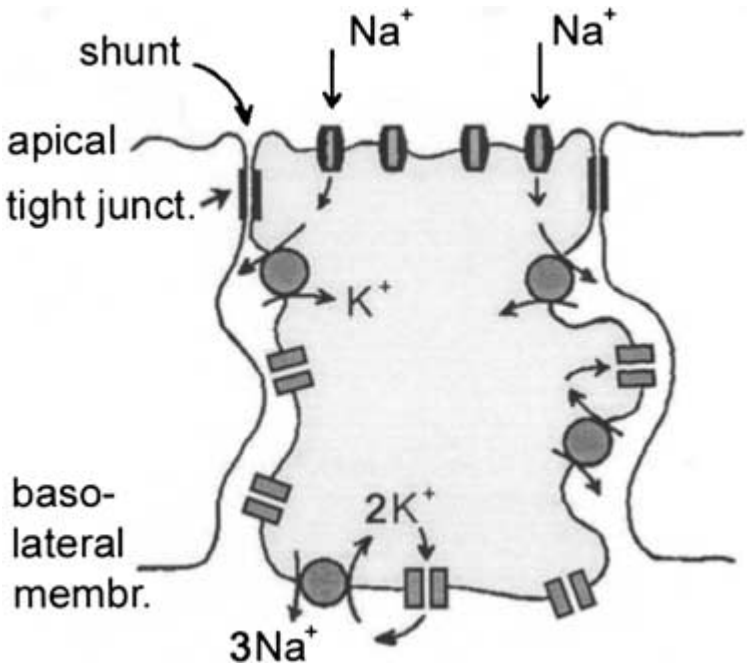

Figure 1-4: Koefoed-Johnsen-Ussing (KJU) Two membrane model of Epithelium sodium uptake. [31]

A modernized view of the KJU model by polarized principle cells of the short-circuited amphibian epidermis from Lindemann *et al*., [31]. Amiloride sensitive Na^+ channels are shown on the apical membrane facing the external environment. K^+ channels (rectangles) and Na^+/K^+ pumps (circles) are shown on the basal membrane facing the interstitial compartment.

1.5.2 NaCl absorption and secretion in epithelial cells

Coinciding with the increased knowledge of ion channel diversity in different cell types, there has also been an increase in the knowledge and understanding of channels that pass ions besides Na^+ & K^+. Following the development of the KJU model, research on the transport of other ions in the context of epithelial cells continued to develop our understanding of the mechanisms involved in ion movement across epithelium. Using small intestine and rabbit gallbladder as a model system, Frizzell *et al*., [32] developed a model of a neutral coupled NaCl influx where the apical membrane mediates the influx of NaCl from the environment in an electrically neutral fashion [32]. Based on their model, sodium and chloride entry into absorptive cells are linked at the mucosal membrane and the presence of 140mM NaCl (extracellular) resulted in a net influx of Na^+ and Cl^- which was eliminated by removal of either sodium or chloride from the apical solution [32].

Continued study of this mechanism led to the development of the proposed model of NaCl transepithelial movement in airway surface epithelium (figure 1-5). In this model, normal physiological conditions would favor absorption of Na^+, Cl^- and H_20 [33-35] according to the previously proposed KJU model [30]. NaCl absorption requires the entry of Na^+ ions through the apical surface sodium channel [36] which results in a depolarization of the apical membrane potential (V_a) value resulting in an increase in the hyperpolarization of the membrane voltage (V_t) across the airway according to the formula:

$$V_t=V_b-V_a$$

Where (V_t) is the transepithelial electrical potential difference, V_b and V_a are the basolateral and apical membrane potential differences respectively. This change in transepithelial potential (V_t) permits chloride absorption into the interstitial fluid by its movement through the paracellular pathway. The sodium that enters the cell is subsequently extruded by the action of the Na^+/K^+-ATPase pump residing in the basolateral membrane [37]. The build up of intracellular K^+ due to the function of the pump, which brings in 2 K^+ for every 3 Na^+ ions excreted, K^+ is recycled out of the cell through potassium channels in the basolateral membrane. The end result of this series of events is the transepithelial movement of NaCl from the mucosal environment through the epithelial cells and into the serosal environment in an electrically neutral fashion with H_20 following along its osmotic gradient.

In addition to NaCl absorption by surface epithelium, the proximal airway is also involved in salt secretion. In contrast to NaCl absorption, the epithelial cells which are responsible for salt secretion in glandular structures lie deeper within the proximal airway than the airway surface epithelial cells [38], although airway epithelium can secrete NaCl if apical membrane Na^+ conductance is inhibited [35, 39] [Figure 1-5A&B]. Chloride secretion in airway epithelia is a two step process that is regulated by increases in the intracellular cAMP concentration [40]. In this process, chloride enters the cell across the basolateral membrane by means of an electrically neutral sodium/potassium/2-chloride co-transporter (NKCC1) [41]. The action of NKCC1 along with the Na^+K^+-ATPase, allows for an increase in intracellular chloride concentrations above its electrochemical equilibrium, creating an electrical driving force for chloride exit across the apical membrane [42-46]. The subsequent movement of Cl^- out of the cell through a cAMP

activated Cl^- channel hyperpolarizes the apical membrane potential providing a strong driving force for Na^+ exit via the paracellular pathway (figure 1-5) resulting in a net flux of NaCl from the serosal solution across the epithelium into the mucosal environment.

Willumsen *et al.,* [39] characterized this process in human nasal epithelium and determined the intracellular and extracellular concentrations of sodium and chloride to be (Na^+_i=22mM; Na^+_o=100mM; Cl^-_i=40mM; Cl^-_o=80mM) as well as an apical membrane potential of -25mv and a basal membrane potential of -35mV. Using the equation for electrochemical driving force

$$\Delta\mu_{i\text{-}o}=(RT/zf) *(\log[in]/[out]) + (\varphi_i-\varphi_o)$$

Where $\Delta\mu$ is the total driving force for an ion, R is the universal gas constant, T is the absolute temperature, *f* is Faraday's constant, z is the valence of the ion, φ_i is the transepithelial electrical potential difference (V_t) and φ_o is the basolateral membrane potential difference (V_b). Using their measured values, they reported a driving force for Na^+ (-55mV) and Cl^- (3.5mV) which favor absorption in airway epithelia. However, when the apical Na^+ conductance was blocked they observed hyperpolarization of both apical and basal membrane potentials to -36mV and -41mV and a V_t of -5mV. From these values they determined that blocking the apical membrane Na^+ conductance resulted in a -12mV driving force for Cl^- secretion consistent with the model presented in figure 1-5B of chloride secretion in the proximal airway.

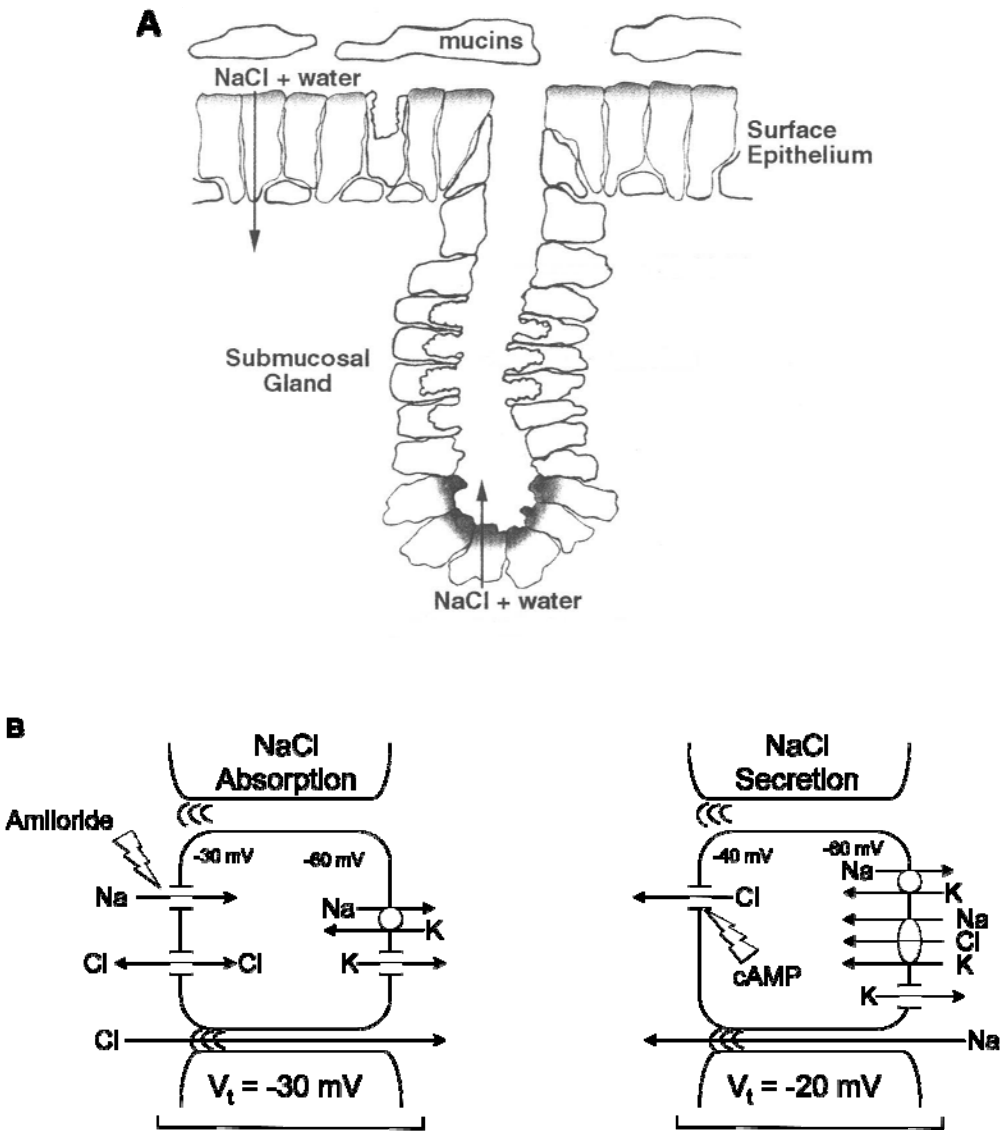

Figure 1-5: Model of cellular NaCl absorption and secretion [47].

Models of NaCl absorption and secretion in proximal airway. A) Schematic of proximal airway showing sites of NaCl and water transport. Expression of CFTR chloride channel indicated by shading. B.) Cellular models for NaCl absorption in surface epithelium and secretion in serous cells of submucosal gland under open circuit conditions. The apical Cl^- channel shown in both models is CFTR. V_t is lumen negative in both models with physiological solutions at both surfaces.

With the model for NaCl absorption and secretion firmly established, diseases which were thought to be the result of a defect in NaCl transport were examined. A known characteristic of patients with the disease cystic fibrosis (CF) is a high NaCl concentration in the sweat which led to the expression, "Woe to that child which when kissed on the forehead tastes salty". Studies on isolated sweat glands from CF patients suggested that low Cl^- permeability resulted in poor reabsorption of NaCl in the sweat duct resulting in an increase in the concentration of salt in the sweat [48, 49].

Knowles *et al*., [50, 51] reported that the nasal and bronchial epithelia of patients with CF had an increased basal transepithelial potential difference, treatment of the airway surface with amiloride (a blocker of Na^+ transport) increased the transepithelial potential difference and that removal of Cl^- from the airway surface resulted in a smaller Cl^- diffusion potential difference. These three characteristics of CF tissue indicated that the disease is the result of altered ion transport or permeability which results in deranged airway surface liquid volume and composition, thickened mucus and recurrent lung infections common in patients with cystic fibrosis [52]. Continued study of epithelia from subjects with CF showed that Na^+ channel activity was significantly higher while the Cl^- permeability was drastically reduced [49, 51] which left the actual defect in CF unknown (i.e. increased Na^+ absorption or decreased Cl^- permeability).

Support for the CF defect being a decrease in chloride permeability came from studies by Widdicombe *et al*., [53]. In their studies, they compared the responses of normal and CF trachea cells to treatment with isoproterenol which had been shown to stimulate short circuit currents (I_{sc}) across dog and human cells in culture [54, 55]. Treatment of normal cells with isoproterenol resulted in an increase in transepithelial

potential difference and a depolarization of the apical membrane along with a decrease in the fractional resistance of the apical membrane indicating that isoproterenol stimulates chloride secretion by increasing Cl^- permeability [53]. However, when CF cells were treated with isoproterenol no change in transepithelial potential difference, apical membrane potential or fractional resistance was reported suggesting that cystic fibrosis decreases apical Cl^- permeability [53].

Although the evidence to implicate defective Cl^- transport as the cause of cystic fibrosis was compelling, without identification of the mutated chloride transporter a conclusive disease model could not be developed. Although the previous studies were unable to identify a specific chloride transporter, the identification of isoproterenol activation proved a useful diagnostic tool in the search. Welsh *et al.,* and Halm *et al*., [56, 57] identified apical chloride channels from human epithelium that were anion selective, stimulated by increasing intracellular cAMP, outwardly rectifying (larger outward currents than inward currents), and not sensitive to Ca^{2+}. Despite the efforts of the researchers involved none of these channels were able to be definitively shown to be "the cystic fibrosis channel".

Efforts to identify the "CF channel" using chromosome walking/jumping and complementary DNA hybridization isolated DNA sequences, encompassing more than 500,000 base pairs on the long arm of human chromosome 7 which contained at least four transcribed sequences from a region thought to contain the CF locus [58]. Of the four segments, three were shown to not be the CF locus by DNA sequence analysis and the fourth segment was indicated as containing at least a portion of the cystic fibrosis gene locus [58-60]. Two DNA segments in the fourth segment were used as probes to

screen cDNA libraries which led to the identification of an open reading frame on chromosome 7 capable of encoding a protein of 1480 amino acids with expression highest in those tissues which were severely affected by cystic fibrosis [1]. Additionally, when sequences derived from CF patients were compared to those from unaffected patients the deletion of a phenylalanine residue at position 508 was identified only in the CF patients [1]. These observations led Riordan *et al*., [1] to conclude that they had identified the cystic fibrosis gene and that the major genotype of cystic fibrosis patients was the deletion of a phenylalanine at position 508 (the mutation was designated ΔF508). From their findings, they proposed that the protein encoded was 1480 amino acids in length, contained two repeated motifs each capable of spanning the plasma membrane 12 times, as well as two sequences that resembled ATP binding folds separated by a unique regulatory domain which contains multiple consensus phosphorylation sites (figure 1-6) [1]. The similarity of the nucleotide binding domains to those of the mammalian multidrug resistance P-glycoprotein suggested that the CF gene product is probably involved in transport across the plasma membrane [1]. They named the identified gene product the cystic fibrosis transmembrane conductance regulator (CFTR).

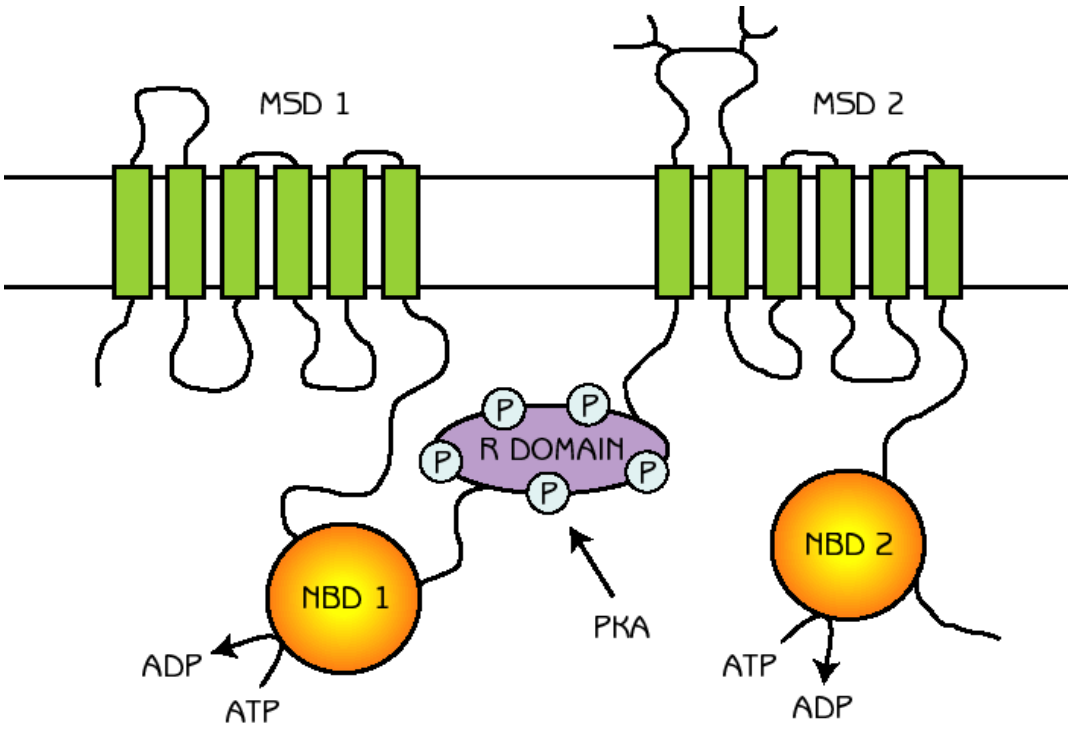

Figure 1-6: Model of CFTR Structure [1].

The proposed structural model of CFTR has a cytosolic NH_2 terminus leading into six membrane-spanning domains (MSD1) followed by the first nucleotide-binding domain (NBD1). A unique feature of CFTR is the cytoplasmic regulatory domain (R-domain) linking the NH_2 and COOH halves of the channel, which contains multiple protein kinase A (PKA) phosphorylation sites. The R-domain connects to six more membrane-spanning segments (MSD2), finally terminating in an intracellular nucleotide binding domain (NBD2), followed by the COOH terminus of the channel.

1.6 CYSTIC FIBROSIS TRANSMEMBRANE CONDUCTANCE REGULATOR (CFTR):

1.6.1 CFTR & Cystic Fibrosis.

Mutations in CFTR result in the disease cystic fibrosis, one of the most common human genetic diseases, affecting nearly 1 in 2500 people in northern Europe and the United States [3]. As of 2007, over 1500 CFTR mutations of various types have been identified (Table 1-1). The most important pathological abnormalities of CF occur in the lungs, where mucous accumulation leads to chronic infection, progressive tissue destruction, fibrosis and air trapping due to occlusion of the distal airways [61-64]. However, cystic fibrosis pathology is not restricted to just the lungs, exocrine glands are also affected. In the pancreas the lack of digestive enzyme secretion results in pancreatic insufficiency and malabsorption in the gut [65-68]. Additionally, cystic fibrosis can lead to obstruction or congenital absence of the vas deferens in males leading to infertility [69-73].

Mutation Type	Count	Frequency %
Missense	652	41.85
Frameshift	246	15.79
Splicing	198	12.71
Nonsense	150	9.63
In frame in/del	31	1.99
Large in/del	44	2.82
Promotor	8	0.51
Sequence variation	227	14.57

Table 1-1: Categorization of detected mutations in CFTR according to the Cystic Fibrosis Mutation Database [74].

Mutations of CFTR that result in a CF phenotype are separated into four categories or classes based on their effect on channel function (Figure 1-7). Class I mutations result in a lack of protein production as a result of splice site abnormalities, frame shifts caused by deletions and insertions or nonsense mutations. Class II is characterized by a defect in trafficking resulting in a significant decrease in the amount of CFTR expression at the plasma membrane. An example of this type of mutation is ΔF508 (the most common CFTR mutation) which is associated with minimal cAMP-activated chloride conductance as a result of incorrect folding. The misfolding of ΔF508 results in its targeting to the Endoplasmic Reticulum Associated Protein Degradation (ERAD) pathway for ubiquitination and subsequent degradation by the proteasome, preventing the channel from reaching the plasma membrane [75, 76]. Class III mutations are correctly processed but cAMP stimulation fails to elicit channel opening, such as the G551D mutation that occurs in NBD1, which results in a decrease in ATP binding [77]. Class IV is characterized by alterations in channel conduction properties which can occur by different means. For example, R334Y and R347P result in a significant decrease in single channel conductance possibly through disruption of the channel pore, while R117H reduced chloride conduction by decreasing the P_o of CFTR [78, 79].

Although this classification system is very useful, it is not without limitations. For example, the most common CF causing mutation ΔF508 falls into more than one class. As stated earlier, ΔF508 results in a channel that is misfolded thus preventing its trafficking from the ER to the plasma membrane typical of a Class II mutation. Studies have shown that indeed some ΔF508 does escape the ER and moves to the plasma membrane where it can conduct chloride [80-88]. However, once at the membrane the

ability of the channel to conduct chloride is significantly reduced due to a decrease in the open probability (WT-CFTR P_o=0.4; ΔF508 P_o=0.1) leading to a decrease in the I_{Cl} at the apical membrane [84] which is characteristic of a Class IV mutation, indicating that a single CFTR mutation can adversely affect multiple steps in the proteins processing and/or function.

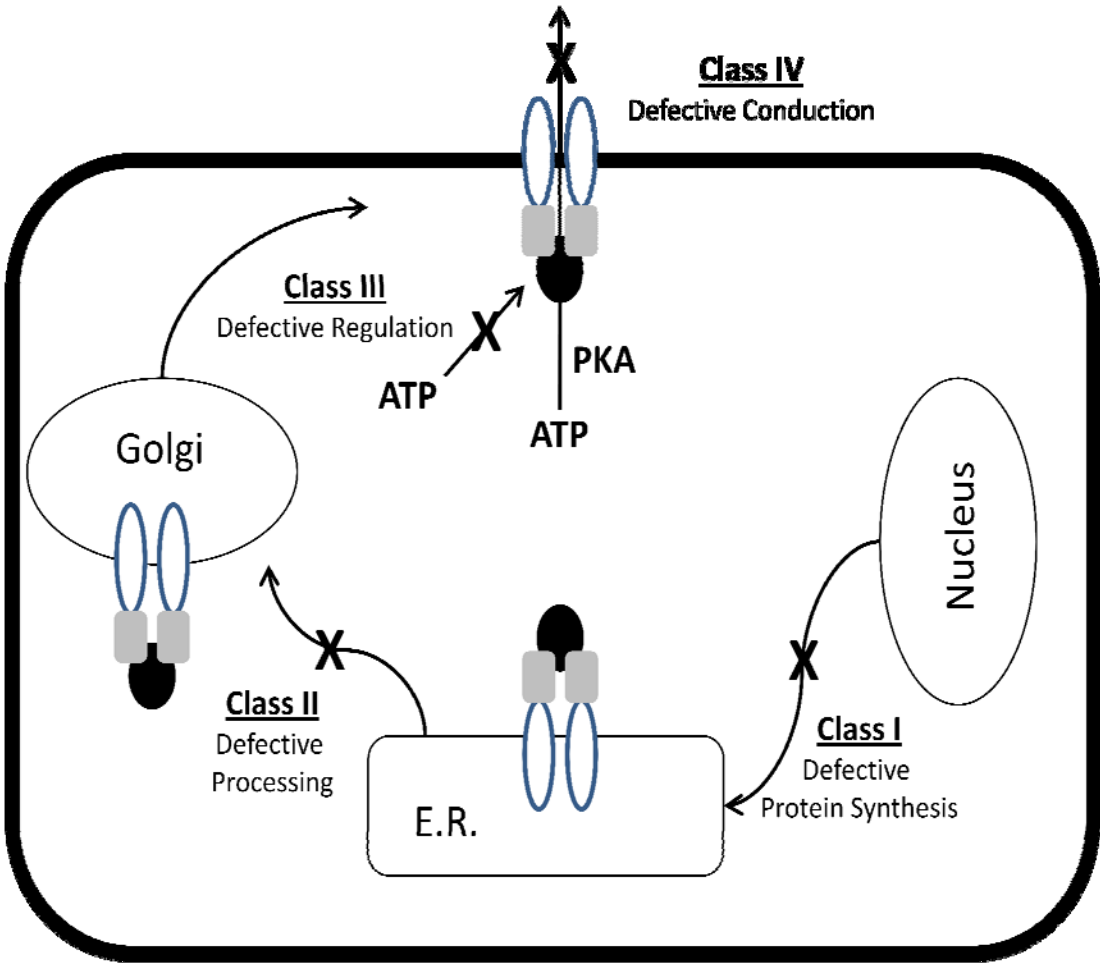

Figure 1-7: Representation of Classes of CFTR mutations [89].

1.6.2 CFTR and Anion Conduction.

The primary sequence of CFTR has considerable homology to a family of proteins called ATP binding cassette (ABC) transporters. They are one of the largest and most ancient protein families with representatives in all extant phyla from prokaryotes to humans. The family includes a large number of bacterial permeases and in eukaryote cells, the multi-drug resistance protein (p-glycoprotein) and the sulphonylurea receptor. ABC transporters are transmembrane proteins that function in the transport of a wide variety of substrates across extra- and intracellular membranes, including metabolic products, lipids, sterols and drugs. Proteins are classified as ABC transporters based on the sequence and organization of their ATP-binding domain(s), also known as nucleotide-binding folds (NBFs). However, unlike bacterial ABC transporters, the individual domains of CFTR are not encoded by separate genes; all functional domains of CFTR are encoded by a single gene.

Because of CFTR's homology to other ABC transporters, initially it was believed that it was not an ion channel. Following the cloning of CFTR, the first successful expression of the protein was in CF epithelial cells. Although the expression of CFTR was able to correct the chloride channel defect [90, 91], it was believed that this effect was not the result of CFTR conducting chloride [92, 93]. However, when CFTR was expressed in various systems that do not normally express CFTR or have cAMP dependent chloride channels, cAMP dependent chloride currents were detected [94-96]. Moreover, when Anderson and co-workers mutated CFTR they observed the anion selectivity of the channel was altered suggesting that CFTR is itself a channel, as opposed to it acting as a regulator of another channel [97]. Definitive evidence of CFTR being a

chloride channel was provided by reconstituting CFTR in planar lipid bilayers where a low pS, chloride selective ion channel activity was detected that was protein kinase A and ATP dependent [98, 99].

With CFTR being firmly established as a Cl^- channel, investigations into the biophysical properties of the channel were performed. From an electrophysical stand-point, CFTR channels possess several unique characteristics (Figure 1-8), such as regulation of channel activity by cAMP-dependent phosphorylation and intracellular nucleotides, a small single channel conductance of 6-10pS, linear current voltage relationship, time and voltage independent gating. The channel is also selective for anions over cations with an anion permeability sequence of $Br^- \geq Cl^- > I^- > F^-$ [100]. In addition to being permeable to ions, CFTR was also shown to be able to conduct a large number of polyatomic anions in the sequence $NO_3^- > Cl^- > HCO_3^- >$ formate > acetate [101].

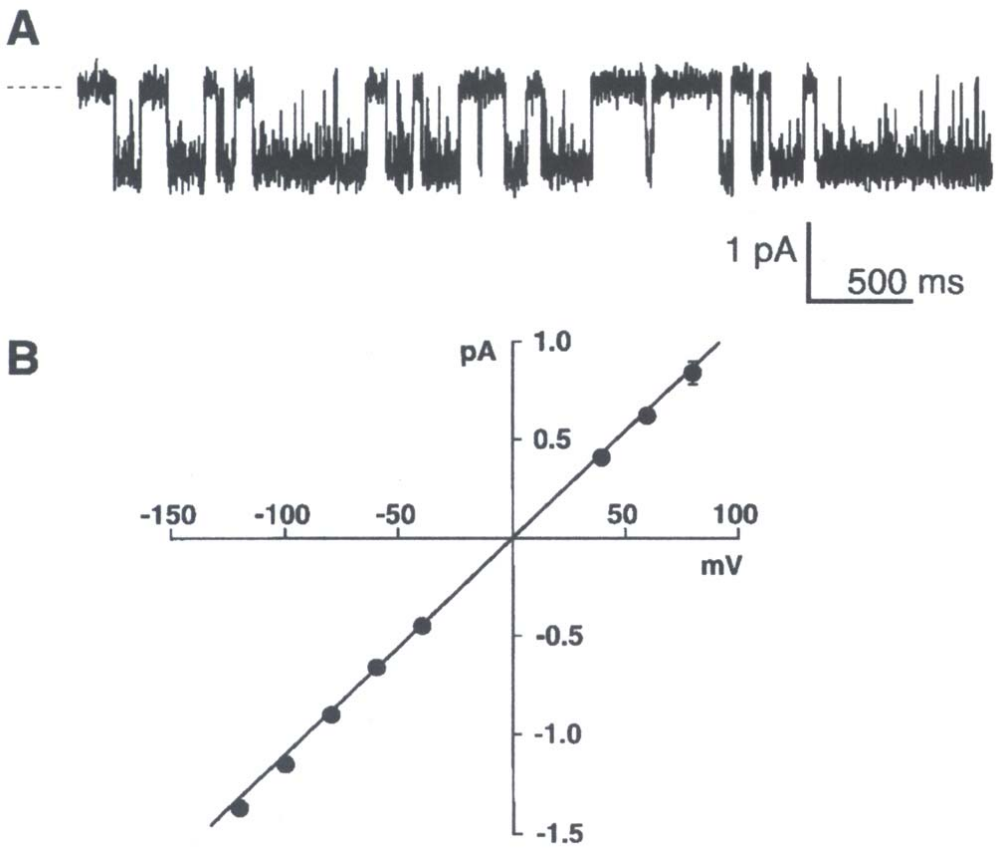

Figure 1-8: Single Channel Recording and Current/Voltage relationship of WT-CFTR [102, 103]

A) 5 sec. trace from excised inside-out patch containing 1 CFTR channel held at -80 mV. Stimulation with 75nM PKA and 1mM ATP. Dashed line is closed state [102]. B) current/voltage (I/V) relationship of channel at 35° C with symmetrical N-methyl-D-glucamine chloride (140mM) [103].

1.6.3 CFTR Structure /Function:

1.6.3.1 Nucleotide Binding Domains.

One of the characteristic features of CFTR is that for the channel to open, the intracellular membrane surface must be exposed to (hydrolysable) ATP. The coupling of CFTR gating to ATP hydrolysis occurs at the two nucleotide binding domains (NBDs). The binding of ATP to the NBDs results in conformational changes that open and close the channel and allow transmembrane flow of Cl^- or HCO_3 down its electrochemical gradient.

The importance of the NBD's of CFTR is emphasized by the number of disease associated mutations in these domains [2]. The highly conserved nucleotide binding motifs (Walker A & Walker B) and LSGGQ motifs (which stabilize ATP binding and catalyze its hydrolysis) of CFTR's NBDs have been shown to bind and hydrolyze intracellular ATP respectively, to regulate channel gating [104, 105]. To discern the mechanism of NBD regulation of CFTR gating Anderson *et al*., [97] studied ATP regulated Cl^- activity in excised inside-out membrane patches. They found that addition of ATP to the intracellular solution had no effect, but once the channel was phosphorylated by PKA, the channels were activated suggesting that ATP regulates the channel only after it has been phosphorylated by PKA [97]. Further studies on phosphorylated channels revealed that as the ATP concentration increased, the mean closed time decreased but mean open time did not change which led to the proposed kinetic model of CFTR gating that consisted of two closed states and one open state [$C_1 \leftarrow \rightarrow C_2 \leftarrow \rightarrow O$] [105-109]. In this model the progression of activation first requires

the phosphorylation of CFTR in the C_1 state, the transition from C_1 to C_2 requires the binding of ATP to the NBDs which then leads to channel opening.

Further analysis of CFTR gating and the role of NBDs using homology models from several NBD crystals was performed by Vergani *et al*., [110]. As seen in figure 1-9 in the model they propose, ATP binding to NBD1 triggers its binding to NBD2. Additional ATP binds to NBD2 which results in a slow opening of the channel (C_2-to-Open) through a transition state that requires the formation of the NBD1/NBD2 heterodimer. The open state of the channel is destabilized by the hydrolysis of ATP on NBD2, which results in disruption of the heterodimer NBD and leads to closing of the channel

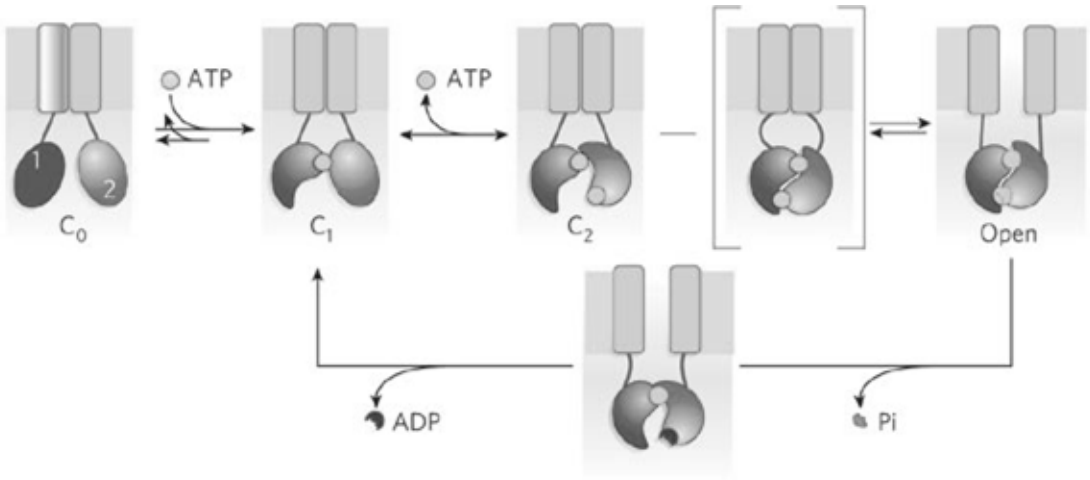

Figure 1-9: Model of nucleotide binding domain regulation of CFTR gating [110].

Diagram illustrating the proposed mechanism coupling the opening of channel pore in the transmembrane domains to the hydrolysis cycle through the dimerization of NBDs (C_n= Closed states O= Open state).

1.6.3.2 The R-domain:

In addition to the above structures, CFTR also contains a unique stretch of amino acids located between NBD1 and TMD2 that contains multiple sites for PKA phosphorylation called the regulatory, or R-domain (Figure 1-10 & table 1-2). The boundaries of the R-domain have been up to some debate. Originally, the R-domain was defined aa590-830 or those amino acids encoded by exon 13 [1]. However, severing CFTR after aa634 and before aa835 and co-expressing it as two half channels produced a functional channel which was constitutively active [111] indicating that the N- and C-terminal boundaries of the R-domain are 634 and 835 respectively.

The most obvious feature of the R-domain upon analysis of its sequence is the presence of multiple highly conserved consensus sequence sites for PKA phosphorylation. Other than the phosphorylation sites, there is little sequence similarity between species of the remaining residues although there is a "conservation of charge" of approximately 28% with sixteen of the 24 basic residues in the PKA sites and several are clustered between aa817-838 [112].

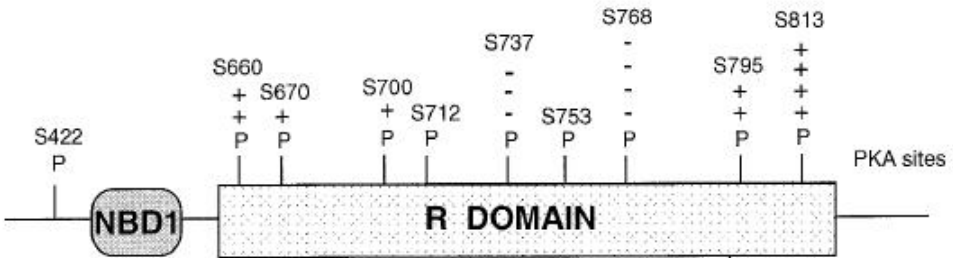

Figure 1-10: Summary of CFTR phosphorylation by cAMP-dependent protein Kinase A [113]

Summary of CFTR phosphorylation by cAMP-dependent protein kinase (PKA). Illustrates relative levels of phosphorylation of individual sites observed (except for Ser-768) after brief stimulation of PKA in intact cells, with relative contribution of each site to regulation of CFTR channel activity inferred from site-directed mutagenesis reflected by (+) or (-). Note distinction between stimulatory (+) = stimulatory site sites and inhibitory (-) = inhibitory sites.

Table 1-2: Biochemical and functional analysis of phosphorylation sites on the R-domain [113].

Residue Number	Amino Acid Sequence	*In Vitro* PKA Phosphorylation	*In Vivo* PKA Phosphorylation	Function discerned by Mutagenesis
S660	RKTS	√	ND	++
S670	RF**S**	√	ND	+
S686	KKQ**S**FK	ND	ND	Nil
T690	KQ**T**	ND	ND	Nil
S700	KRKN**S**	√√√	√√	+
S712	RKF**S**	√√	ND	Nil
S728	ED**S**DE	ND	ND	Nil
S737	RRL**S**	√√√	√√√	---
S742	PD**S**EQ	ND	ND	Nil
S753	RI**S**	√	√	+
S756	VI**S**TG	ND	ND	Nil
T757	IS**T**GP	ND	ND	Nil
T760	GP**T**LQ	ND	ND	Nil
S768	RRRQ**S**	√√√√	ND	----
T787	RK**T**	ND	ND	Nil
T788	RKT**T**	ND	ND	Nil
S790	**S**TRK	ND	ND	Nil
S795	RKV**S**	√√√√	√√√	++
S813	RRL**S**	√√	√√√√	++++

In vitro data from amino acid sequencing, mass spectrometry, and kinetic analysis of phosphorylation of intact CFTR, of an R-domain peptide, and of short peptides derived from R-domain sequences. *In vivo* information comprises results from ^{32}P labeling followed by immunoprecipitation and two-dimensional peptide mapping. In all cases, indicated relative level of phosphorylation of a particular site reflects acute cAMP-dependent PKA mediated incorporation of ^{32}P over a 5-15 min period. Sites are indicated as stimulatory (+) when mutation caused rightward shifts of IBMX dose response curves and mutation of sites labeled inhibitory (-) caused leftward shifts but mutation of other sites (nil) had no effect. √ indicates residue was phosphorylated by PKA; ND indicates phosphorylation by PKA was not detected, nil mutation had no effect. Number of (+), (-) or (√) indicate magnitude of effect.

Analysis of the PKA sites on the R-domain has shown that only five (ser-660; 700; 737; 795; 813) appear to be readily phosphorylated by PKA *in vivo* in cells that express native or recombinant CFTR [114, 115]. Further analysis of the R-domain's phosphorylation sites via site-directed mutagenesis and two-dimensional peptide mapping have shown that ser-660; 700; 712; 737; 753; 768; 795 and 813 may be phosphorylated *in vitro* by PKA when applied to R-domain peptides or NBD1-R-domain peptides [114-118]. The ability of some of the serines to be phosphorylated *in vitro* while not being phosphorylated *in vivo* likely reflects variation in the kinetics of phosphorylation at each site which may be overcome by higher levels of PKA treatment for a longer period of time.

To determine which of the sites on the R-domain are important for regulation of CFTR, individual and groups of serine residues were mutated to alanine. This series of experiments revealed that mutation of any one of the five readily phosphorylated serine residues or even groups of two to three did not have any effect on grossly measured cAMP-stimulated anion permeability [114, 119] indicating a functional redundancy where one particular site is not essential for proper R-domain regulation of CFTR. However, mutation of four or more serine residues resulted in a two-fold decrease in cAMP-stimulated iodide efflux and channel open probability (P_o) [119, 120]. Further reduction in P_o and anion conduction was observed when the eight *in vitro* phosphorylated serines were mutated to alanine. Moreover, continued mutation of ten, eleven or 16 serine residues only slightly reduced cAMP/PKA induced channel activity compared to the eight ser/ala mutations [119, 120]. Taken together, these data clearly

indicate the PKA phosphorylation of at least eight of the serines on the R-domain of CFTR is required for optimal channel activity.

The reduction in channel P_o due to mutation of serine residues suggested that when not phosphorylated, the R-domain acts as an inhibitory particle preventing Cl^- conduction even in the presence of ATP. This hypothesis was tested by a two-pronged approach using site-directed mutagenesis and examination of R-domain deletions. Csanady *et al*., [111], demonstrated that when the entire R-domain was deleted (aa634-836), the result was a channel that was constitutively active and P_o was only slightly increased by cAMP/PKA stimulation. Furthermore, when this construct was treated with the PKA inhibitor Rp-cAMPSA, the elevated basal conductivity was not substantially reduced [111].

Another approach used to examine the inhibitory property of the R-domain was site-directed mutagenesis, where individual serine residues were mutated to aspartic acid, mimicking phosphorylation at that residue. Mutation of four readily phosphorylated serine residues (660; 737; 795; 813) did not result in an increase in the basal chloride current when mutated individually or simultaneously [119]. Similar to the serine-to-alanine mutations, which required eight point mutations to inhibit activity, no observed changes in channel function were observed with the serine-to-aspartic acid point mutations until eight amino acids (660; 686; 700; 712; 737; 768; 795; 813) were changed from serine to aspartic acid [119]. This S-oct-D construct was constitutively active and was able to be activated to a greater extent by the addition of cAMP to the channel.

Under non-stimulated conditions, the prevailing view is that channel gating is inhibited by R domain elements that perhaps interfere with NBD dimer formation. This

is similar conceptually to the 'ball and chain' model of Shaker K channel inactivation [121, 122], and this model is supported by the finding that addition of the non-phosphorylated R domain to the cytoplasmic face of active CFTR channels is inhibitory [123]. Conversely, a stimulatory action of the R domain was implicated by the properties of CFTR channels bearing a large R domain deletion (708-835), which gate with reduced open probability, but are stimulated by the addition of a phosphorylated R region polypeptide (aa 645-835) [124]. It also appears that the location of the R domain, at the center of the repeated ABC structure, is not critical to channel regulation, since its transplantation to the C-terminus of CFTR, together with a sufficient linker region, also confers regulated CFTR channel function [125].

Taken together, these data fit the model of R-domain regulation proposed by Chappe *et al*.,[126] in which they describe the R-domain as having both a stimulatory and inhibitory function depending on its phosphorylation state (figure 1-11). When unphosphorylated, the R-domain is bound to a site on the channel which indirectly blocks the flow of Cl^- through the channel, possibly by blocking NBD dimer formation. Phosphorylation of the channel results in the movement of the R-domain away from the pore where it associates with a stimulatory site permitting chloride conduction.

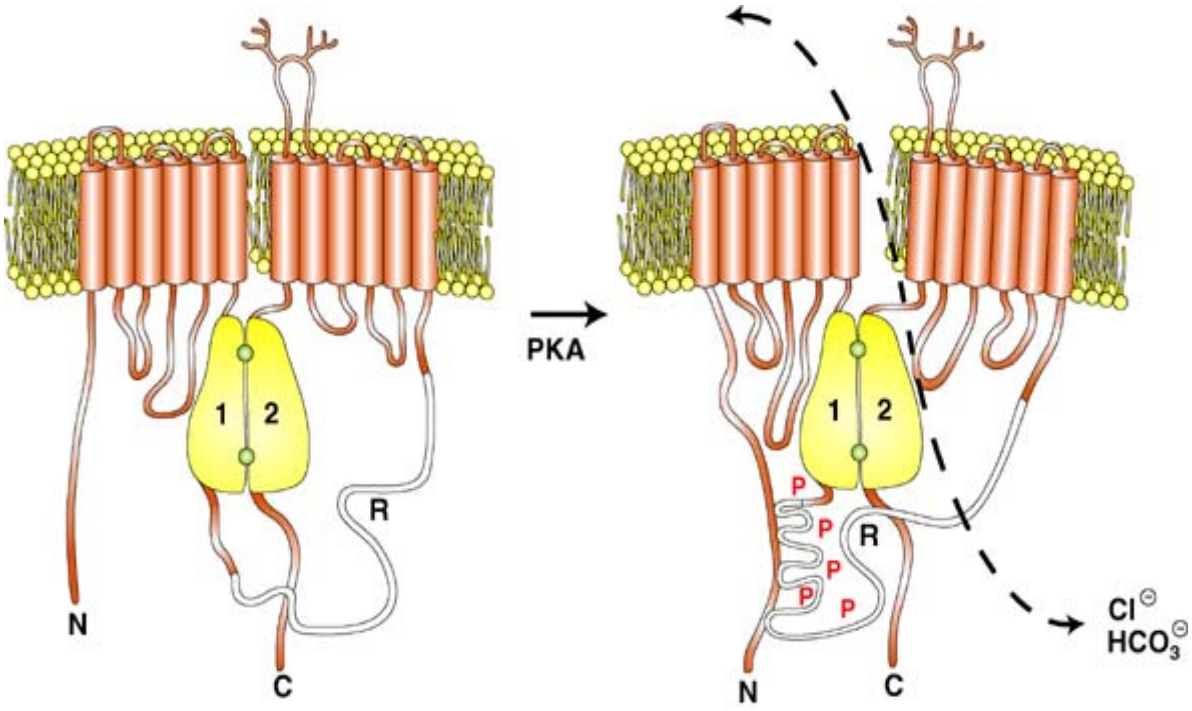

Figure 1-11: Model of effect of phosphorylation of the R-domain of CFTR [126]

In this model following the NBD1/NBD2 dimerization, PKA phosphorylates the R-domain which results in its interaction with the N-terminus of the channel allowing for anion conduction.

1.6.4 Regulated CFTR Trafficking:

Much attention has been focused on elucidating the mechanisms which regulate CFTR's ability to conduct chloride ions. Although regulation of channel gating is a critical element in the regulation of CFTR it is not the only component of a system that regulates the channels response to stimulation. This is evident from the formula for the total current.

$$I=iNP_o$$

This identity states that the total current (I) is a product of (*i*) the single channel conductance, open probability (P_o) and the number of channels in the membrane (N). This leads to the central question of regulated CFTR trafficking: Is the CFTR that contributes to plasma membrane chloride conduction present only in the apical membranes or does at least a portion of the channels reside in a sub-apical compartment from which it is mobilized to the surface following stimulation.

Studies of CFTR localization in cells provided support of the hypothesis of regulated CFTR trafficking. Lehrich *et al*., [127] examined the shark rectal gland using confocal microscopy in order to study the localization of CFTR under basal and stimulated conditions. When no agonist was present, they reported CFTR immunofluorescence from the apical membrane and extended into the sub-apical and supernuclear regions. Stimulation with secretagogues resulted in movement of the signal toward the apical membrane resulting a decrease of the depth of CFTR signal by ≈50% [127]. Quantification of CFTR fluorescence intensity as a function of distance from the apical membrane confirmed the movement of the signal toward the apical membrane. Additionally, it has been shown that the vasoactive intestinal peptide (VIP) produced a

redistribution of CFTR to the apical membrane domain in rat small intestine [128]. Using F-actin as a brush border marker in duodenal villus cells, VIP elicited a reversible three-fold increase in brush border associated CFTR with the channel being redistributed within the cell apex to the plasma membrane within 30 min [128, 129].

Subsequent studies of regulated CFTR trafficking examined the endo- and exocytic properties of CFTR expressing cells. Prince *et al*., [130], using biotinylation of carbohydrate residues on the extracellular surface of T84 cells followed by immunoprecipitation and radioisotope labeling using [^{32}P]-ATP found that CFTR was rapidly internalized by T84 cells with a half time of ≈3 min [130]. They also reported that cAMP stimulation resulted in an approximately 60% decrease in CFTR endocytosis. Moreover, they reported a small increase in apical membrane CFTR of ≈12%. However, the method they employed might have had serious limitations on its ability to detect phosphorylated CFTR. That is to say that using *in vitro* phosphorylation to detect CFTR following biotinylation and immunoprecipitation may be hindered by the phosphorylation state of the protein (i.e. if CFTR is phosphorylated by agonist there may be limited phosphorylation sites available for the *in vitro* phosphorylation assay) reducing the observed CFTR signal. To overcome this, Lukacs and co-workers developed a method for detecting CFTR where immunoprecipitation of the biotinylated CFTR was achieved with M3A7 and L12B4 monoclonal anti-CFTR antibodies [131]. Using this method they were able to show a forskolin-dependent inhibition of CFTR endocytosis and increase in plasma membrane CFTR as well as a depletion of the channel from intracellular compartments [131].

Studies of CFTR exocytosis have also demonstrated regulated channel trafficking in response to cAMP/PKA stimulation. Pulse labeling the plasma membrane of cells expressing WT-CFTR with biotinylated lectin showed that cAMP/PKA stimulation increased the rate of exocytosis of internalized marker nearly three-fold and required the expression of CFTR [132]. Moreover, when recycling/exocytosis was examined in human airway cells via monitoring the release of previously internalized FITC-dextran treatment of cells expressing WT-CFTR with a cAMP analog resulted in an increase in the release of FITC-dextran which was accompanied by an increase in membrane capacitance when monitored by whole cell patch-clamp measurements [133].

In addition to the biochemical analysis of regulated CFTR trafficking, a substantial amount of work has been done to elucidate this process by using measurements of membrane capacitance which are summarized in table 1-3.

Table 1-3: Measurement of stimulated capacitance in CFTR expressing cells [4].

Cell Type	Method	ΔC_m	Agonist	Reference
Xenopus Oocyte	2-electrode voltage clamp (single sine wave)	14nF	100μM 8-CPT-cAMP 1mM IBMX	[134]
Xenopus Oocyte	2-electrode voltage clamp (single sine wave)	23nF	100μM 8-Br-cAMP 1mM IBMX	[135]
Xenopus Oocyte	2-electrode voltage clamp (step)	80nF	10μM FSK 1mM IBMX	[136]
9HTE0-	Whole Cell Patch Clamp	14pF	100μM 8-Br-cAMP	[133]

Multiple studies have demonstrated that CFTR, expressed in the oocytes of the African claw-toed frog *Xenopus laevis,* produces a significant increase in chloride current with a corresponding increase in membrane capacitance following cAMP/PKA stimulation [135-137]. Takahashi *et al*.,[136] also demonstrated that the increases in C_m were accompanied by an increase in membrane surface area measured via morphometry. Along these lines, Peters and co-workers used a FLAG tagged CFTR construct expressed in *Xenopus* oocytes and were able to demonstrate recruitment of CFTR to the cell surface which corresponded to their observed increased in C_m [137]. Additionally, using impedance analysis to examine the effects of cAMP/PKA stimulation on I_{Cl} and C_m, Weber *et al*., [135] verified the previous results [136, 137] which showed a cAMP/PKA dependent increase in both parameters (I_{Cl} & C_m) [135]. Furthermore, they observed that these increases were not produced by cAMP/PKA in non-injected or ΔF508 expressing oocytes and that injection of the cAMP inhibitor (*Rp*-cAMP) abolished the cAMP/PKA induced increases in I_{Cl} and C_m [135]. Increases in plasma membrane CFTR density were also detected using atomic force microscopy (AFM) applied to membrane fragments excised from *Xenopus* oocytes expressing CFTR (25,26).

These findings, together with the unitary relationship between the surface area and the electrical capacitance of biological membranes ($1\mu F/cm^2$) [138], are consistent with the concept that cAMP/PKA stimulation elicits the fusion of CFTR-containing vesicles from intracellular compartments with the plasma membrane. Taken together, these results indicate that in addition to regulating channel gating, cAMP agonists also modulate the density of CFTR channels in the plasma membrane in many systems [133-137, 139-143]. Accordingly, the cAMP/PKA-induced increase in anion current

associated with phosphorylation-dependent increases in CFTR open probability (P_o) is supported also by an increase in the number of channels (N) resident in the surface membrane (22). The collected work from laboratories utilizing different cell types has suggested that this regulated trafficking function of CFTR is more significant in some systems than others; nevertheless, the trafficking pathways and associated protein interactions that underlie this response remain poorly defined.

In the present study, we examined the structural basis of regulated CFTR trafficking using a series of CFTR deletion constructs, by assessing their cAMP/PKA-induced membrane current and capacitance responses. Our goal was to determine whether there were regions of CFTR that were required for its cAMP/PKA-dependent membrane trafficking. We found that the removal of the R domain from CFTR, in addition to producing a spontaneous Cl current in the absence of stimulation, eliminated the cAMP/PKA-induced membrane capacitance increase. In addition, both agonist stimulation and removal of CFTR's R domain significantly reduced the channel's functional half-life, implying that these conditions, which bring CFTR to the cell surface, also increase its exposure to degradation pathways. Structure-function analysis of R-domain deletion constructs showed that removal of its C-terminal region produced a channel that retains agonist-dependent current regulation, but eliminated the cAMP/PKA-mediated increase in C_m. These findings suggest that this ordered R domain segment can stabilize CFTR within intracellular compartments, whereas R domain phosphorylation, by interfering with this stabilization, permits a redistribution of CFTR to the cell surface

2.0 MATERIALS & METHODS:

2.1 XENOPUS OOCYTES:

Xenopus oocytes are egg precursors from the African claw toed frog *Xenopus laevis* that can pass through the female frog's oviduct and be fertilized to develop into another frog. An individual oocyte is a large cell with a diameter of approximately 1-1.2 mm, surrounded by a glycoprotein matrix (vitelline membrane) which gives the oocyte some amount of structural stability and helps maintain its spherical shape [144].

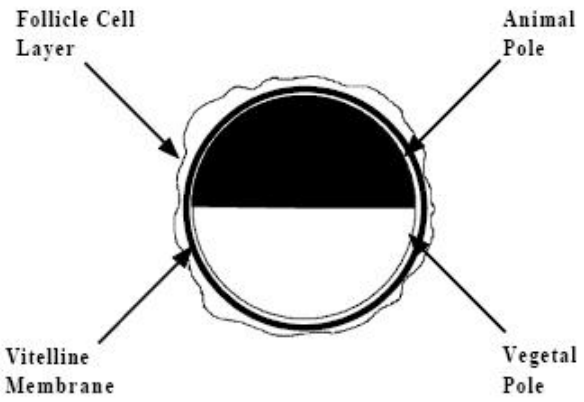

Figure 2-1: Individual stage V or VI oocytes from *Xenopus* laevis [144]

The most obvious feature of a *Xenopus* oocyte is its two-toned color scheme; the animal pole is dark (brown) and the vegetal pole is light (yellow) [figure 2-1]. This polarization is maintained inside the oocyte, in that the nucleus is found in the animal pole and there are different populations of mRNAs in each pole. Because *Xenopus* oocytes contain very few types of endogenous channels and receptors, they are an ideal system in which to study ion channel function.

Gurdon and co-workers were among the first to use the unfertilized oocytes from the *Xenopus* laevis as an expression system to study gene expression [144]. They demonstrated that injection of haemoglobin mRNA into the nucleus or mRNA into the cytoplasm resulted in the expression of a functional protein. The potential for the use of *Xenopus* to study ion channels was not realized until Miledi and co-workers showed that when ion channel cRNA was injected into oocytes, they produced a functional channel [144].

From these initial experiments, the use of *Xenopus* oocytes to study ion channels has expanded to examine various aspects of ion channel structure and function.

According to Axon Instruments [144], the use of *Xenopus* oocytes includes, but is not limited to: 1.) analysis of the properties of mutated channels 2.) analysis of receptor-effector coupling 3.) screening of cloned ion-channel genes 4.) comparison of ion-channel properties from various tissues expressed in common environment 5.) examination of multi-subunit assembly and post-translational processing of ion channels 6.) studies of the effects of second messengers on channel function.

Because oocytes contain a layer of follicle cells surrounding the vitelline membrane, individual oocytes must be separated from the follicular cells. Typically, this involves an extensive collagenase treatment to completely strip off the follicle cells. This is done by immersing the oocytes in a calcium free saline solution containing collagenase for one to three hours, until approximately half of the oocytes have been removed from the ovarian lobe. Once the oocytes are separated from the connective tissue, they are then sorted according to developmental stage. An oocyte exists in one of six developmental stages (I-VI), where only the more highly developed stage V and VI oocytes are sorted out and used for expression of a particular cRNA due to their high expression of translation machinery.

2.2 OOCYTE PREPARATION*:*

Isolation and cRNA injection of oocytes was performed as described previously in Cunningham *et al*., [145], and Gurdon *et al*., [146]. Female *Xenopus laevis* were purchased from *Xenopus* I (Ann Arbor, MI). When oocytes were to be extracted, the frog was anesthetized in a solution that contained 1.5L dH_2O and 1.8g of trichina [ethyl-3-

aminobenzoate methanesulfonic acid] and 4g Na-bicarbonate (Sigma-Aldrich, St. Louis, MO). This solution was then brought to 2L by the addition of ice. Individual frogs were placed into the solution for a minimum of 1 hour. Following incubation in the anesthetic, the frog was brought out and placed on a tub of ice with its head covered in ice. To remove the oocytes from the frog, two one-inch incisions were made in the frogs starting from the lower pelvis to the middle of the thorax at about 45˚. This exposed the underlying muscle layer which was cut with scissors to reveal the ovaries. Each ovary was removed through the incision with forceps and placed in non-sterile 1X Modified Barth's Solution (MBS) (table 2-1). This protocol was approved by the University of Pittsburgh Institutional Animal Care and Use Committee.

Table 2-1: Solutions Used.

ND-96	96 mM NaCl, 1mM KCl, 1.2mM $CaCl_2$, 5.8mM $MgCl_2$, 10mM N-2 hydroxyethylpiperazine-N'-2-ethanesulfonic acid (HEPES)
Modified Barth's Solution (MBS) (10X)	879 mM NaCl; 10mM KCl; 24mM $NaHCO_3$; 8mM $MgSO_4*7H_2O$; 3mM $Ca(NO_3)*4H_20$; 4mM $CaCl_2*2H_2O$; 100mM HEPES (½ Na salt)
MBS^{++} (10X)	Above plus: 25mM Na-Pyruvate; 500mg/ml penn/strep; 50ml horse serum/L
Forskolin	10 mM stock in EtOH; Used at 10mM
IBMX	500mM stock in DMSO; Used at 1mM
C7-intracellular Buffer	255 mM Potassium Glutamate; 10mM NaCl; 14mM MgSO4; 40mM HEPES
Isoproterenol	10mM stock in DMSO; Used at 10mM
Propranolol	100mM stock in DMSO; Used at 100nM
Ca^{2+} - Free ND-96 (10X)	959 mM NaCl; 10mM KCl; 10mM $MgCl_2*6H_2O$; 50 mM HEPES (½ Na salt)

The isolated ovaries were placed in a large weigh boat filled with non-sterile MBS and cut into small pieces. The cut ovaries were then placed into 6ml of collagenase solution (200mg/12ml Ca^{2+}- Free ND-96) until the volume of the tube reached 10ml. At this point, the oocytes were placed on an orbital rocker for 50 minutes at room temperature. While the oocytes were being treated with collagenase, a hypertonic solution of 250 mM KH_2PO_4 was prepared (200ml 250 mM KH_2PO_4 + 200mg BSA) and placed on a stir plate. Following the collagenase treatment, oocytes were washed three times with the KH_2PO_4/BSA solution to remove collagenase, the presence of BSA gives the remaining collagenase another substrate to react with in order to minimize any additional effects on the oocytes. After the third wash the oocytes were bathed three times for five minutes in the KH_2PO_4/BSA solution without being disturbed in order to shrink any vasculature on the outside of the oocytes remaining following isolation. After the washes in hypertonic solution, the oocytes were washed three more times with 1X-Ca^{2+} Free-ND-96 (table 2-1) followed by 1 wash with MBS^{++} (table 2-1). Following the wash in MBS^{++}, the oocytes were placed in a 100mm Petri dish, filled with MBS^{++} and allowed to incubate at 18˚ C for a minimum of 2 hours prior to sorting individual oocytes. Stage 5 & 6 oocytes were isolated in a 100mM petri dish containing 1X MBS^{++} under a dissecting microscope. The sorted oocytes were then placed at 18˚ C overnight in MBS^{++}.

2.3 cRNA INJECTION AND EXPRESSION:

cRNA was produced using the mMESSAGE MACHINE™ cRNA production kit from Ambion (Huston, TX) according to manufacturer's suggestions (see section 2.4)

and then injected into oocytes for expression. To accomplish this, we followed a modification of the protocols described in Cunningham, *et al*., [145], and Gurdon, *et al*., [146]. In our protocol, we injected cRNA constructs into oocytes in 50nl volumes using a micro-injection apparatus (World Precision Instruments, Sarasota, FL). Injections were performed using RNAse-free glass pipettes which had the tips broken to the desired diameter using forceps. The glass pipette was backfilled with mineral oil and placed in the micro injector. The apparatus was then placed in position, and the cRNA to be injected was drawn up into the pipette. To obtain the desired amount of cRNA to be injected, we diluted the stock cRNA using DEPC-treated H_20 (Ambion, Houston TX). When multiple cRNAs were to be injected, they were co-injected into the oocyte in the same 50nl volume. Following injection of cRNA the oocytes were placed in one well of a six well plate depending on which cRNA(s) were injected and allowed to incubate for 1-3 days at 18˚ C to allow for maximal expression.

2.3.1 Co-injection of NEG2 peptides

The NEG2 peptide, derived from the C-terminus of the R domain and two modified peptides sNEG2 and hNEG2 (see Figure 3-9D), were synthesized via solid-phase peptide synthesis (SPPS), and kindly provided by Dr. Robert Bridges (Rosalind Franklin University). Each peptide was solubilized at a concentration of 50 μM in an intracellular buffer [147] containing (mM): 128 K glutamate; 5 NaCl; 7 $MgSO_4$; 20 HEPES; pH 7.0, titrated with ultra pure KOH), aliquoted and stored at -20˚C. Oocytes expressing ΔNEG2-CFTR were voltage clamped as described in section 2.7 and allowed to equilibrate for 5 min. NEG2, or a modified peptide, was drawn into an injection tip

similar to that used for cRNA injections, the clamp was interrupted, and oocytes were impaled and injected with 23 nL of NEG2 peptide solution. Twenty minutes following peptide injection, experimental recordings were initiated using the standard agonist addition and recording protocols described in section 2.7.

2.4 cRNA SYNTHESIS:

In our experiments, we injected cRNA into individual oocytes for protein expression. Because most eukaryotic mRNAs have 7-methyl guanosine cap structures at the 5' end, these RNAs can be synthesized using the SP6, T3 or T7 polymerases via *in vitro* transcription reactions by including the cap analog (m^7G(5')ppp(5')G) in the reaction. To perform the reaction, the double-stranded DNA was linearized with the XHO-1 restriction enzyme (New England Biolabs, MA) that cut the DNA 3' to the end of the coding sequence. When linearized, the template was purified by phenol/chloroform extraction and ethanol precipitation. The linearized DNA was then used as a template to synthesize cRNA using the mMESSAGE MACHINE™ kit from Ambion (Houston, TX) according to the manufacturer's instructions. For CFTR preparation, a double reaction was used to give a higher cRNA yield. Briefly, the *in vitro* transcription reactions contained a mixture of linearized DNA template, ribonucleotide mix, cap analog and SP6, T3 or T7 RNA polymerase, as appropriate. Following cRNA production, the remaining DNA template was degraded by the addition of DNase and cRNA was recovered by lithium chloride extraction and precipitation with ethanol and isopropyl

alcohol. The concentration and purity of cRNA was examined by spectrophotometric measurement and gel electrophoresis.

2.5 MOLECULAR BIOLOGY:

For all of our experiments, the human WT-CFTR in the pBQ expression vector was used as a template. CFTR deletion constructs were generated by polymerase chain reaction (PCR) using this template and various primers (Invitrogen, CA). For deletion constructs, forward (deletion fwd) and reverse (1480 rev) primers were designed which bound to either the 3' or 5' end of the CFTR cDNA in pBQ. These primers also had a restriction digestion site at the 3' end of each primer (KPN1 on forward primer & XHO1 on reverse primer) (figure 2-2A). Either one of these primers was used in conjunction with another forward or reverse primer to generate a deletion at the desired site on CFTR using the 3-temperature PCR protocol shown in figure 2-2B. Following the PCR generation of our deletion construct, it was then subcloned into the vector pcDNA3.1-V5-His/Topo (Invitrogen, CA) using a topo-cloning kit according to manufacturers instructions. This system uses topoisomerase attached to the open ends of the pcDNA3.1 vector to subclone in a desired DNA fragment or PCR product. Once the DNA was inserted into the vector it was transformed into top-10 competent cells (Invitrogen, CA), and 100 μl was plated on LB-AMP plates (100mg ampicillin/L of LB agar) and grown overnight at 37˚ C. Following incubation, individual colonies were selected and used to seed 5ml liquid cultures in LB/AMP (10μl of 100mg/ml ampicillin per 5ml LB-broth). These cultures were then shaken at 37˚ C overnight. When the cultures had reached log-

phase growth 1ml of each sample was removed and used in a spin-mini-prep plasmid DNA isolation kit (Qiagen, CA). The isolated plasmid DNA was used to in a series of restriction digests to assess the size and orientation of the inserted PCR product. The three restriction digestions that were performed on each sample were 1.) XHO-1 2.) KPN-1 3.) XHO-1+KPN-1; with restriction enzymes from (New England Biolabs MA), This allowed for determining the correct size of the insert as well as ensuring that the topo-sub-cloning placed the insert in the correct orientation. In figure 2-2C the result of the restriction digests are shown on a sample of DNA that was generated via the above PCR protocol. In this example, lanes 1-3 and 7-9 are the result of PCR generated mutant being inserted in the correct orientation in that only the double digest with KPN1 & XHO1 were able to excise a band of the proper size from the vector. The digests in lanes 4-6 show the results of the PCR fragment being inserted in the wrong orientation, since each enzyme results in excision of the PCR fragment from the vector.

Figure 2-2: Overview of PCR protocol used to generate R-domain deletion constructs.

A) Representation of primer design used to generate R-domain deletion constructs where the forward primer contains a KPN-1 site and the reverse primer contains a XHO-1 site to allow for analysis of orientation. B) Three temperature PCR protocol used for generation of deletion constructs. C) Restriction digestion analysis of orientation of insertion of R-domain deletion construct generated by PCR. Correct orientation is indicated by a double band only in the KPN-1/XHO-1 double digest (i.e. lane #3 & #9) (see text for description)

When the band size and orientation were assured, we used the remaining bacterial culture to seed a 50ml liquid culture for bulk plasmid isolation using a midi-prep plasmid DNA isolation kit (Qiagen, CA). Following bulk isolation of the plasmid DNA, we then used phenol/chloroform extraction of the DNA to remove any impurities in the sample. The clean sample was then sequenced at the University of Pittsburgh DNA Core sequencing facility. The sequencing of each produced deletion construct provided definitive proof that the deletion was in the desired location as well as determine if any undesired mutations had been inserted into the construct during the PCR process. Finally, the cDNA of the deletion construct was used as a template to produce cRNA for oocyte injection or transfected into mammalian cells as the experiment required.

2.6 LUMINOMETRY:

Labeling of CFTR at the cell surface utilized an externally epitope tagged CFTR construct (EXT-CFTR, [148]), kindly provided by Dr. John Riordan (UNC-CH). HEK 293 cells were transiently transfected with cDNA constructs encoding EXT-CFTR or WT CFTR (control), 4μg/35mm dish, 24 h prior to experiments using lipofectamine 2000 (Invitrogen, CA) according to the manufacturers instructions. Following transfection, cells were incubated in HEK 293 media (DMEM + 10% FBS) at 37˚ C overnight. Cells were stimulated with 10 μM forskolin (EMD Biosciences, CA) at 37^{o}C for 12 min and placed on ice. For oocyte studies, EXT-CFTR (10ng) or WT CFTR (1ng) cRNA was injected together with β-AR and incubated in MBS^{++} for 3 days at 18˚C. Oocytes were stimulated with 10 μM isoproterenol (Sigma, MO) as in the electrophysiological studies.

Non-stimulated HEK cells or oocytes, treated identically except for agonist additions, served as controls. For chemiluminescence measurements, cell surface EXT-CFTR was labeled by sequential incubations in primary monoclonal HA antibody (1:1,000, 90 min) [Covance, New York, NY], secondary biotin-conjugated goat anti-mouse IgG (1:200, 90 min) [Invitrogen, Eugene, OR], and streptavidin conjugated to HRP (1:500; 90 min) [Zymed, San Francisco, CA]. All steps were performed at 4°C to block CFTR trafficking. The cells were then washed extensively, HRP-labeled proteins were detected using SuperSignal West Femto chemiluminescent substrate (Pierce). This process involves the oxidation of luminal by hydrogen peroxide which is catalyzed horse raddish peroxidase (HRP), resulting in the creation of an excited state product (3-aminophthalate), which decays to a lower energy state by releasing photons. The photons released were read in a TD20/20 luminometer (Turner, Sunnyvale, CA).

2.7 TWO ELECTRODE VOLTAGE CLAMP:

To record currents from *Xenopus* oocytes injected with CFTR cRNA, we used the two electrode voltage clamp technique (2EVC). A diagram of a conventional 2EVC is shown in figure 2-3.

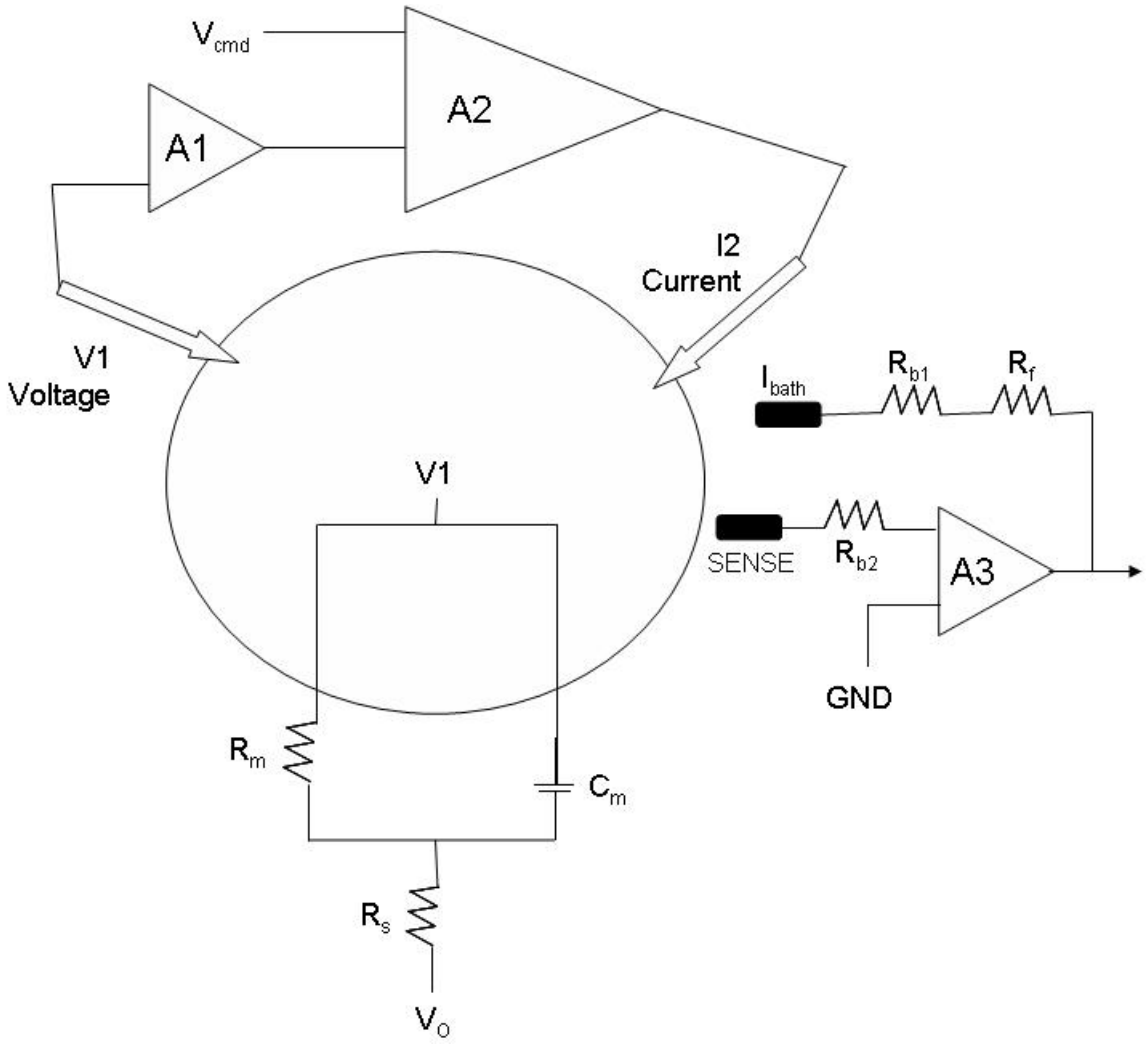

Figure 2-3: Conventional two electrode voltage clamp [144].

V1: voltage sensing microelectrode; I2 current passing microelectrode; SENSE: bath ground electrode voltage V1 for ground; I_{bath}; ionic carrier electrode to make the SENSE close to GND for current I2 ground. R_{b1} and R_{b2} are series resistances between cell membrane and the bath electrodes I_{bath} and SENSE. V_{cmd}: command voltage generated by computer. R_m: membrane resistance. C_m; membrane capacitance. R_s: series resistance from the bath solution and recording system.

Oocytes were impaled with two 3M KCl-filled electrodes which were connected to a GeneClamp 500 amplifier (Axon Instruments, CA) via Ag-AgCl pellet electrodes and referenced to the bath by two Ag-AgCl pellet bath electrodes. The voltage clamp was controlled by an AXOLAB 1100 analog-to-digital/digital-to-analog interface board (Axon Instruments, CA) using a modification of the pClamp-5 software (described in section 2-7-1) which was generated by Takahashi & Qi *et al.*, [136, 149] For our experiments, the membrane potentials were allowed to stabilize prior to starting to record current and capacitance.

Using the voltage clamp technique requires the membrane potential to be held constant (clamped) while measuring the current flowing across the membrane at that voltage. Our system (figure 2-3) used two different electrodes to measure the potential (V1) and pass current (I2). The membrane potential (V_m) was recorded by the amplifier (A1) connected to the voltage sensing electrode (V1). The V_m was then compared to the command potential (V_{cmd}) of the amplifier (A2) which was generated by the digital-to-analog interface board using the modified pClamp-5. A2 output was proportional to the difference between V_m and V_{cmd}, which forced current to flow through the current passing electrode (I2) to nullify the difference.

During recording of *Xenopus* oocytes or any large cell, the membrane current is sufficiently large so as to cause a significant drop across the resistance of the ground electrode. Given that the potential recorded by V1 is the sum of the transmembrane potential (V_m) and the bath potential (V_b, potential across R_{b1}), then to accurately record V_m the value of V_b had to be zero or nearly zero or the value of V_b had to be independently measured and subtracted from the potential recorded by V1. To

accomplish this, we used a two electrode virtual ground circuit. In this configuration, one ground was designated as the "sense" or voltage sensing electrode was placed near the cell surface. There was no current flow through the "sense" electrode, thus eliminating any voltage drop across R_{b2}. The other ground electrode (I_{bath}) carried ionic current in our system. These two electrodes worked in a feedback loop along with A3 to ensure that the potential at the "sense" electrode is equal to the potential at the negative amplifier input (GND).

In the repetitive pulse protocol (figure 2-4B), V_m was held at -30 mV, approximating the Cl^- equilibrium potential, and pulsed to -40 mV (50 ms) to obtain C_m, as described (section 2-7-1). To Measure I_m, V_m was returned to -30 mV (100 ms) and then pulsed to -60 mV (200 ms) to obtain the reported transmembrane current, I_m, which was sampled 10 ms before the end of each pulse. This protocol was repeated every 5 sec throughout the experiment. Using this protocol we were able to record CFTR-dependent Cl^- currents and membrane capacitance from *Xenopus* oocytes.

2.7.1 Capacitance Measurements:

A capacitor can be defined as two parallel conducting plates of large area separated by a thin sheet of insulator. The thickness (≈10nm) and amphipathic nature of the lipid bilayer make them an excellent approximation of a parallel plate capacitor. Capacitance is measured in Farads, which is defined as the ratio of the magnitude of the charge on either conductor to the magnitude of the potential difference between them. The general formula for capacitance is:

$$Q=C\Delta V$$

where (Q) is the charge, (C) is capacitance, and ΔV is the change in voltage. Since charge is only stored in a capacitor when there is a change in voltage across the capacitor, the current flow through the capacitor is proportional to the voltage change with time. This can be expressed in terms of current by the following equation:

$$I=C(\Delta V/\Delta t)$$

The stored charge on the membrane capacitance approximates the resting potential in that any change in voltage across the membrane is accompanied by a change in stored charge [144]. This indicates that if a current is applied to the membrane, it must first satisfy the requirement for charging the membrane capacitance, and then it can change the membrane voltage. This can be graphically represented by depicting the membrane as a resistor of value (R_m) in parallel with capacitance (C_m) [Figure 2-4].

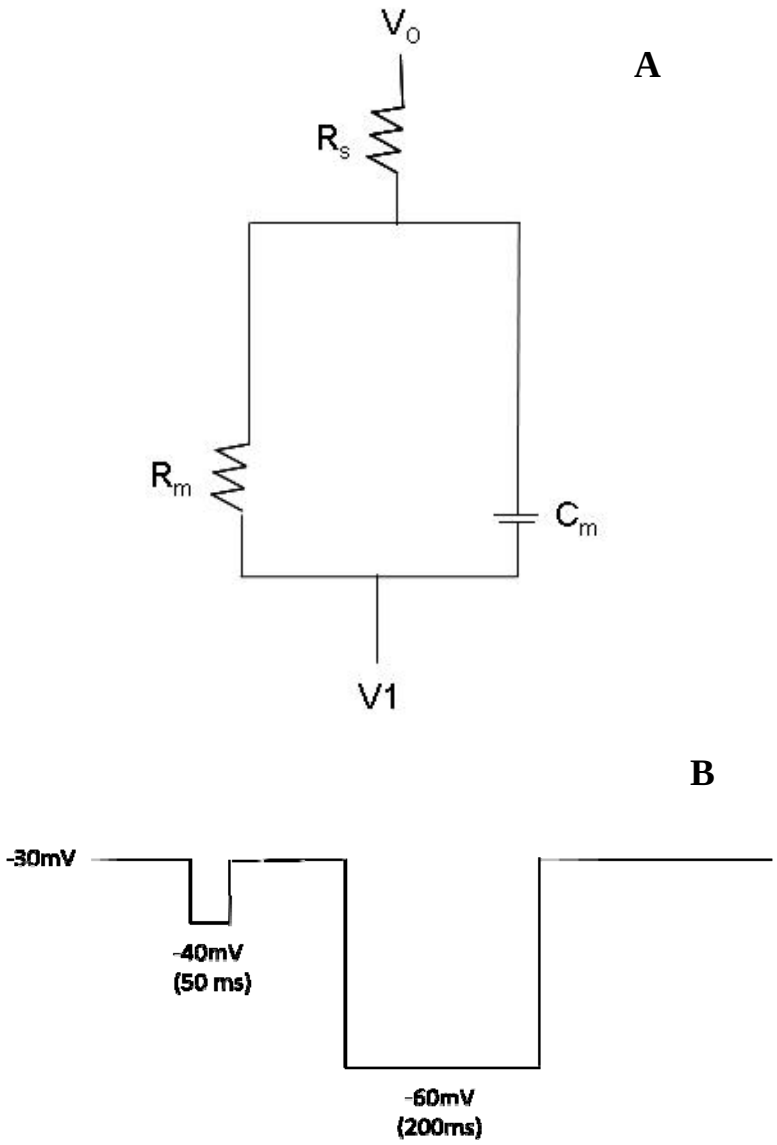

Figure 2-4: Model of biological membrane as an RC circuit [144]

A) This model of a biological membrane clearly indicates that if a current pulse is applied to the circuit it must first charge the capacitance only then can the voltage change to a steady state value. B) Model of our 2EVC pulse protocol used during our experiments to measure I_m and C_m. First pulse to -40mV was used to calculate C_m and the second pulse to -60mV was used to measure I_m. (see text for details)

The requirement of charging the membrane in response to an induced current prior to a change in voltage indicates that a time element must be taken into account. The charging of the membrane is approached along an exponential time course of:

$$V(t)=V_{inf}(1-e^{-t/\tau})$$

where V_{inf} is the infinite time or equilibrium value and does not depend on the capacitance. Instead it is determined by the current (I) and the membrane resistance (R_m), which can be represented by Ohm's law:

$$V_{inf}=IR$$

However, when the membrane capacitance is in the circuit, the voltage is not reached immediately. Instead, it is approached with the time constant τ which is given by:

$$\tau=R_mC_m$$

This implies that the charging time constant increases when either the membrane capacitance or the resistance increases. This is particularly important when recording from *Xenopus* oocytes because they are large cells with extensive membrane invaginations and have a large charging phase.

If biological membranes can be represented by a simple RC circuit where (R_m) is resistance and (C_m) is the capacitance of a parallel place capacitor, then it can be assumed that there is a relationship between the membrane capacitance and the membrane surface area. This relationship was determined by Almers *et al.*, [138], to be 1μF/cm^2. This relationship implies that a change in membrane surface area results in a concurrent change in membrane capacitance. To measure these changes, we used modifications of the formulas presented previously in conjunction with the modified pClamp5.0 software

[136, 149]. In our experiments, the membrane potential was clamped to the reversal potential of Cl^- (-30mV) followed by a 10mV hyperpolarizing pulse to -40mv (50ms duration) to drive chloride out of the oocyte generating a chloride current that can be used to calculate membrane capacitance. The effects of this pulse protocol on the recording of V_m and I_m can be seen in figure 2-5.

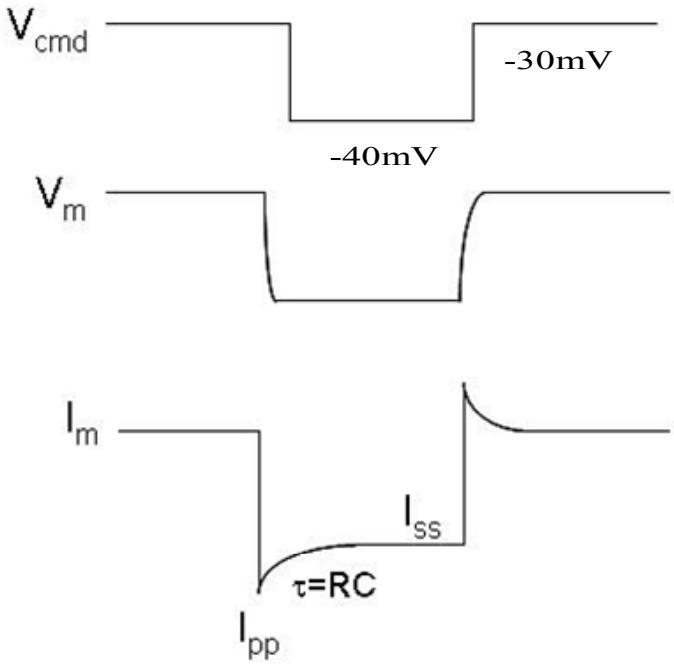

Figure 2-5: RC parallel circuit response to a voltage step

Measurement of the membrane voltage (V_m) and membrane current (I_m) in response to a step change in the command voltage (V_{cmd}). The current decay constant (τ) is determined by the modified pClamp-5 software by fitting the current decay from peak potential current (I_{pp}) to steady state current (I_{ss}) with a single exponential decay curve.

Using this protocol, we were able to calculate the I_{ss} or steady state current and the I_{pp} or peak current which was given by:

$$I_{ss}=V_{cmd}/(R_s + R_m)$$

$$I_{pp}=V_{cmd}/R_s$$

These equations allowed us to measure the current that was induced by the change in voltage, but for us to determine membrane capacitance; we had to calculate the time constant of the decay (τ) of the current from the I_{pp} to the I_{ss}. This was accomplished by the modified pClamp-5 software, which fit this current decay with a single exponential decay constant. When we obtained the decay constant we were then able to calculate the membrane capacitance which was given by:

$$\tau=[(R_m*R_s)/(R_m + R_s)]C_m$$

All of the data points necessary to determine membrane capacitance were calculated online using the modified pClamp-5 software.

The Axon Instruments pClamp-5 program was modified to generate a brief command voltage pulse and acquire the resulting membrane potential (V_m) and membrane current (I_m). The algorithms used to fit the current decay curve and calculate R_m, R_s and C_m were developed by Dr. Akira Takahashi and Dr. Juanjuan Qi in our laboratory. To measure C_m oocytes were voltage clamped at -30mv and the pClamp5 software generated a 10mV hyperpolarizing voltage pulse to -40 mV with a duration of 50ms was applied to the oocyte. During the pulse we sampled current 10ms before the end of the pulse at a sampling rate of 170kHz (maximum sampling rate of our digitizer),

allowing for the collection of 1700 data points. To compensate for the possible contribution of the pipette glass to the measured $C_{m,}$ the first 20 points of the collected data were discarded. Starting at data point 21, the next 250 data points (i.e. points 21-271) near the peak current (I_{pp}) were fit with a first order exponential decay function. The I_{ss} was calculated by averaging the three measurements taken at points 1660, 1680 and 1700 from the 1700 point data array. Figure 3-1 A&B shows the curve fitting obtained by this method before and after a large change in membrane current is induced in oocytes expressing WT-CFTR.

Validation of this method was performed using a three-fold approach. The first method was the use of model cells which were designed to mimic an oocyte membrane expressing WT-CFTR under basal and stimulated conditions. During these experiments Qi & Takahashi found that when measuring the stimulated C_m, there was an 11% underestimation of C_m (observed C_m of 330nf vs. 370nF measured C_m). This was explained by the marked value of the capacitor used in the model circuit possibly not actually being 370nF. We also tested our system using the MEO-2U oocyte model cell (Molecular Devices, CA). In these experiments our program measured an average C_m of 210±1.7nF (n=9). Compared to the model cell C_m of 220 nF, our measured value corresponded to a 5% underestimation of membrane capacitance by our system.

In addition to using model circuits, the effect of stimulation of Ca^{2+} activated Cl^- currents was measured and showed that increasing the activity of endogenous Cl^- conductance did not have an effect on the measured membrane capacitance [149]. Furthermore, the injection of the GABA-C receptor into *Xenopus* oocytes and the subsequent stimulation of GABA-gated Cl^- currents did not result in a measured increase

in membrane capacitance. In light of these control experiments, it was clear that changes in membrane capacitance measured by the modified pClamp 5.0 software were not correlated with increases in membrane conductance.

2.8 WESTERN BLOT ANALYSIS:

Western blotting of *Xenopus* oocyte extracts was performed as described [150]. Briefly, oocytes were homogenized in 15 mM Tris, pH 6.8 (20 μL buffer/oocyte). An equal volume of 1,1,2-tricloro-trifluorethane (Freon) was added and the oocytes spun for 10 min. at maximum speed (13,000xg) in a bench top centrifuge. The upper phase was recovered and the remainder treated again with Freon. Proteins from the upper fraction were precipitated with ice-cold methanol and chloroform. Sample buffer was added, the proteins separated by SDS-PAGE, and transferred to Immobilion™-P. Blots were probed with R domain specific α-hCFTR mouse monoclonal IgG_1 (1:1000) from R&D systems (Minneapolis) or the mouse monoclonal antibody (1:2500) whose epitope lies at the CFTR C-terminus (clone 24-1), which was purified from hybridoma supernatant (HB-11947; ATCC) by Mark Silvis in the lab. The secondary antibody was donkey α-mouse-HRP (horse radish peroxidase) from Amersham (1:5000).

2.9 STATISTICS & CALCULATIONS

All data are presented as mean ± S.E.M. where *N* indicates the number of experiments and *n* is the total number of oocytes studied. Statistical analysis was performed using the Student's unpaired *t* test. A value of $p \leq 0.05$ is considered statistically significant and shown by an (*) in graphs. All experiments were performed on oocytes harvested from at least three *Xenopus laevis* to judge reproducibility. The functional half-life of different CFTR constructs was determined by fitting current decay curves obtained in the presence of brefeldin A with the two-parameter, single exponential decay regression function of SigmaPlot 2001 (SPSS, Chicago, IL).

We calculated the number of vesicles (N_v) inserted into the plasma membrane in response to cAMP/PKA stimulation as described by Bertrand *et al*. [4], using the equation

$$N_v=\Delta C_m/C_s \cdot 4\pi r_G^2$$

where ΔC_m is the measured increase in membrane capacitance, C_s is the specific capacitance of a biological membrane ($1\mu F/cm^2$) and r_G is the radius of a spherical vesicle, assumed to be 100 nm for this purpose.

To calculate the number of channels we used the formula:

$$N_c=I_m/(P_o\gamma\Delta V)$$

Where I_m is the measured membrane current, P_o is the open probability of a CFTR channel (0.4), γ is the single channel conductance of a CFTR channel (8pS) and ΔV is V_m-V_R or membrane potential minus reversal potential.

3.0 RESULTS:

3.1 β-AGONIST INDUCED CURRENT AND CAPACITANCE RESPONSES.

Representative I_m and C_m responses from oocytes expressing WT CFTR are illustrated in Figs. 3-1 A&B, and mean data for basal and peak stimulation values from 15 recordings are summarized in Fig. 3-1C. In prior experiments of this type, stimulation was produced by addition of forskolin plus IBMX [136, 137]. In this study, co-expression of the β2-adrenergic receptor allowed cAMP/PKA stimulation by addition of isoproterenol (10 μM) as employed in previous studies [151, 152]. Stimulation with isoproterenol obviated the increase chloride conduction without affecting intracellular cAMP that has been reported with various xanthine derivatives such as IBMX [153].

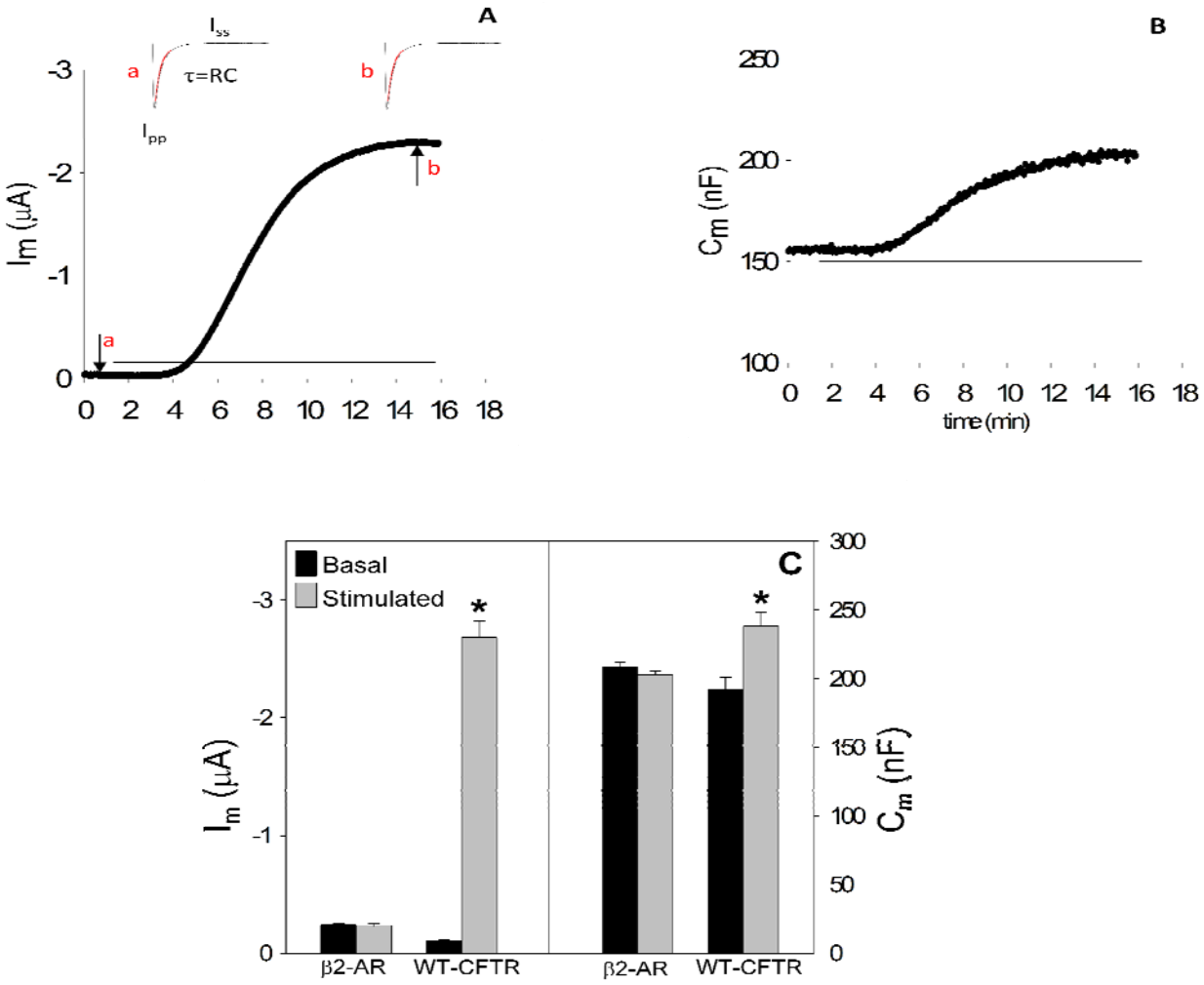

Figure 3-1: Stimulation increases I_m and C_m in *Xenopus* oocytes expressing WT-CFTR.

I_m (A) and C_m (B) recordings from a WT CFTR expressing oocyte during stimulation by bath addition of isoproterenol (10 μM), horizontal line. V_m was held at -30 mV and I_m obtained during a 10 ms pulse to -60 mV. C_m was calculated from currents recorded during a 20 mV hyperpolarizing voltage pulse, and the inserts (a & b) of panel A provide current recordings obtained from pulses before and after isoproterenol stimulation at the times indicated. The red line shows the fit of the current transient used to obtain C_m as described in Experimental Procedures where I_{ss} is steady state current and I_{pp} is the peak point of the current. Each oocyte was injected with 1 ng WT CFTR plus 1 ng β2-adrenergic receptor cRNAs in 50 nl water. C) Average basal and stimulated I_m and C_m values are from β2-adrenergic receptor injected oocytes [N=3; n=10] or oocytes expressing WT CFTR [N=4; n=15]. A value of $p < 0.05$ is considered statistically significant and shown by an (*) in all experiments.

Prior to stimulation, basal Cl current was 0.10 ± 0.01 μA, and isoproterenol produced a current increase (ΔI_m) that averaged 2.5 ± 0.13 μA. This current stimulation was paralleled by a 24% increase in membrane capacitance, ΔC_m = 46 ± 9.4 nF, from 192± 8.8 to 238 ± 10.4 nF. These changes in I_m and C_m are CFTR dependent; they are not observed in oocytes lacking exogenous CFTR expression (fig. 3-1C). The magnitudes of these responses are consistent with previously published data obtained using forskolin plus IBMX as the cAMP/PKA agonists [4, 135, 136]. The observed increases in membrane capacitance have been linked to the augmented delivery of CFTR to the plasma membrane, detected in prior studies by immunofluorescence labeling of CFTR bearing a flag epitope in its fourth extracellular loop [137]. Based on the relationship between biological membrane capacitance and surface area (1μF/cm^2) and using the equations in section 2.9, the corresponding increase in plasma membrane area predicted by this capacitance change corresponds to the net fusion of 3.6x10^7 vesicles of 100 nm diameter with the plasma membrane. From the measured ΔI_m, the single channel current of CFTR at the holding voltage (based on CFTR's single channel conductance of 8 pS), and a P_o of 0.4, we predict that a number of channels equivalent to the calculated number of vesicles contributed to the measured current. However, given the limitations of our assumptions, the contribution of membrane resident CFTR channels to the measured membrane current cannot be eliminated. Therefore, within the limitations of these assumptions, our data suggest that a large portion of the cAMP/PKA stimulated chloride current is the result of CFTR trafficking to the cell surface.

3.2 STIMULATION INCREASES THE CELL SURFACE EXPRESSION OF EXTOPE (EXT) CFTR.

Next, we determined cell surface CFTR expression using a different epitope-tagged CFTR from Peters *et al*., [137] construct and examined the response to β-agonist stimulation. EXT-CFTR contains a hemagluttinin (HA) tag in an expanded second extracellular loop of CFTR [148]. It was kindly provided by Dr. John R. Riordan (UNC-CH) and sub-cloned into pCDNA3.1$^-$, the construct employed to generate other cRNAs. Functional expression of EXT-CFTR exhibited behavior similar to WT CFTR, but required ~10-fold more CFTR cRNA (10 ng/oocyte) to obtain quantitatively similar stimulated current levels. As for WT CFTR, basal Cl^- currents were low, and addition of isoproterenol increased I_m and C_m ($\Delta I_m = 1.9 \pm 0.21$ μA , $\Delta C_m = 26 \pm 4.1$ nF) (Fig. 3-2 A). These values were similar to those obtained from injection of 1 ng WT CFTR (Fig. 3-1). The reduced expression efficiency of EXT-CFTR could reflect less effective processing of the protein within the ER.

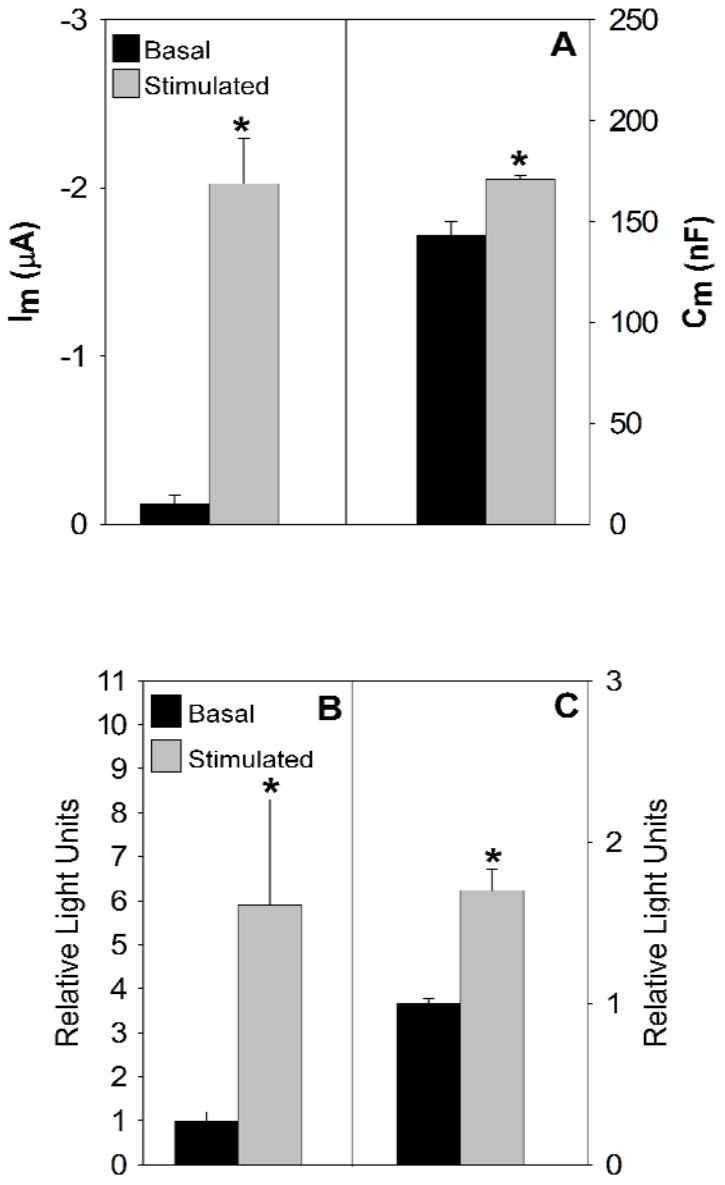

Figure 3-2: Current, capacitance and cell surface expression of EXT-CFTR are increased by cAMP/PKA stimulation

A) I_m and C_m were obtained from *Xenopus* oocytes injected with 10 ng EXT-CFTR and 1ng β2-AR cRNA 3 days prior to measurements [N=4; n=17]. Mean luminometry values from oocytes (B) or HEK 293 cells (C) expressing EXT-CFTR (10ng cRNA or 4 μg cDNA/35 mm plates, respectively). Values were background subtracted and normalized to mean values obtained under basal, non-stimulated conditions (oocytes: N=4; n=20; HEK cells: N=5; n=20).

We next used the EXT-CFTR construct to evaluate the influence of cAMP/PKA stimulation on its surface expression by enzyme linked immuno-labeling and luminometry, as described in Experimental Procedures. Similar experiments were performed in both oocytes and HEK 293 cells. The measurements employed modifications of the protocols described by Devor *et al*. and Jan *et al*. [154, 155] in which cells or oocytes were incubated with primary α-HA followed by an α-mouse-biotin conjugated secondary, and finally with a streptavidin-HRP conjugated tertiary antibody. As shown in Figs. 3-2 B&C, cAMP/PKA stimulation produced significant, 6- and 2-fold increases in cell surface EXT-CFTR detection of oocytes and HEK cells, respectively. Taken together with the agonist-dependent increases in C_m, the β-agonist induced surface labeling of EXT-CFTR supports the concept that cAMP/PKA stimulation increases CFTR density in the plasma membrane via fusion of CFTR containing vesicles that are derived from intracellular compartments. The response in oocytes was more robust than that found in HEK cells. In relation to prior studies [137], these data also indicate that this response does not depend on the position of the epitope tag in CFTR since both studies reported a stimulation dependent increase in membrane expression with epitope tags at different positions on the channel.

3.3 STIMULATION OF CFTR REDUCES ITS FUNCTIONAL HALF-LIFE

Next, we evaluated the hypothesis that the stimulation of CFTR trafficking may alter its functional stability in the plasma membrane. Results consistent with this interpretation have emerged from prior studies of other transporters/channels whose

trafficking is subject to acute regulation [156, 157]. To examine this possibility, we determined the decay of CFTR currents following the inhibition of anterograde membrane traffic with brefeldin A (BFA), both before and during isoproterenol stimulation of channel trafficking to the cell surface. This method is used commonly to examine the functional half-life of channels in this expression system [158].

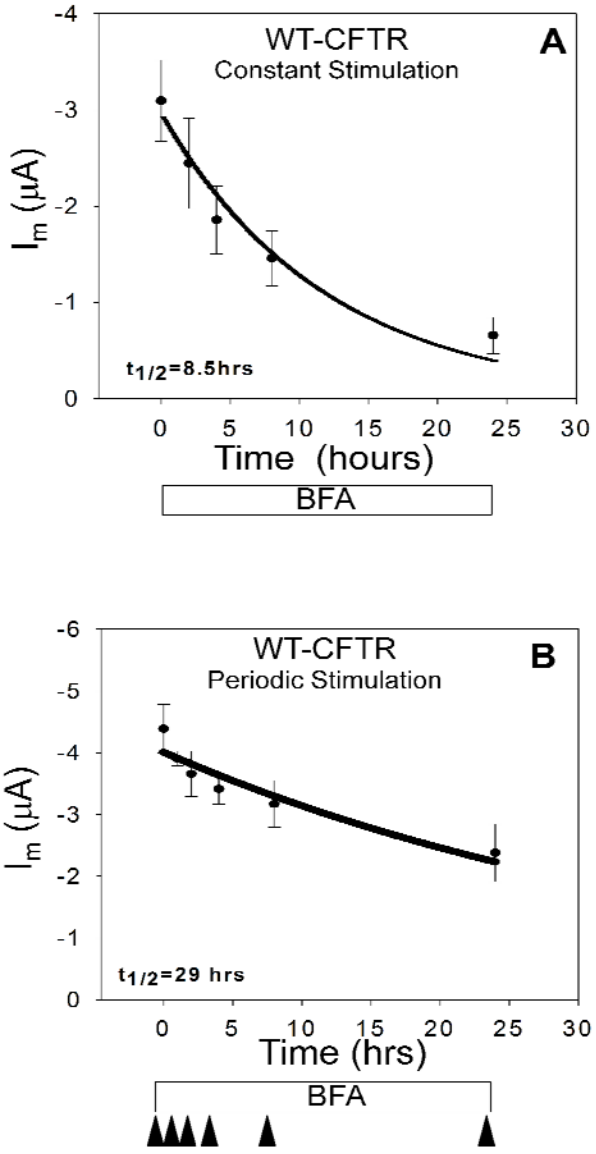

Figure 3-3 The functional half-life of CFTR is reduced during cAMP/PKA stimulation.

Current decay curves were produced by continuous incubation of oocytes expressing WT-CFTR (1ng) and β2-AR (1ng) with brefeldin A (10 μM). The data were fit with a single exponential function using SigmaPlot (Systat Software,CA). A) Oocytes were stimulated continuously with 10 μM isoproterenol and currents were recorded at 0, 2, 4, 8 and 24 hrs [N=5; n=20, each data point]. B) Currents were recorded from oocytes after (0, 1, 2, 4, 8, 24) hours of treatment with 10μM BFA. Current measurements were obtained at maximal stimulation following isoproterenol stimulation at the indicated times by (▲) [N=4; n=16].

As shown in Fig. 3-3, oocytes expressing WT CFTR were bathed continuously in 10 μM BFA. One group was exposed to continuous stimulation, with agonist present throughout the indicated time-course (Fig. 3-3A). The other group was stimulated periodically at the indicated times (arrowheads, Fig. 3-3B). When the cells were continuously exposed to agonist, their currents declined more rapidly ($t_{1/2}$ = 8.5hrs) than those stimulated only at the indicated measurement times ($t_{1/2}$ = 29hrs). The more rapid decline in current with constant stimulation was not due to β2-AR desensitization, since similar data were obtained also in response to stimulation by forskolin plus IBMX ($t_{1/2}$ = 6.4 hrs for constant stimulation and $t_{1/2}$ = 24.71hrs for periodic stimulation). The decrease in functional channel half-life observed with constant stimulation is consistent with the hypothesis that CFTR is relatively stable when it resides within intracellular compartments prior to stimulation, but that in response to agonist, the channel traffics more rapidly through plasma membrane-endosomal pathways, resulting in reduced functional stability. Similar findings have been obtained for GLUT4 and ENaC. In response to insulin, the half-life of GLUT4 was reduced from 50 to 15 hrs [157], while that of ENaC was decreased from 20 to 5 hrs in response to cAMP stimulation [156]. Similarly, the functional half-life of CFTR was reduced by a factor of ~3.5 during continuous cAMP/PKA stimulation.

3.4 R DOMAINLESS CFTR LACKS MEMBRANE CURRENT AND CAPACITANCE STIMULATION

Prior studies by Csanady *et al.*, [111] have shown that regulated CFTR channel activity could be expressed from half-channels encoded by two cRNA constructs (so-called split CFTR). In addition to the ability of the split CFTR constructs to function similar to WT-CFTR, the ease in generating deletions using the split constructs also made them an attractive alternative to full-length WT-CFTR. In preparation for the expression of split CFTR lacking the R domain, we first examined the agonist-evoked changes in current and capacitance of split CFTR expressed from two co-injected cRNAs. Our first series of split CFTR constructs contained the R-domain, which when co-injected into oocytes contained a complete CFTR cRNA which was "split" into two constructs. The R domain containing constructs encoded amino acids 1-834 or 635-1480, and they were co-expressed with the remaining CFTR sequence from a separate co-injected cRNA, i.e. 1-834 + 835-1480 or 1-634 + 635-1480. Figure 3- 4A shows that these split CFTRs behaved indistinguishably from the intact protein (compare with Fig. 3-1), having low basal currents and substantial increases in both I_m and C_m during cAMP/PKA stimulation. The current findings replicate those of Csanady *et al.*, [111], but the increased C_m values show also that the regulated CFTR trafficking property of the intact protein is retained. In addition, as illustrated in Fig. 3-4B, the functional turnover of the split CFTR (1-834 + 835-1480) was similar to that of WT CFTR under constant stimulation conditions. Thus, the regulated gating and trafficking properties of WT CFTR are retained in these split constructs, permitting their further modification.

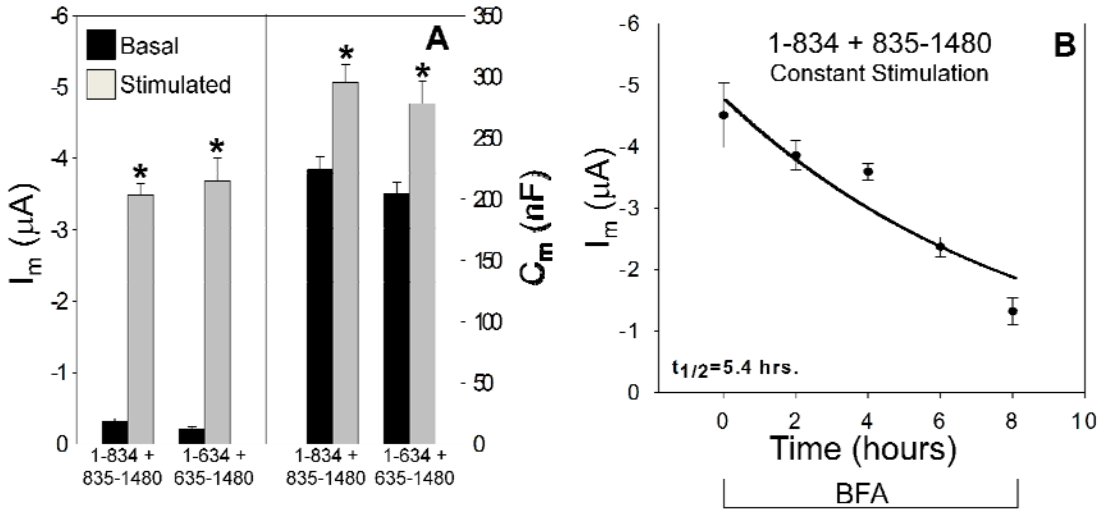

Figure 3-4: The functional properties of split CFTR constructs resemble those of WT CFTR.

A) Oocytes were co-injected with 0.5 ng of the CFTR half-channel cRNAs (1-834 + 835-1480, [N=4; n=16] or 1-634 + 635-1480, [N=3; n=10] and 1 ng β2-AR, and I_m and C_m were recorded in response to 10 μM isoproterenol, as in Fig. 1. B) Oocytes co-injected with split CFTR (1-834 + 835-1480 and β2-AR, as in A) were bathed continuously in 10 μM BFA and 10 μM isoproterenol and I_m measured at the indicated times [N=4; n=20].

The expression of split CFTR lacking the R domain (1-634 + 835-1480; termed ΔR-N/C) resulted in a high basal current that was not further augmented by cAMP stimulation, as found in previous studies of this construct [111]. Figure 3-5 A-C show representative current and capacitance recordings and the summary data from oocytes expressing ΔR-N/C CFTR. The spontaneous basal currents produced by omission of the R domain **(**1.9 ± 0.18 μF) were similar to the stimulated currents of WT CFTR (2.5 ± 0.13 μA) and EXT-CFTR (1.9 ± 0.21μA). In addition to the absence of an isoproterenol-induced current, stimulation of oocytes expressing ΔR-N/C CFTR did not elicit an increase in C_m (Fig. 3-5 B&C). Thus, in addition to forming a constitutively active channel, ΔR-N/C CFTR does not undergo a regulated trafficking response; rather, CFTR lacking its R domain is trafficked constitutively to the plasma membrane. These findings suggest that the presence of a non-phosphorylated R domain is necessary for CFTR to enter a regulated intracellular compartment from which it is trafficked to the plasma membrane in response R domain phosphorylation.

Figure 3-5: CFTR lacking the R domain does not exhibit regulated current or capacitance responses.

A&B) Time-courses of I_m and C_m in an oocyte injected with ΔR-N/C cRNAs (0.5ng each, 1-634 + 835-1480) plus 1ng β2-AR. Horizontal bar indicates addition of 10 μM isoproterenol. C) Summary I_m and C_m data for ΔR-N/C expressing oocytes [N=6; n=29]. D) Following addition of 10 μM brefeldin A, decay of spontaneous ΔR-N/C CFTR I_m yields a functional $t_{1/2}$ of ~30 min; expression conditions as in A [N=3; n=8].

The functional half-life of WT CFTR was reduced by its continuous stimulation (Fig. 3-3), which was attributed to its mobilization from a stable intracellular compartment. Accordingly, it was of interest to examine the turnover of ΔR-N/C, since this combination of half-channels behaves as if it were cAMP/PKA stimulated. Oocytes expressing ΔR-N/C CFTR were incubated with 10 μM BFA. Since preliminary experiments indicated that the current decline following BFA addition was rapid, the decay of the spontaneous currents of ΔR-N/C CFTR was measured during continuous recordings. As shown in Fig. 3-5D, the half-life of the ΔR-N/C construct was very brief, at 0.5 ± 0.1 hrs. Thus, the R domainless CFTR exhibited the least functional stability of any CFTR construct we examined, and this property likely contributes to its somewhat lower overall current level relative to WT CFTR. Data obtained with the split CFTR that retains the R domain (Fig. 3-4B) suggests that the rapid turnover of ΔR-N/C is not due to the use of a split CFTR construct. The short half-life of ΔR-N/C CFTR suggests that structures within the R domain contribute to the stability of CFTR at the plasma membrane

In prior studies, we found that the ΔC_m response of WT CFTR reached a plateau as CFTR expression and the corresponding ΔI_m was increased, which was done by augmenting cRNA dose [136]. To verify that the lack of a ΔC_m for ΔR-N/C was not compromised in some way by assessing only a restricted expression level, we determined its ΔC_m-ΔI_m relation over a range of cRNA expression, in comparison with WT CFTR. As figure 3-6 shows, the ΔC_m response of ΔR-N/C to stimulation was minimal over a broad range of expression. In addition, these data show that the expression level of WT

CFTR used in these studies (yielding ~2 μA current) was within the range where ΔC_m is directly proportional to the ΔI_m response.

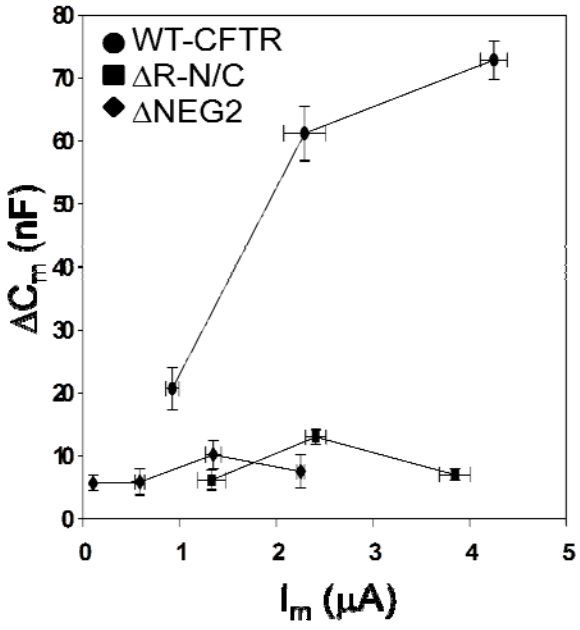

Figure 3-6: Varying amount of cRNA injected does not affect the Cm response of R-domain deletion

ΔC_m-ΔI_m relations for WT, ΔR-N/C and ΔNEG2 CFTRs. Isoproterenol- induced changes in current and capacitance were varied by injecting different amounts of cRNAs (ng): WT CFTR and ΔR-N/C, 0.5, 1, 2.5; ΔNEG2, 2.5, 3.5, 7, 15; N=2, n=8.

3.5 INDIVIDUAL HALF CHANNEL CONSTRUCTS DO NOT FORM A FUNCTIONAL CHANNEL.

Next, we addressed the possibility that the properties of ΔR-N/C might have arisen from the function of individual half-channels rather than association of the channel halves. Previous studies by Devidas and co-workers [159] suggested that CFTR constructs comprised of TM1 + NBD1 or TM2 + NBD2 formed constitutively active channels when expressed in *Xenopus* oocytes. In view of the high level of cRNA used in those studies (50 ng/oocyte), we asked whether the half-channel constructs would generate significant currents at the lower cRNA levels employed here (i.e. 0.5 ng). Expression was allowed to proceed for the same time period (3 days). The basal and stimulated currents obtained from these cRNAs, and others used in the present studies, are provided in Table 3-1. Relative to WT CFTR, split CFTR or ΔR-N/C, the individual half channels did not produce significant currents. Therefore, the currents obtained from split and ΔR-N/C CFTRs derive from the assembly of half-channels.

Table 3-1 Basal and stimulated currents recorded from *Xenopus* oocytes expressing WT CFTR and individual half-channel cRNAs.

cRNA	Basal I_m (μA)	Stimulated I_m (μA)	μg cRNA	n
WT-CFTR	-0.10±0.01	-2.7±0.14	1	15
1-634	-0.10±0.04	-0.02±0.002	0.5	8
835-1480	-0.09±0.02	-0.04±0.01	0.5	10
1-834	-0.16±0.02	-0.02±0.03	0.5	8
635-1480	-0.20±0.04	-0.20±0.02	0.5	9

Column one shows the cRNA construct injected into each oocyte. Columns 2 and 3 show the average basal and stimulated I_m recorded with 2EVC. Column 4 & 5 list the amount of cRNA injected and the number of 2EVC recordings for each construct.

3.6 EXPRESSION OF THE R DOMAIN DID NOT RESTORE REGULATION TO ΔR-N/C

Since a regulated CFTR trafficking response required the R domain, we asked whether its co-expression with ΔR-N/C would restore a stimulation-dependent current and capacitance responses. This outcome would facilitate studies designed to identify a region within the R domain that contributes to the ΔC_m. In BHK cells, Chappe *et al*. [126] found that co-expression of the R domain with CFTR half-channels encoded by a bisistronic construct partially reduced the spontaneous anion efflux and channel activity of split ΔR expressing cells and also partially restored their cAMP/PKA responsiveness. However, as seen in Fig. 3-7A, the co-expression of R domain cRNA with ΔR-N/C failed to significantly reduce its spontaneous current or restore cAMP/PKA regulation, despite a five-fold excess of R domain cRNA. To ensure that the R domain polypeptide was expressed, western blot analysis was performed using lysates from oocytes co-injected with R domain and ΔR-N/C cRNAs, or with ΔR-N/C alone. The blot of Fig. 3-7B shows that the lack of recovery of regulated current was not due to a lack of R domain expression, but likely results from an inability of the R domain to properly assemble with the half-channels.

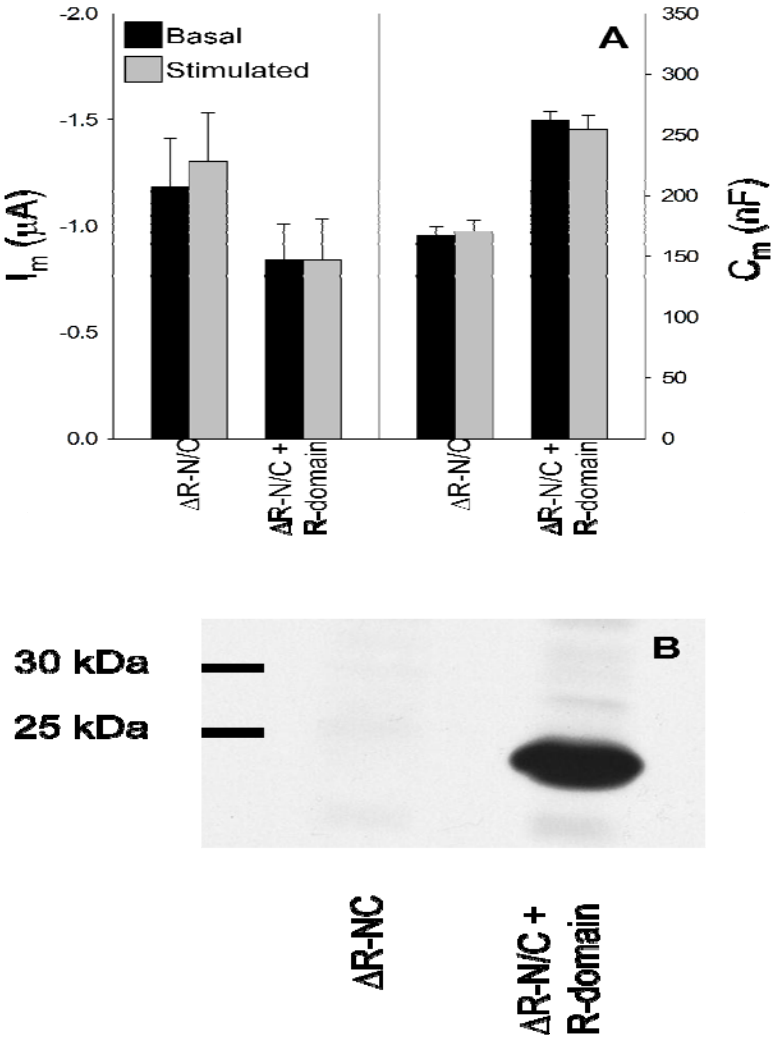

Figure 3-7: Expression of the R domain does not induce regulated behavior of ΔR-N/C

cRNA expression conditions: 0.5ng each ΔR-N/C cRNAs, with or without 5 ng R domain, plus 1ng β2-AR cRNA. A) Mean basal and stimulated I_m and C_m values ΔR-N/C [N=3; n=14] and ΔR-N/C + R-domain, [N=3; n=17]. The source of the difference in mean C_m values of these groups is not known; however, these values are within the range observed and variation does arise from oocyte size and membrane folding [135]. B) Immunoblot of lysates from oocytes expressing ΔR-N/C or ΔR-N/C + R-domain; expression conditions as in A. Membranes were probed with R domain specific anti-CFTR mAb (1:1000); see Experimental Procedures for protocol.

3.7 THE NEG2 REGION IS REQUIRED FOR CAMP/PKA-DEPENDENT CFTR TRAFFICKING

The co-expression of R domain constructs with ΔR-N/C did not allow us to narrow the R region involved in regulated CFTR trafficking. Therefore, we progressively deleted amino acid segments from the C-terminus of the 1-834 construct and co-expressed these with the complementary C-terminal construct, 835-1480. Of those examined (Table 3-2), only the split CFTR combination 1-784 + 835-1480 generated significant currents above baseline levels.

Table 3-2: R-domain deletion constructs examined and results of cAMP/PKA stimulation on I_m

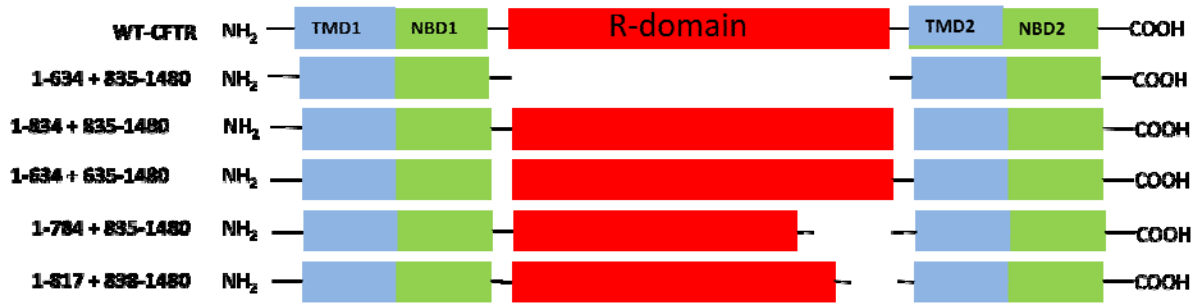

R-Domain deletion cRNAs	Basal I_m (μA)	Stimulated I_m (μA)	ng cRNA	n
1-634 + 835-1480	-1.9±0.17	-2.1±0.18	0.5	29
1-653 + 835-1480	-0.07±0.04	-0.11±0.02	5	7
1-673 + 835-1480	-0.17±0.01	-0.15±0.04	5	8
1-693 + 835-1480	-0.11±0.03	-0.10±0.02	5	7
1-713 + 835-1480	-0.09±0.06	-0.11±0.04	5	10
1-733 + 835-1480	-0.12±0.05	-0.11±0.01	5	8
1-753 + 835-1480	-0.06±0.02	-0.08±0.05	5	11
1-773 + 835-1480	-0.12±0.01	-0.11±0.03	5	7
1-784 + 835-1480	-0.33±0.02	-1.5±0.30*	3.5	11
1-816 + 839-1480	-0.84±0.25	-1.9±0.51*	3.5	14

Graphical representation of split CFTR constructs used. Table lists the construct(s) injected and the average basal and stimulated I_m recorded with 2EVC. The amount of cRNA of each half channel construct injected and the number of experiments performed with each construct is shown in columns 4 and 5. (*) indicates significant difference between basal and stimulated data ($p<0.05$).

As illustrated in Fig. 3-8 A&B, this 51 amino acid deletion, which retained 12 of 19 PKA phosphorylation sites, produced somewhat elevated basal currents while remaining responsive to cAMP/PKA stimulation unlike ΔR-N/C [113]. However, 1-784 + 835-1480 CFTR showed no stimulation-dependent increase in membrane capacitance (Fig. 3-8C). Therefore, this combination of half-channels structurally dissociates the ΔC_m and ΔI_m responses of CFTR to cAMP/PKA stimulation. In addition, this data verifies that the measured ΔC_m is not a technical artifact that is linked in some way to the ΔI_m. The absent C_m response suggests that 1-784 + 835-1480 CFTR lacks regulated recruitment to the plasma membrane and indicates that this region of the R domain accounts for the similar properties of ΔR-N/C.

Figure 3-8: Partial R domain deletions mimic the absence of a trafficking response in ΔR-N/C.

A&B) I_m and C_m recordings of split CFTR (1-784 + 835-1480) co-expressed with β2-AR; all cRNAs 1 ng/oocyte. Horizontal bar indicates the addition of 10 μM isoproterenol. C) Summary data for 1-784 + 835-1480 CFTR [N=3; n=11]. D) Summary data for split ΔNEG2 (1-816 + 839-1480) injected oocytes; cRNAs 1 ng/oocyte [N=4; n=16].

3.8 CFTR TRAFFICKING DEPENDS ON THE NEG2 REGION AND ITS HELICAL PROPERTIES.

Lying in the 784-835 region of the R domain is a stretch of negatively charged amino acids (aa 817-838) designated by Ma and coworkers as NEG2 [5, 6]. In their prior studies, this region of the R domain influenced CFTR gating. Its 22 amino acids have a net charge of -9, and the peptide exhibits significant α-helical content, assessed by CD spectroscopy [6]. On this basis, we developed split CFTR constructs lacking the NEG2 region (1-816 + 839-1480), and designated their co-expression as ΔNEG2 CFTR. As shown in Fig. 3-8D, their behavior was qualitatively similar to the larger deletion, 1-784 + 835-1480. As shown in Table 3-2, the basal currents of ΔNEG2 were more elevated, but the stimulated current levels were similar. As found for ΔR-N/C and 1-784 + 835-1480 CFTR, this channel did not display the cAMP/PKA-dependent stimulation of C_m that is characteristic of WT CFTR.

To determine whether the NEG2 peptide itself could influence the regulated trafficking of CFTR, we injected the peptide (817-838) into oocytes expressing ΔNEG2. Based on prior experience with similar protocols [160], the 20 min period prior to initiation of stimulation should be more than sufficient for peptide diffusion within the oocyte. Figure 3-9A provides the mean data from this set of experiments.

Figure 3-9: Peptide injection restores regulated trafficking to ΔNEG2

A) Summary data for ΔNEG2 expressing oocytes injected with 23 nl of 50 mM NEG2 peptide (~1 nmol) prior to I_m and C_m recordings [N=4; n=14]; cRNA 7 ng/oocyte). B) Oocytes co-injected with split ΔNEG2 and β2-AR cRNAs were bathed continuously in 10 μM BFA and I_m measured at the indicated times [N=3; n=18]. C) Summary data for changes in C_m (%) evoked by 10 μM isoproterenol following injection of the indicated peptide into oocytes expressing split ΔNEG2 CFTR (as in A). Sequences of peptides: NEG2, GLEISEEINEEDLKECFFDDME; sNEG2, LIKEFSEEDGECLMIDEDENEF; hNEG2, GLEISEQINQQNLKQSFFNDME See [6] for discussion of peptide structures as determined by circular dichroism. sNEG2, [N=3; n=12]; hNEG2, [N=4; n=16]. D) 3D rendering of WT and mutant NEG2 peptides generated using the Kinemage, Next Generation (KiNG) display software available from (http://kinemage.biochem.duke.edu/software/king.php) with negatively charged amino acids shown in red

Following NEG2 peptide injection, the basal and stimulated currents were not markedly different from those of ΔNEG2 alone; however, a significant ΔC_m (29.2±2.03 nF) response to cAMP/PKA stimulation was now observed. Within this time frame, peptide injection was unable to reproduce the full magnitude of the ΔC_m response of WT CFTR, and this may result from incomplete structural complementation by the peptide or to the need for additional time for the formation of a regulated trafficking compartment within the cell. Despite this quantitative difference, the data is consistent with the view that the NEG2 region is required for regulated CFTR trafficking.

To further assess the properties of NEG2, as done originally by Ma *et al*. [6], two additional peptides were synthesized that eliminated the helical content of NEG2 or reduced its net negative charge (see fig. 3-9D for graphic). One peptide (sNEG2) consists of a scrambled NEG2 sequence that disrupts the helical structure but preserves the negative charge; the other peptide, (hNEG2) has reduced negative charge (-9 to -3) but retains helical structure [6]. The remaining negative charge of hNEG2 was necessary to maintain peptide solubility [6].

As shown in Fig. 3-9C, we determined the influence on agonist-dependent I_m and C_m of introducing these peptides into oocytes expressing ΔNEG2 CFTR. The sNEG2 peptide did not restore the agonist stimulated increase in C_m, while hNEG2 peptide injection reproduced a similar ΔC_m response as that observed with NEG2 peptide injection. Elimination of the agonist induced ΔC_m with sNEG2 and its preservation with hNEG2 suggest that the helical content of NEG2 is a primary requisite for this region to support the regulated trafficking of CFTR.

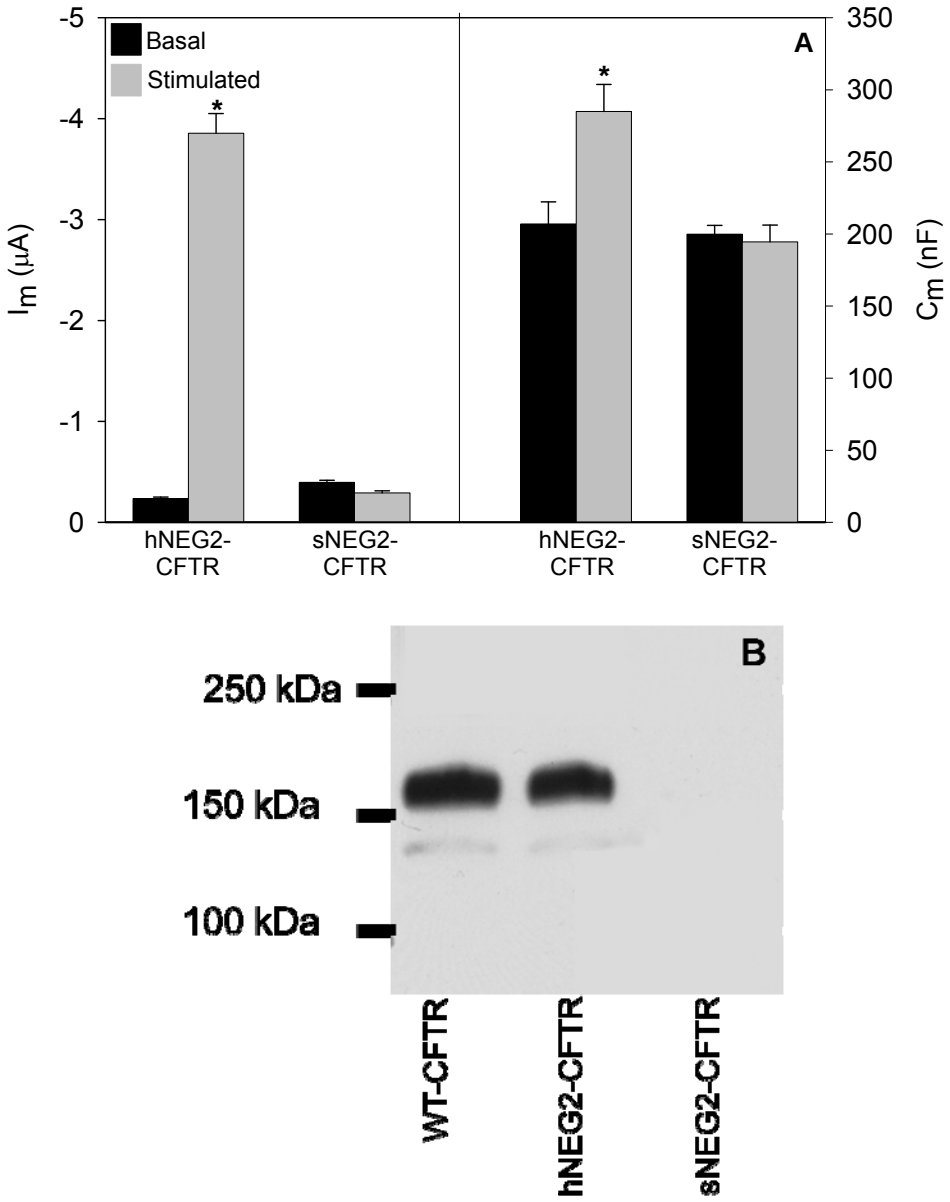

Figure 3-10: hNEG2-CFTR retains regulated trafficking properties.

A) I_m and C_m summary data for hNEG2-CFTR [N=3; n=13] & sNEG2-CFTR [N=3; n=10]. B) Western blot of HEK 293 cells transfected with WT CFTR, hNEG2-CFTR or sNEG2-CFTR. Cells were transfected with 4 μg cDNA, each construct; after 24 hrs, cells were harvested and subjected to immunoblot using mAb directed against the CFTR C-terminus (1:2500). Typical of results from 3 experiments.

These findings were further explored by incorporating the sNEG and hNEG sequences into full-length CFTR. PCR-based mutagenesis (see Methods) was employed to generate mutations within the NEG2 region. The resulting constructs were designated sNEG2-CFTR or hNEG2-CFTR. Similar to findings with hNEG2 peptide injection, hNEG2-CFTR yielded agonist induced increases in both I_m and C_m, as illustrated in Fig. 3-10A. In addition, the basal current of hNEG2-CFTR was similar to that observed for WT CFTR expression. In contrast, attempts to express sNEG2-CFTR did not yield currents higher than those observed in non-injected oocytes. The explanation for this negative finding was provided by western blots of HEK 293 cells transfected with WT CFTR, hNEG2-CFTR or sNEG2-CFTR plasmids (Fig. 3-10B): WT and hNEG2-CFTR were expressed at similar levels, whereas the sNEG2-CFTR construct did not produce a detectable product. These data, in conjunction with the peptide co-injection experiments, strongly suggest that the NEG2 region is required for regulated CFTR trafficking and that its helical content is an important structural feature necessary for the response.

3.9 SYNTAXIN 1A INHIBITION IS ELIMINATED IN ΔR-N/C AND ΔNEG2 CFTR

Prior studies have indicated that a physical interaction of syntaxin 1A (S1A) with the CFTR N-terminus reduces the regulated currents of CFTR expressed in oocytes [161, 162]. Other work [137] attributed the action of co-expressed S1A to an inhibition of CFTR trafficking, detected using membrane capacitance measurements and external epitope tag labeling, similar to the present studies.

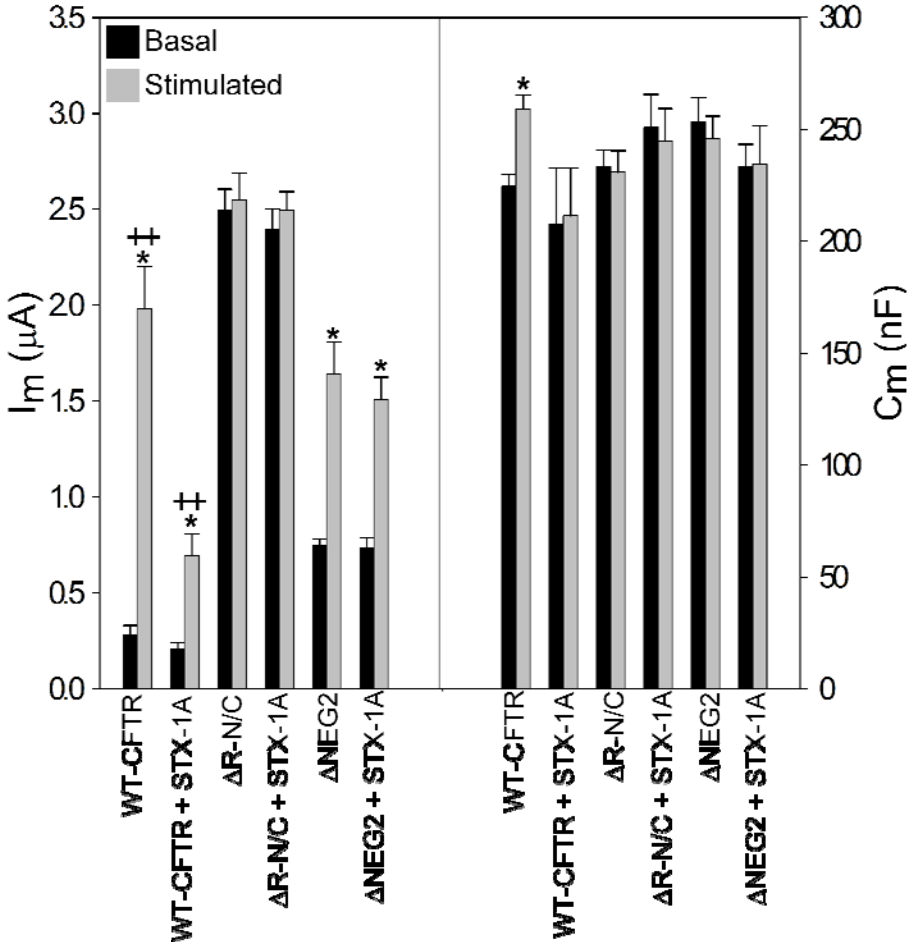

Figure 3-11: Deletion of NEG2 region eliminates the effect of syntaxin 1A on CFTR-mediated ΔI_m and ΔC_m.

cRNA injections: WT-CFTR (1ng), ΔR-N/C (1ng total) or ΔNEG2 (7.5ng) with or without S1A (10ng), as indicated, plus β2-AR (1ng); stimulation with 10μM isoproterenol. (*) significant difference between basal and stimulated conditions ($p<0.05$); ($^{++}$) indicates a significant difference with S1A co-expression ($p<0.05$). N=2; n=9, all groups.

Given the requirement for the R domain and specifically the NEG2 region in regulated CFTR trafficking, we examined the influence of co-expressed S1A on the properties of ΔR-N/C and ΔNEG2 CFTR. As illustrated in Fig. 11, the action of S1A on WT CFTR recapitulated the results of prior studies in which its co-expression reduced cAMP/PKA stimulated CFTR currents and eliminated the agonist-evoked ΔC_m. However, these inhibitory effects were absent when S1A was co-expressed with ΔR-N/C or ΔNEG2 CFTR. The elevated basal currents of ΔR-N/C and ΔNEG2 CFTR were not altered by S1A, nor was the current response of ΔNEG2 CFTR to stimulation. Thus, these R domain deletion mutants, which exhibit no ΔC_m response to agonist, are also unresponsive to S1A inhibition. The functional interaction between this SNARE protein and CFTR, like the regulated trafficking response of CFTR, requires the NEG2 region

.

4.0 DISCUSSION:

The primary goal in this work was to determine whether a structural feature, within CFTR itself, contributes to its cAMP/PKA regulated trafficking at the plasma membrane. Our rationale was that the identification of a CFTR component that is required for the trafficking response could lead ultimately to elucidation of the trafficking mechanism, and potentially provide targets for modulating the apical membrane density of CFTR mutants (see Introduction).

Xenopus oocytes display a robust CFTR trafficking phenotype, and calculations based on the present data suggest that the recruitment of CFTR from intracellular compartments accounts for most of the current response in this system. Oocytes exhibit agonist evoked, CFTR-dependent increases in membrane capacitance and in plasma membrane CFTR labeling using an expression construct containing a flag epitope tag in CFTR's fourth extracellular loop, ECL4 [137] This approach has been used by others to measure the cell surface expression of ENaC [163, 164] and other channels [165]. In the present studies, we confirmed this finding using a CFTR construct bearing an HA tag in ECL2, so-called EXT-CFTR. Gentzsch *et al*. [148] developed EXT-CFTR and characterized its regulated function using halide efflux measurements. As for WT CFTR, we observed increases in I_m and C_m from EXT-CFTR upon cAMP/PKA stimulation. The current/capacitance responses of WT and EXT-CFTR were similar (57 vs. 67 pA/pF), indicating

that its regulated plasma membrane trafficking properties replicate those of WT CFTR and CFTR tagged in ECL4. Thus, the detection of a stimulus-induced increase in plasma membrane CFTR is independent on the position or composition of the epitope tag.

cAMP/PKA evoked changes in membrane capacitance were used to assess the trafficking of CFTR as its structural features were manipulated. Given that the initiation of both gating and trafficking responses require phosphorylation of the CFTR R domain, it was logical to begin this process using constructs in which the R domain was deleted. Csanady *et al*. [111], showed that CFTR's gating properties were maintained when split CFTR half-channels lacking the R domain were co-expressed in *Xenopus* oocytes, providing the opportunity to examine the relation of CFTR trafficking to R domain structure. As in prior studies [111], we found that split CFTR lacking the R domain, ΔR-N/C, exhibited spontaneous currents that were not significantly increased by cAMP/PKA stimulation. In addition, the agonist-induced ΔC_m, reflecting the regulated trafficking of WT CFTR to the cell surface, was eliminated, identifying the R domain as a necessary structural feature in this process.

R-domainless and ΔNEG2 CFTRs exhibited a reduced functional half-life, resembling that of WT CFTR during continuous stimulation by cAMP/PKA. These findings suggested that under non-stimulated conditions, CFTR resides in an intracellular compartment where it is relatively stable. This stability may arise from the kinetics of plasma membrane trafficking steps that distribute CFTR predominantly to intracellular compartments in the absence of stimulation. As noted above, similar behavior is observed in response to the acute stimulation of GLUT4 and ENaC trafficking.

To further resolve the R region involved in stabilizing CFTR within the cell, segments of the R domain C-terminus were progressively deleted from the half channel construct that included

the R domain (e.g. 1-835). Large R region deletions were problematic, however. As demonstrated previously [166, 167], functional CFTR expression was lost when regions at the N-terminus of the R domain were eliminated. Nevertheless, the expression of constructs that eliminated smaller C-terminal segments of R revealed that removal of the NEG2 region eliminated agonist-stimulated trafficking of CFTR while retaining most of CFTR's regulated conductance function.

Confirming the importance of this segment, prior injection of NEG2 peptide restored a regulated trafficking response to ΔNEG2 CFTR, although the agonist-induced ΔC_m was reduced by approximately 35% compared to that of WT CFTR. The functional complementation of regulated CFTR trafficking by peptide injection depended on the previously determined helical structure of NEG2 [6], as peptide lacking helical content failed to recover agonist-evoked capacitance changes, despite the retention of NEG2's negative charge. This feature was confirmed for full-length CFTR in which the NEG2 region was substituted by the helical counterpart, hNEG2. Nevertheless, hNEG2 retains a net negative charge of -3, which was minimally required for peptide solubility [6], and this may contribute to the regulated trafficking response observed.

The relatively short time for recovery of cAMP/PKA regulated trafficking following NEG2 peptide injection (~30 min between injection and stimulation) suggests that the intracellular CFTR trafficking compartment that contributes to the increase in C_m with stimulation can be re-filled relatively quickly. Previous studies of CFTR turnover at the cell surface are compatible with this short timescale for recovery. For example, in T84 cells, ~50% of CFTR on cell surface was internalized within 15 min [130], and similar CFTR endocytic internalization rates were observed in COS-7 cells expressing WT CFTR [168]. Time courses of CFTR internalization

and recycling with similar kinetics were reported recently for polarized human airway cells [169]. These findings suggest that CFTR endocytosis and recycling at the plasma membrane domain are sufficiently rapid to permit the formation of a trafficking compartment within the timeframe of these experiments.

Evidence for the ability of the NEG2 peptide to functionally associate with NEG2 deleted CFTR was provided by Ma and co-workers [6]. They showed that the addition of NEG2 to the cytoplasmic surface of WT or ΔNEG2-CFTR in lipid bilayers altered CFTR open probability in a biphasic, concentration-dependent manner. Since low NEG2 concentrations enhanced P_o, while higher NEG2 concentrations reduced CFTR P_o, Ma *et al.,* [6] proposed that the amphipathic nature of the NEG2 helix facilitates its interaction with a gating inhibitory site in the non-phosphorylated channel, stabilizing the closed state, while its interaction with a stimulatory site in the phosphorylated channel augments channel opening [6]. Overlaid on this concept, the present findings suggest that the NEG2 region interrupts the constitutive trafficking of CFTR to the plasma membrane when the channel is not phosphorylated, permitting its entry into a kinetically stable intracellular compartment. Subsequently, R domain phosphorylation would suppress these interactions of NEG2, which may include its association with components of the trafficking machinery, permitting the progression of phosphorylated CFTR to the surface membrane.

As a prototype for this model, we examined the influence of syntaxin 1A on the behavior of ΔR-N/C and ΔNEG2 CFTRs. The regulation of CFTR by this SNARE protein is complex, involving its physical interaction with the CFTR N-terminal tail, which itself influences channel open probability [170]. In addition, prior work in oocytes showed that S1A co-expression with WT CFTR reduced its regulated trafficking to the cell surface [137], and this action was

confirmed here by the inhibition of stimulated WT CFTR current and the block of agonist-induced ΔC_m associated with S1A co-expression (Fig. 11). As previously [137], we attribute this effect of S1A to its ability to retain CFTR within intracellular compartment(s), similar in principle to the concept that the NEG2 region is required for intracellular stabilization of CFTR under basal conditions. Thus, elimination of the NEG2 region, allows CFTR to traffic constitutively to the plasma membrane, and this deletion also obviates the block of CFTR progression to the cell surface elicited by S1A expression. In this light, when CFTR is not phosphorylated, NEG2 may interact with a traffic regulatory protein, such as a SNARE protein, and that this interaction causes intracellular CFTR retention within non-stimulated cells. It is possible also that this regulatory protein interaction is effected by another part of CFTR with which NEG2 associates. Nevertheless, attempts to further resolve the molecular details are outside the scope of the present work.

In summary, cAMP/PKA stimulation increases cell surface expression of CFTR in addition to augmenting CFTR channel gating, and both modes of regulation require the R domain. Its removal permits CFTR gating in the absence of agonist stimulation and also eliminates the ability of the channel to enter a regulated trafficking pathway, resulting in the constitutive delivery of CFTR to the plasma membrane. Our findings identify the NEG2 region of the R domain, aa 817-838, as the critical structural element of CFTR that is required for its phosphorylation-dependent trafficking. Accordingly, the intracellular retention of CFTR under non-phosphorylated conditions may involve interactions of the NEG2 region with proteins that mediate regulated membrane trafficking events. Since NEG2 also influences channel gating [6], these findings imply that regulation of the gating and trafficking functions of CFTR are structurally linked. The identification of NEG2 as a required structural component should lead

to a better understanding of CFTR trafficking mechanisms, including the associated protein-protein interactions.

APPENDIX:

In this section, the work presented was not directly part of the thesis project described previously. Instead, the data presented in this section, are collaborations in which several investigators contributed to the totality of the work.

5.0 SERUM-GLUCOCORTICOID-INDUCED KINASE (SGK-1) REGULATION OF CFTR.

5.1 INTRODUCTION:

Serum-glucocorticoid-induced kinase (SGK-1) is an inducible Ser/Thr kinase that belongs to the family of AGC (PKA/protein kinase G/protein kinase C) kinases. It was originally isolated from a mouse tumor cell line during a differential screening for glucocorticoid-induced transcripts [171, 172]. The most understood functions of SGK-1 are that of a kinase involved in cell survival in various situations as well as its ability to regulate multiple membrane, transport and channel proteins [173]. Studies have shown that SGK-1 is tightly regulated by numerous signaling molecules through its sub-cellular localization, expression levels and its intrinsic kinase activity, thus allowing it to integrate numerous signaling pathways [173].

To date, two paralogues of SGK-1 have been identified (SGK-2 & SGK-3) which share 80% amino acid identity in their catalytic domains with SGK-1 and each other

[174-176]. The consensus phosphorylation motifs for SGK-1 require arginines at positions 5 and 3 while basic residues C-terminal of S/T are inhibitory with no requirement for bulky hydrophobic residues which translates into a consensus site of RXRXXS/T for SGK-1 [177-179].

5.1.1 Regulation of SGK-1 by phosphorylation.

A characteristic of many AGC kinases is the conserved phosphorylation motifs in their catalytic domain and the C-terminal region as shown in figure 5-1. The phosphorylation sites located in the catalytic domain are situated in the activation loop (A-loop) which was first identified in PKB/Akt (Protein kinase B/Akt) as a target for the PI-3K dependent kinase PDK-1 (3-phosphoinositide-dependent protein kinase 1) [180, 181]. Generally PDK-1 activation involves interaction of PDK-1 and its target with phosphoinositides through its pleckstrin homology (PH) domains. This interaction recruits both kinases to the plasma membrane and allows PDK-1 to phosphorylate the AGC kinase on the A-loop. However, SGK-1 does not have a PH domain, instead SGK-1 is phosphorylated on Ser-422 in the C-terminal hydrophobic (H-motif) by an as yet unknown kinase that is PI-3K dependent [179, 182] (figure 5-1). This indicates that the activation of SGK-1 by PDK-1 is independent of phosphoinositides, or the PH-domain in PDK-1, which makes activation of SGK-1 much slower that that of PKB/Akt.

Other kinases may also activate SGK-1. For example, PKA may also activate SGK-1 via phosphorylation of a consensus sequence surrounding Thr-369 (KKITP). However, this site is imperfect and other groups have not been able to detect activation of SGK-1 by cAMP under conditions were cAMP was able to phosphorylate the CREB

transcription factor [183]. Evidence suggests that various MAP kinases, specifically bone marrow kinase (BMK) and p38α, phosphorylate and activate SGK-1. Both of these kinases phosphorylated SGK-1 at a site (ser78) which lies outside of the catalytic domain and increase activity independent of the phosphorylation state of Thr256 in the A-loop. [184, 185]. Another potential mechanism of SGK-1 activation is through interaction with WNK1 (with no lysine kinase 1) [176]. Like activation of SGK-1 by BMK and p38α, the mechanism of WNK1 activation is not completely understood. However, there is some evidence that phosphorylation of SGK-1 at Ser-422 in addition to phosphorylation of Thr-256 is required [176].

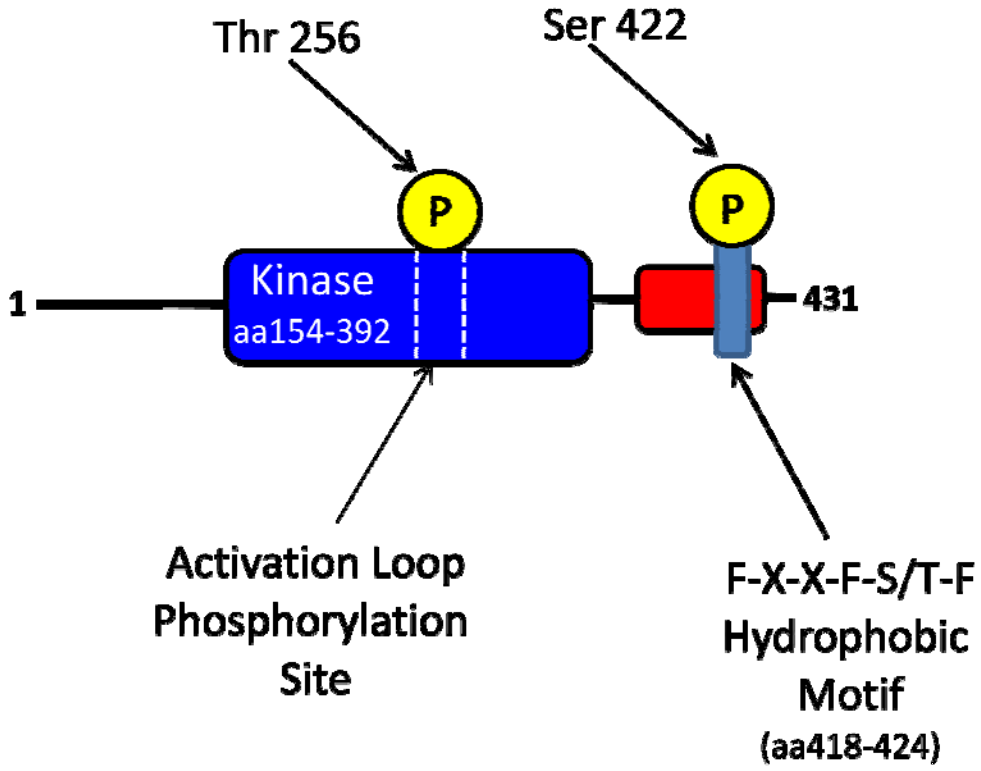

Figure 5-1: Model of human SGK-1 [186]

Structural representation of serum-glucocorticoid induced kinase (SGK-1). The drawing illustrates that SGK-1 contains two regulatory features: phosphorylation of the activation loop and phosphorylation of a hydrophobic motif (blue box), located in the tail region (red box) C-terminal to the kinase domain.

5.1.2 Regulation of SGK-1 by ubiquitylation.

Another mode of SGK-1 regulation is mediated by ubiquitylation. Studies by Brickly *et al.*, [187] have shown that the rapid internalization and proteosome degradation of SGK-1 requires ubiquitylation [187]. The E3 ubiquitin ligase, NEDD4-2 (neuronal precursor cells expressed developmentally down regulated 2) has been shown to increase SGK-1 ubiquitylation and degradation but only when the N-terminus of SGK-1 is present [188]. Further analysis of the role of the N-terminus of SGK-1 in ubiquitinylation by NEDD4-2 has shown that a six amino acid hydrophopic motif (GMVAIL) is required for its ubiquitinylation [189]. In addition, it was shown that six lysine residues within the amino terminus that srrround the GMVAIL motif are also needed for ubiquitin modification [187, 189]. Deletion of the the GMVAIL residues was shown to prevent rapid SGK-1 degredation and disrupted its localization to the endoplasmic reticulum, where mutation of all 6 lysine residues also led to decreased ubiquitinylation and protein stabilization but did not disrupt SGK-1's endoplasmic reticulum localization indicating that SGK-1 is ubiquitinylated in the ER [189]. Taken together, these results suggest that the activity of SGK-1 is regulated through its consititutive degredation which requires a unique N-terminal hydrophobic motif (GMVAIL).

5.1.3 The Role of SGK-1 in aldosterone-dependent Na^+ reabsorption.

SGK-1's involvement in aldosterone dependent Na^+ reabsorption is the most studied function of the kinase with respect to epithelial transport. The last point of control of renal Na^+ excretion is the aldosterone-sensitive distal nephron (ASDN), [i.e. late distal convoluted tubule, connecting tubule, the cortical and medullary collecting ducts] [190]. In these segments of the kidney, Na^+ transport is accomplished by Na^+ entry through ENaC (epithelial sodium channel) in the apical membrane and Na^+ exit by its transport via the Na^+K^+-ATPase in the basolateral membrane.

ENaC is composed of three subunits (α,β,γ) and each subunit contains a C-terminal PY (PPXY) motif that is involved in protein/protein interactions with tryptophan rich WW domains [191, 192]. Studies have shown that the PY motifs are binding sites for the NEDD4-2 ubiquitin ligase family and specifically NEDD4-2 [192-199]. The mechanism of NEDD4-2 regulation of the channel requires the binding of the ENaC's PY motif to NEDD4-2's WW domain allowing for ubiquitylation of the channel resulting in its internalization and degradation.

Alverez de la Rossa *et al.,* [200] have shown that co-expression of ENaC with SGK-1 in *Xenopus* significantly increases the activity of the channel by increasing the number of channels present in the membrane as well as increasing the activity of channels already present in the membrane [190, 200-207]. The increase in channel number is likely due to interaction of SGK-1 with NEDD4-2 via interaction of SGK-1's PY-motif with the WW-domain on NEDD4-2 followed by phosphorylation of NEDD4-2 by SGK-1 (figure 5-2).

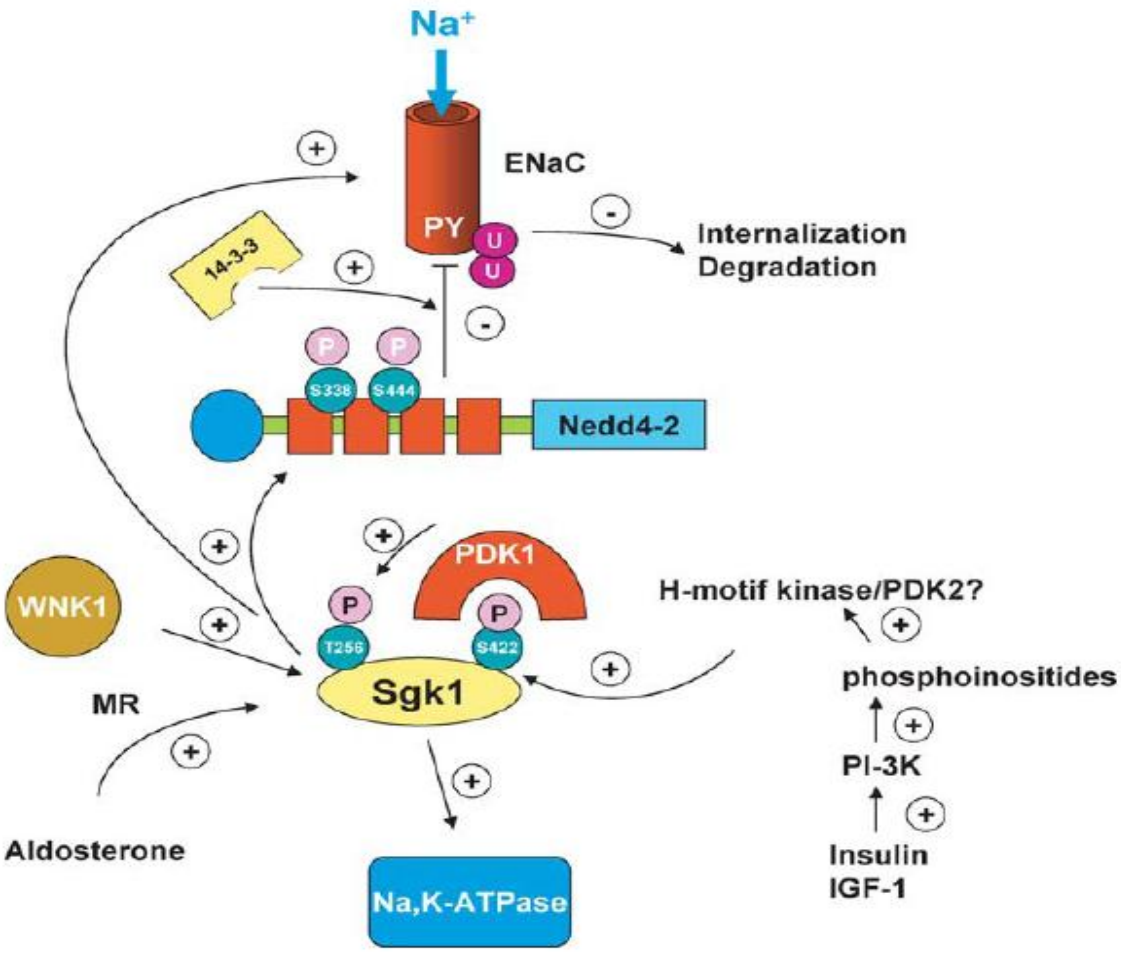

Figure 5-2: Regulation of ENaC by SGK-1 [173].

Aldosterone induces the expression of SGK-1 by binding to the mineralocorticoid receptor (MR) and translocating into the nucleus. SGK-1 becomes phosphorylated on Ser422 by an unknown kinase referred to tentatively as 3-phosphoinositide-dependent protein kinase (PDK)-2 or hydrophobic motif (H-motif) kinase; this latter kinase depends on the PI-3K pathway and is stimulated by insulin or IGF-1. Phosphorylated Ser422 then serves as a binding site for PDK-1 via PIF-pocket, leading to the phosphorylation of Thr256 on the activation loop and activation of SGK-1. Alternatively, SGK-1 is also activated by WNK1 via an unknown mechanism. Once activated, SGK-1 phosphorylates Nedd4-2 on Ser444 and Ser338, which allows binding of 14-3-3 on Ser444. This interferes with Nedd4-2/ENaC interaction, causing reduced ubiquitylation of and accumulation of epithelial Na^+ channel (ENaC) at the plasma membrane.

This mechanism has been examined in *Xenopus* oocytes, where it was discovered that SGK-1 induces NEDD4-2 phosphorylation of Ser-444 and Ser-338 resulting in the creation of a binding site for the scaffold protein 14-3-3 [208]. Binding of NEDD4-2 to 14-3-3 prohibits its association and ubiquininylation of ENaC, resulting in a decrease in ENaC endocytosis and an increase in the number of channels in the membrane [202, 208-210].

Another proposed method of SGK-1 regulation of ENaC is via direct interaction with the channel resulting in phosphorylation of the α-subunit, leading to a two to three fold increase in channel activity [211, 212]. Additional studies using *Xenopus* A6 cells, which endogenously express SGK-1 and ENaC, confirmed the previous findings as well as raising the possibility that the increase in ENaC activity is not only the result of activation of membrane resident channels, but also due to insertion of more channels into the membrane [213]. In addition to ENaC, SGK-1 has been shown to regulate an increasingly large number of transport proteins. Multiple studies have been dedicated to the role of SGK-1 in regulation of such proteins such as ROMK and Na^+-K^+-$2Cl^-$ co-transporter as well as mediation of the stimulation of NHE3 (Na^+/H^+ exchanger isoform 3) [214-216].

5.1.4 SGK-1 and CFTR.

It has been well established that the gill operculum of the killifish, *Fundulus heteroclitus,* is stimulated to secrete chloride in response to increased salinity when the fish moves from fresh water to a saltwater environment [217-219], requiring the gills to

switch from NaCl absorption to NaCl secretion [220, 221]. Transepithelial Cl^- secretion in the gills involves Cl^- entering the cell from the basolateral membrane via NKCC1, which is dependent on the action of the sodium-potassium-ATPase generating a sodium gradient across the basolateral membrane. The Cl^- entering the cell is secreted via CFTR which generates an apical negative transepithelial voltage providing the driving force for paracellular sodium secretion [220]. Sufficient chloride export is facilitated by a 9-fold increase in CFTR mRNA levels in the first 24hrs following the move to a high salt environment, leading to an increase in CFTR expression in the apical membrane [222, 223]. The increased expression of CFTR is preceded by a dramatic increase in the plasma levels of the steroid cortisol, a signal that activates SGK-1. These observations suggest that SGK-1 may play a role in increased chloride secretion by activation of CFTR. This was confirmed by studies in *Xenopus* oocytes in which SGK-1 was shown to stimulate CFTR while the kinase dead SGK-1 mutant (K127N) had no effect [224]. Furthermore, studies by Sato *et al.,* [225] have shown that in addition to stimulating chloride currents, SGK-1 also has the ability to increase the maximal stimulated current elicited by cAMP/PKA agonists, possibly by increasing the number of channels in the membrane. Moreover, they also report that SGK-1 stimulation may be mediated by protein/protein interactions involving the PDZ interacting motif [225].

The effect of SGK-1 on CFTR currents is well documented [220, 221, 224-226], however the mechanism of its action is not very well understood. The focus of this study was to elucidate the mechanism of SGK-1 action on CFTR which result in the observed increased chloride currents. To this end, we used *Xenopus* oocytes as a heterologous expression system to examine the effects of SGK-1 stimulation on various CFTR

constructs. Our studies show that co-expression of the constitutively active SGK-1 (S442D) with WT-CFTR resulted in a significant increase in stimulated chloride current (ΔI_m) but did not increase the change in membrane capacitance (ΔC_m) following stimulation compared to WT-CFTR alone, suggesting that SGK-1 does not increase the trafficking response of CFTR upon stimulation. To examine the effects of SGK-1 on CFTR surface expression we used we used a CFTR construct with an HA tag in the second extracellular loop (EXT-CFTR) provided by Dr. J. Riordan (UNC-CH). When co-expressed with S422D-SGK, EXT-CFTR functioned similarly to WT-CFTR, stimulation resulted in an increase in ΔI_m without an increase in ΔC_m. Using the EXT-CFTR construct to examine cell surface fluorescence, we demonstrated that SGK-1 co-expression increased cell surface expression following stimulation, similar to WT-CFTR. However, when cell surface expression was measured prior to stimulation, SGK-1 co-expression resulted in a significant increase in the amount of CFTR resident in the plasma membrane.

To examine the effect of the elimination of the kinase activity on ΔI_m, ΔC_m and cell surface expression, we co-expressed WT-CFTR or EXT-CFTR with the kinase dead SGK-1 mutant K127N. As Stato *et al,* [225] reported, K127N co-expression with WT-CFTR did not increase I_m over that observed in its absence and it did not have an effect on the ΔC_m upon stimulation. Additionally, measurements of cell surface expression using EXT-CFTR, show that the removal of the kinase activity of SGK-1 eliminated the increase in the amount of channels in the membrane prior to cAMP/PKA stimulation indicating that the kinase activity of SGK-1 is critical for the increase in channel trafficking to the membrane prior to stimulation.

To determine the structural element(s) of CFTR that mediates the effect of SGK-1 on CFTR activity, we examined the effects of co-expression of S422D with the R-domainless construct ΔR-N/C. The elimination of the R-domain had no effect on the basal I_m or the stimulated current when co-expressed with S422D, indicating that the presence of the R-domain is essential for SGK-1 regulation of CFTR activity. Taken together our results suggest that SGK-1 regulates CFTR chloride currents by increasing the number of channels in the membrane prior to stimulation and this process requires the kinase activity of SGK-1 and the presence of the R-domain of CFTR.

5.2 MATERIALS AND METHODS.

5.2.1 Preparation of *Xenopus* oocytes.

The preparation and isolation of individual stage V or VI oocytes was performed as stated previously (section 2.2). Briefly, ovaries were surgically removed from female *Xenopus* laevis frogs and placed in 1X MBS (table 2.1). The ovaries were then cut into small sections and placed in a collagenase solution for 50 min to separate individual oocytes. Following collagenase treatment the oocytes were washed three times in hypertonic solution followed by a 15 min incubation in the same solution with agitation every 5 min. After the treatment in hypertonic solution the oocytes where then washed three times in 1X Ca^{2+} free ND-96 and placed in a 100mm pitri dish containing 1X MBS^{++} (table 2.1) at 18˚ C for a minimum of two hours prior to sorting. Sorting of individual oocytes was performed using a dissection microscope with oocytes bathing in 1X MBS^{++}. When a sufficient amount of individual stage V or VI oocytes were sorted they were incubated overnight at 18°C in 1X MBS^{++}.

After incubation, individual oocytes were injected with cRNA as detailed previously (Section 2.3). cDNA constructs of SGK-1 used to generate cRNA were kindly provided by Dr. Bruce Stanton (Dartmouth, NH). cRNA was produced using the mMessage machine RNA production kit from Ambion (Huston, TX) according to manufacturer's suggestions (see section 2.4) and then injected into oocytes for expression. To accomplish this, we followed a modification of the protocols described in Cunningham, *et al*., [145], and Gurdon, *et al*., [146]. In our protocol, we injected cRNA constructs into oocytes in 50nl volumes using a micro-injection apparatus (World

Precision Instruments, Sarasota, FL). To obtain the desired amount of cRNA to be injected, we diluted the stock cRNA using DEPC-treated H_20 (Ambion, Houston TX). When multiple cRNAs were to be injected, they were co-injected into the oocyte in the same 50nl volume. Following injection of cRNA the oocytes were placed in one well of a six well plate depending on which cRNA(s) were injected and allowed to incubate for 1-3 days at 18˚ C to allow for maximal expression.

5.2.2 Electrophysiology.

In this series of experiments, we used two electrode voltage clamp to measure chloride currents from *Xenopus* oocytes expressing various cRNA transcripts. The theory behind the technique was the same as previously described (section 2.7). Briefly, oocytes were impaled with two 3M KCl-filled electrodes which were connected to a GeneClamp 500B amplifier (Axon Instruments, CA) via Ag-AgCl pellet electrodes and referenced to the bath by two Ag-AgCl pellet bath electrodes. The voltage clamp was controlled by an AXOLAB 1100 analog-to-digital/digital-to-analog interface board (Axon Instruments, CA) using a modification of the pClamp5.0 (Axon Instruments, CA) software which was generated by Takahashi & Qi *et al.,* [136, 149]. Using the method detailed in section 2.7, we were able to record CFTR-dependent membrane currents (I_m) and membrane capacitance (C_m) from *Xenopus* oocytes injected with various cRNA's.

To generate the current/voltage plots the voltage clamp was controlled by a GeneClamp-500B amplifier (Axon Instruments, CA) in conjunction with an AXOLAB Digidata 1200 analog-to-digital/digital-to-analog interface board (Axon Instruments, CA)

using pClamp 8.0 software (Axon Instruments, CA). Once oocytes were impaled the holding potential was set to -30 mV. The pulse protocol in these experiments was a series of step voltages starting at -100 mV and moving to +100 mV in 20 mV increments following stimulation with 10μM isoproterenol. Measurements were taken at a point prior to stimulation of oocytes followed by a measurement every 5 min until maximal stimulation was observed. The I/V curves shown are from individual oocytes where measurements were taken prior to stimulation and at maximal stimulation.

5.2.3 Luminometry

The protocol for luminometry used in these experiments is described in detail in section 2.6. Briefly, labeling of CFTR at the cell surface utilized an externally epitope tagged CFTR construct (EXT-CFTR, [148]), kindly provided by Dr. John Riordan (UNC-CH). For oocyte studies, EXT-CFTR (10ng) or WT CFTR (1ng) cRNA was injected together with β2-AR and incubated in MBS^{++} for 3 days at 18˚C. Oocytes were stimulated with 10 μM isoproterenol (Sigma, MO) as in the electrophysiological studies. Non-stimulated oocytes were treated identically except for agonist additions. For chemiluminescence measurements, cell surface EXT-CFTR was labeled by sequential incubations in primary monoclonal HA antibody (1:1,000, 90 min) [Covance, New York, NY], secondary biotin-conjugated goat anti-mouse IgG (1:200, 90 min) [Invitrogen, Eugene, OR], and streptavidin conjugated to HRP (1:500; 90 min) [Zymed, San Francisco, CA]. All steps were performed at 4°C to block CFTR trafficking. The cells were then washed extensively and HRP-labeled proteins were detected using SuperSignal

West Femto chemiluminescent substrate (Pierce), and read in a TD20/20 luminometer (Turner, Sunnyvale, CA).

5.2.4 Statistics and Calculations.

All data are presented as means ± S.E., where N- indicates the number of individual *Xenopus* laevis frogs from which oocytes were extracted and n- is the number of individual oocytes measured. Statistical analysis was performed using a Student's unpaired *t* test. A value of $p \leq 0.05$ is considered statistically significant and indicated by a (*). All 2EVC recordings were performed on oocytes harvested from at least 3 different *Xenopus* frogs to ensure the reproducibility of our results. Half-life determination was accomplished by calculating the τ values using the exponential decay, single, two-parameter regression function of SigmaPlot 2001 (SPSS, Chicago, IL).

5.3 RESULTS

5.3.1 SGK-1 increases stimulated chloride currents but does not increase C_m.

Previous work by Sato *et al*., [225] demonstrated that co-expression of WT-CFTR with the constitutively active form of SGK-1 (S422D) resulted in an increase in stimulated chloride currents from *Xenopus* oocytes. The results shown in figure 5-3 A&B confirm their findings, showing that stimulation of oocytes expressing WT-CFTR + S422D resulted in approximately a 1.7 fold increase in isoproterenol induced I_m (WT-CFTR 3.9±0.8 μA vs. WT-CFTR/S442D 6.8±0.8μA) which is similar to the increase reported previously [225]. Both WT-CFTR & WT-CFTR + S422D) showed a stimulation dependent increase in C_m (figure 5-3C) but co-expression of S422D did not result in a significant increase in the capacitance change (ΔC_m) compared to oocytes expressing only WT-CFTR (WT-CFTR ΔC_m=80±26 nF vs. WT-CFTR + S422D ΔC_m=113±22 nF).

As described in sections 3&4, cAMP/PKA stimulation mobilizes CFTR containing vesicles from an intracellular pool to fuse with the plasma membrane which is reflected as an increase in C_m. Figure 5-3 shows that co-expression of SGK-1 with WT-CFTR increases ΔIm but has no effect on ΔCm which indicates that the effect of SGK-1 on CFTR Im is not the result of stimulation induced trafficking of the channel. These data indicate that SGK-1 does not act like PKA. Rather, SKG-1 either increases CFTR Po or results in trafficking of the channel to the plasma membrane prior to stimulation by PKA.

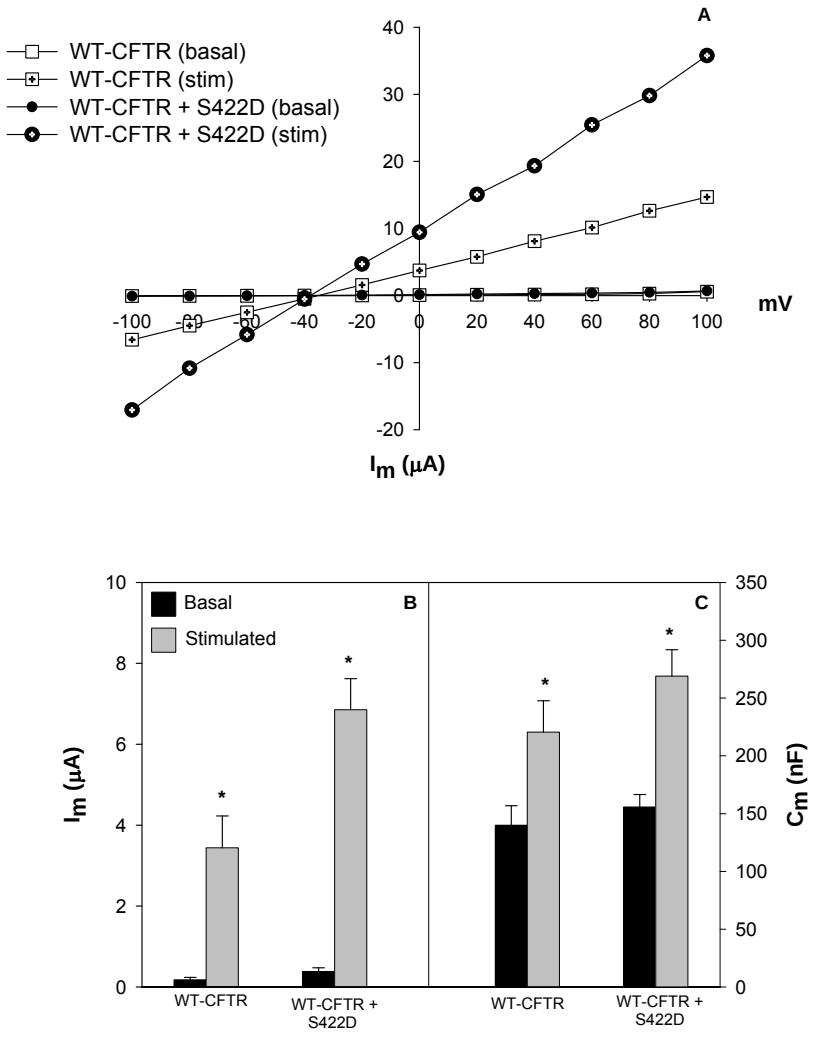

Figure 5-3: SGK-1 expression increases CFTR chloride current.

Xenopus oocytes injected with 1ng WT-CFTR, 5ng S422D and 1ng β2-adrenogeric receptor cRNA. A; current/voltage relationship from individual oocytes expressing WT-CFTR or WT-CFTR + S422D before and after the addition of 10μM isoproterenol. Stimulated recording data was taken at maximal stimulation which was achieved by bathing oocyte in 10μM isoproterenol for 12 min. B & C show summary data of I_m and C_m from 2EVC recordings. Current data shown was recorded from a hyperpolarizing pulse to -60 mV from a holding potential of -30mV. [WT-CFTR: N=4; n=19; WT-CFTR + s442D: N=4; n=14].

5.3.2 SGK-1 increases surface expression of CFTR prior to stimulation.

To determine whether SGK1 increased CFTR cell surface expression, we used a CFTR construct with an HA tag in the second extracellular loop (EXT-CFTR) provided by Dr. J. Riordan (UNC-CH) which behaves functionally like WT-CFTR [148] [described in section 2.6]. Figure 5-4 shows the results of two-electrode voltage clamp recordings of oocytes injected with EXT-CFTR cRNA alone or together with cRNA encoding constitutively active SGK1 (S422D). SGK1 co-expression elicited a 2.5-fold increase in cAMP/PKA-stimulated membrane current (ΔI_m = 6.35±0.4 μA) relative to EXT-CFTR alone (ΔI_m=2.55±0.9μA), without markedly increasing basal currents (figure 5-4B). These results are similar to those for WT-CFTR with and without S422D reported by Sato *et al*., [225], indicating that EXT-CFTR behaves similarly. cAMP/PKA evoked changes in membrane capacitance (Fig. 5-4C) reflect stimulation-induced CFTR trafficking to the plasma membrane, which was not acutely enhanced by SGK1, similar to WT-CFTR co-expression with S422D. Taken together, the data in figure 5-4 indicate that S422D effects EXT-CFTR similarly to WT-CFTR.

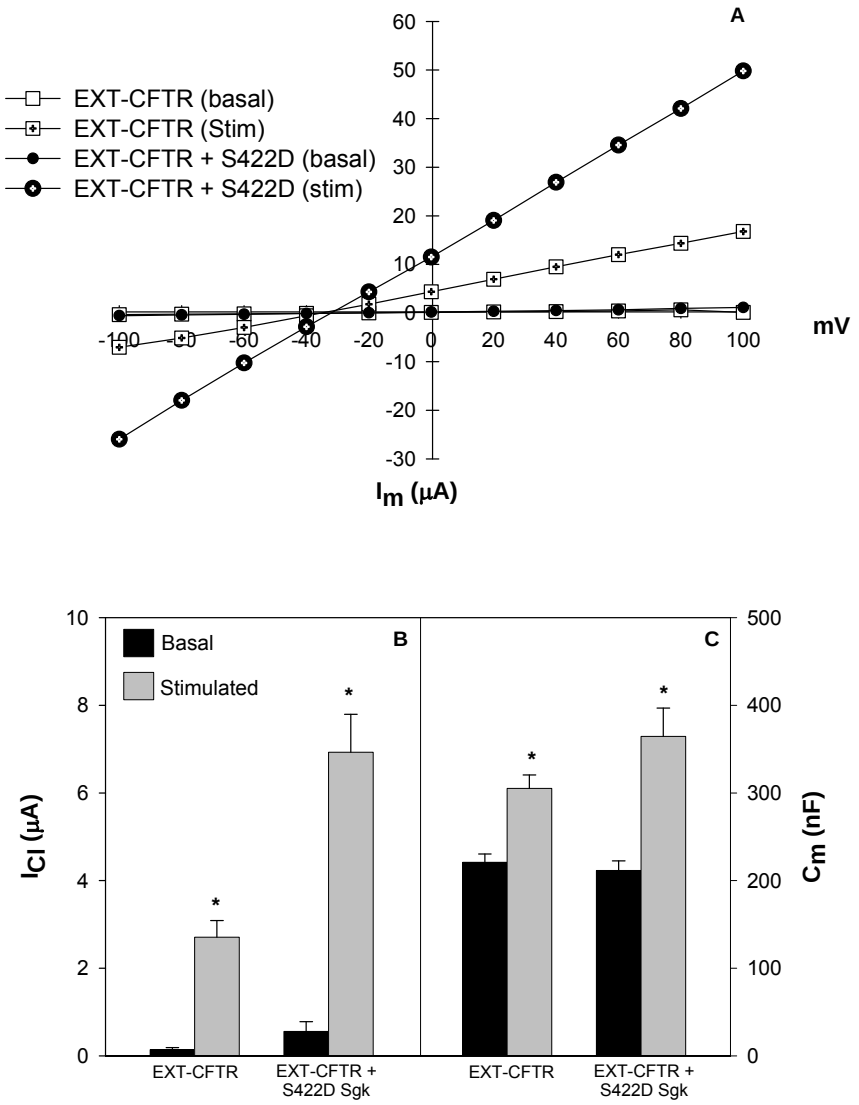

Figure 5-4: SGK-1 effects extope-CFTR similarly to WT-CFTR.

A: I/V plots displaying mean current values at each voltage for oocytes expressing EXT-CFTR or EXT-CFTR + S422D under basal and stimulated conditions (see legend). Stimulated data was taken at maximal stimulation which was achieved by bathing oocyte in 10μM isoproterenol for 10 min. B&C: summary data from *Xenopus* oocytes expressing EXT-CFTR taken at -60mV. A) membrane currents (I_m) in oocytes co-expressing (cRNA): EXT-CFTR (10ng) + β2-adrenergic receptor (1ng) ± S422D SGK1 (5ng) [N=4; n=19,20]. cAMP stimulation by 10μM isoproterenol. B) Corresponding membrane capacitance (C_m) values.

Next, we evaluated the effect of SGK1 on cell surface EXT-CFTR density using enzyme linked immuno-labeling and luminometry [154, 155]. Oocytes were incubated sequentially with primary α-HA, biotin-conjugated α-mouse secondary and streptavidin-HRP conjugated tertiary antibodies. Co-injection of SGK1 produced a 3.5-fold increase in cell surface CFTR luminescence prior to stimulation (figure 5-5A) compared to EXT-CFTR alone. The addition of 10μM isoproterenol resulted in an increase in cell surface expression of both EXT-CFTR and EXT-CFTR + S422D (figure 5-5B). Previous studies have shown that cAMP stimulation mobilizes CFTR to the plasma membrane from intracellular compartments [136, 137, 149]. These findings suggest that SGK-1 can increase the cell surface expression of CFTR in the absence of cAMP stimulation, which augments the subsequent I_m response to isoproterenol.

Figure 5-5: SGK-1 increases CFTR cell surface expression.

Luminescence detection of HA-tagged CFTR at the cell surface using an HRP ELISA sandwich method described in section 2.6. Data are background subtracted and normalized to control. Panel A shows results of measurements taken of oocytes without stimulation [N=3; n=15]. Panel B shows measurements obtained following stimulation (10μM isoproterenol) for 10 min [N=3; n=15]. (*) indicates significant difference compared to EXT-CFTR under basal conditions.

5.3.3 Removal of SGK-1 kinase activity eliminated increases in I_m and cell surface expression of CFTR

To determine if the increases in chloride current and cell surface expression were dependent on the kinase activity of SGK-1 we co-injected WT-CFTR with the kinase dead mutant of SGK-1 (K127N). Figure 5-6-A&B shows the results of 2EVC recordings of oocytes expressing WT-CFTR alone or WT-CFTR + K127N. In panel (A), recordings of I_m clearly show that the previously observed increase in chloride current with S422D co-expression were eliminated when the kinase dead SGK-1 mutant (K127N) were co-injected. Corresponding measurements of C_m show that K127N did not alter the acute increase in membrane capacitance following stimulation, which suggests that the increase in stimulated CFTR chloride currents observed with S422D are dependent on the kinase activity of SGK-1.

Since the kinase dead SGK-1 mutant eliminated the increase in stimulated I_m, we next sought to examine its effect on cell surface expression. In the following experiments, we measured cell surface luminescence on *Xenopus* oocytes expressing EXT-CFTR or EXT-CFTR + K127N. Figure 5-6-C shows that the increase in cell surface CFTR expression under basal conditions is dependent on the kinase activity of SGK-1. Following stimulation, oocytes expressing K127N showed an increase in cell surface luminescence similar to EXT-CFTR alone. Taken together, theses data demonstrate that the elimination of the kinase activity of SGK-1 eliminates its ability to increase the ΔI_m following stimulation by preventing the increase in number of channels in the membrane prior to stimulation.

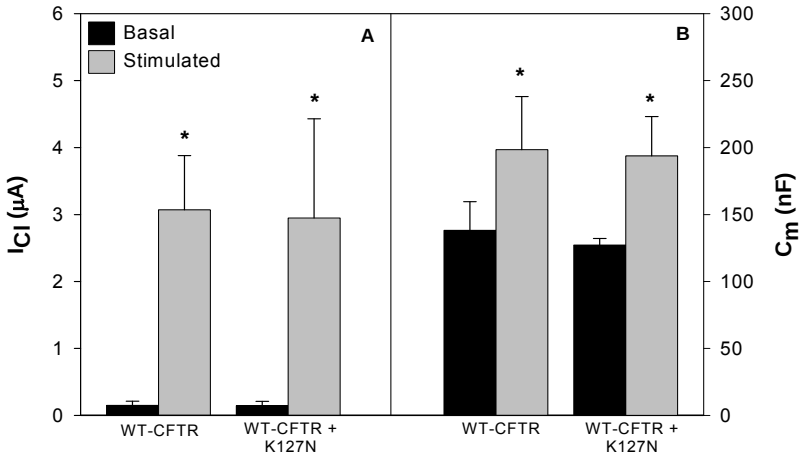

Figure 5-6 Co-expression of WT-CFTR with K127N eliminates increases in I_m and cell surface expression.

Oocytes injected with 1 ng β2-adrenogeric cRNA and 1 ng CFTR or 10ng EXT-CFTR cRNA alone or with 5 ng of cRNA for K127N-SGK-1. On day 3 post injection short circuit currents or luminescence were measured as described in sections 2.6 and 2.7 respectively. A: Short circuit currents at -60 mV are presented as mean currents ± SEM. B: Measurements of membrane capacitance under basal and stimulated conditions. C&D: Luminescence detection of HA-tagged CFTR at the cell surface. All data are background subtracted and normalized to control (basal EXT-CFTR) . C: shows results of measurements taken of oocytes without stimulation [n=15; N=3]. D: measurements obtained following stimulation (10μM isoproterenol) for 10 min [n=15 N=3]. (*) indicates significant difference compared to EXT-CFTR under basal conditions.

5.3.4 Removal of the R-Domain of CFTR eliminates effects of SGK-1

The CFTR R domain contains 5 potential SGK1 phosphorylation sites as assessed by Scansite software [227] (aa 700, 768, 788, 795, 813). Since the R-domain is the major site of phosphorylation-dependent CFTR stimulation, we sought to determine if removal of the R-domain would eliminate the influence of SGK1 on I_m. Therefore, we co-expressed SGK1 with split CFTR cRNAs lacking the R domain (aa 1-634 + 835-1480; termed ΔR-N/C). As shown in Fig. 5-7-A, ΔR-N/C does not respond to cAMP/PKA stimulation, but generates large spontaneous basal currents, similar to those observed during cAMP/PKA stimulation of WT-CFTR**.** Furthermore, SGK1 does not augment ΔR-N/C I_m (Fig. 5-7-B). These findings suggest that the R-domain is required for increases in CFTR current during SGK1 co-expression.

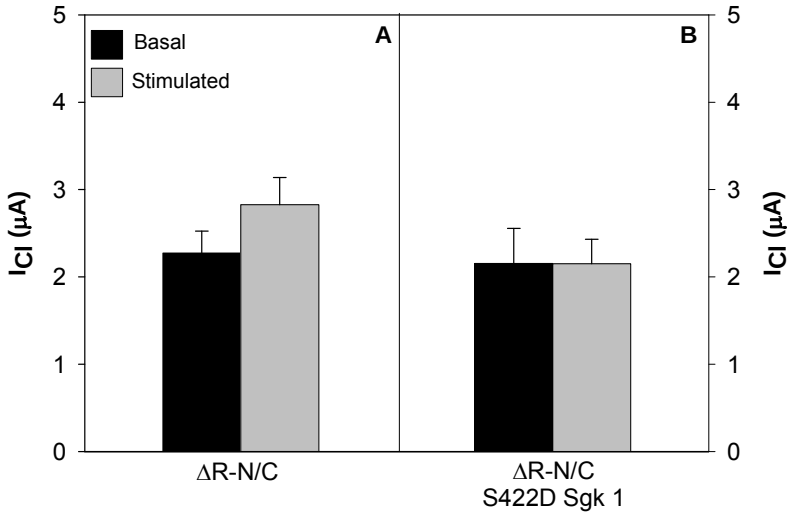

Figure 5-7: Removal of R-domain eliminates the effect of SGK-1

I_m in oocytes expressing ΔR-N (0.5ng) + ΔR-C (0.5ng) + β2-adrenergic receptor (1ng) [n=16]; B) same, with SGK1 (5ng) co-expression [n=20]. Stimulation as in Fig. 5-1.

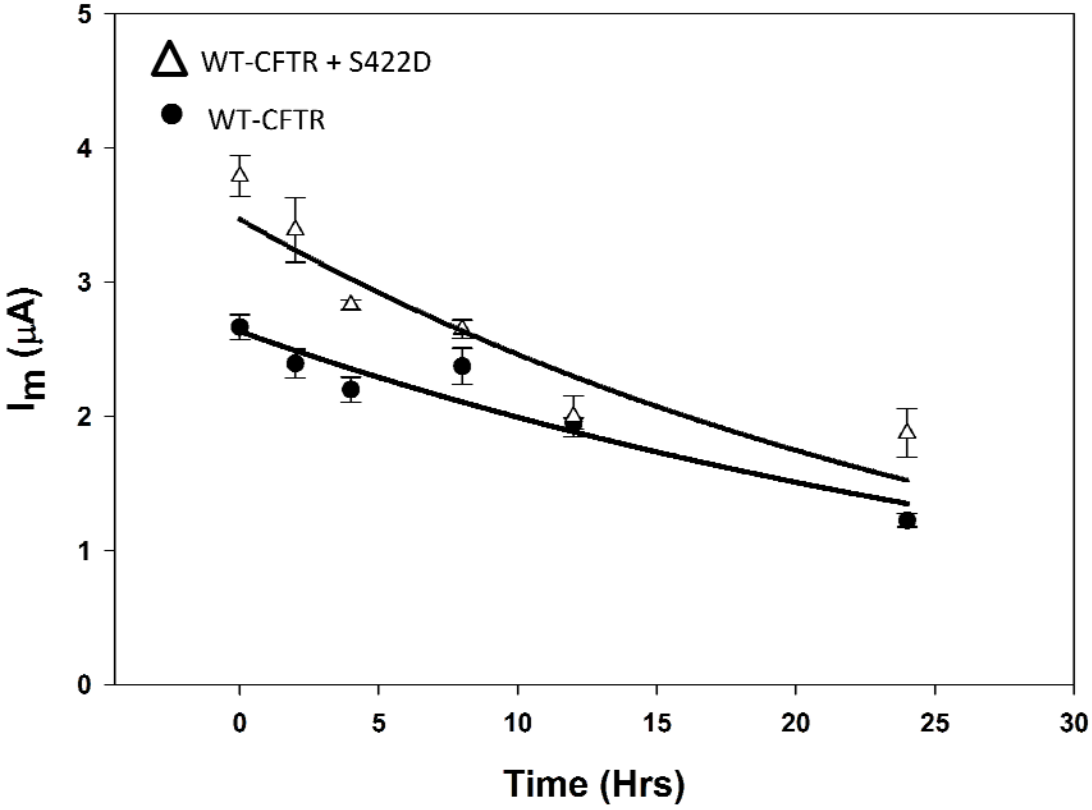

Figure 5-8: S442D-SGK has no effect of functional half life of CFTR.

CFTR current decay in oocytes bathed in 10μM BFA, expressing CFTR (1ng) + β2-adrenergic receptor (1ng) without (●) or with SGK1 (5ng) (Δ); Periodic stimulation as described in Fig 3-3 [n=15 N=3]. [$t_{½}$WT-CFTR= 16.1±4.3hrs; $t_{½}$WT-CFTR+S422D-SGK=10.7±2.4hrs]

5.4 DISCUSSION:

In summary, SGK1 stimulates CFTR I_m by increasing CFTR expression at the cell surface, as determined by labeling of epitope-tagged CFTR. This increase in CFTR density was not due to a decrease in CFTR endocytosis, as indicated by functional studies of plasma membrane CFTR turnover (figure 5-8). Finally, SGK1 stimulation of CFTR current requires its kinase activity and the presence of the R domain. As shown by other work, the non-phosphorylated R domain is responsible for CFTR retention within the cell in the absence cAMP/PKA stimulation [228]. Therefore, the present findings are consistent with two possible mechanisms of SGK1-mediated redistribution of CFTR to the cell surface:

5.4.1 SGK1 phosphorylates the R domain to promote CFTR trafficking to the plasma membrane without markedly increasing its gating,

It is well established that SGK-1 is involved in the regulation of several ion transporters [193, 202, 216, 229-232], and earlier studies have shown that SGK-1 increases CFTR chloride currents [224, 225]. However, the mechanism by which SGK-1 increases CFTR chloride currents is not known. Our data show that the effect of SGK-1 on Im of WT-CFTR expressing ooctyes is dependent on the presence of the R-domain of CFTR. Analysis of the amino acid sequence of the R-domain revealed the presence of five potential SGK-1 phosphorylation sites which when removed (along with the entire R-domain) in the presence of S442D eliminated theincrease in chloride current (figure 5-7). Additional work in our lab has demonstrated that phosphorylation of the R-domain of

CFTR results in an increase in the number of channels resident in the membrane [228]. Our findings with the R-domainless construct (ΔR-N/C) suggest that SGK-1 may be working in a similar manner in that phosphorylation of the R-domain by SGK-1 induces CFTR trafficking to the plasma membrane. Examination of the proposed SGK-1 phosphorylation sites on the R-domain reveals that three of its phosphorylation sites (S768, S795, S813) have been shown to be readily phosphorylated by PKA [113].

Since S442D is a constitutively active kinase, it is likely able to increase the basal phosphorylation state of CFTR, allowing CFTR channels to enter the plasma membrane resulting in an increase in the number of channels in the plasma membrane independent of PKA phosphorylation. Figure 6.4A shows that the presence of S422D resulted in a 3.5 fold increase in CFTR cell surface expression without cAMP/PKA stimulation. Additionally, when the kinase activity of SGK-1 was mutated, the increase surface expression of CFTR was eliminated. Taken together, our findings suggest that the mechanism of SGK-1 regulation of CFTR chloride currents involves phosphorylation of the R-domain of the channel prior to stimulation allowing the channel to enter the plasma membrane increasing the amount of channels in the membrane.

5.4.2 SGK1 phosphorylation of another protein promotes CFTR progression to the cell surface.

Another possible mechanism for SGK-1 regulation of CFTR comes from the work of Martel *et al.,* [233]. In this study, they suggest that aldosterone-induced SGK-1 regulates the activity of myosin Vc by phosphorylation of its tail region, resulting in ENaC's increased association with trafficking proteins, leading to an increase in the amount of ENaC in the plasma membrane [233].

This hypothesis was supported by their observation that SGK-1 phosphorylates myosin Vc tail at Ser-1539 in HEK-293 and M1 cells [233]. The tail region of myosin V family members has been shown to be responsible for binding cargo and regulation of its activity [234-243]. Additionally, ser-1539 is conserved across species and myosin V family members [233], and is part of a putative consensus sequence for other proteins (ex. PKA, PKC and Clk2), which when phosphorylated by calmodulin-dependent protein kinase II, regulated myosin V's ability to interact with cargo [233, 244]. Taken together, these observations suggest that phosphorylation at this site on myosin V is the basis for a common mechanism of regulation of vesicular or organelle transport [233].

A link to this mechanism for CFTR, comes from work of Urban *et al*., [245], where they demonstrated a myosin V family member (myosin V_b) interacts with Rab11a to regulate recycling of CFTR and ΔF508-CFTR in polarized human airway epithelial cells [245]. Immunoprecipitation and western blot analysis on Calu-3 cells showed that endogenous CFTR interacted with myosin V_b and Rab11a [245]. Additionally, si-RNA knockdown of myosin V_b in CFBE41o$^-$ cells resulted in a decrease of CFTR in the membrane and inhibited forskolin induced short circuit currents [245].

The above observations, in conjunction with our findings that SGK-1 co-expression with WT-CFTR increases its trafficking to the plasma membrane prior to stimulation, support a possible mechanism where SGK-1 phosphorylates the C-terminal tail (ser-1539) of myosin Vb resulting in its increased association with CFTR/Rab11a, facilitating its transport to the plasma membrane.

5.4.3 Future Directions:

Future experiments will focus of further elucidation of the mechanism of SGK-1 regulation of CFTR trafficking. Our first experiment will be to mutate the 5 proposed SGK-1 phosphorylation sites within the R-domain (S700, S768, S788, S795, S813) to alanine and examine the effects SGK-1 co-expression on I_m and C_m as well as cell surface expression. Individual mutations will be studied as well as the effects of progressive ser/ala mutations until all 5 residues have been changed to alanine. Additionally, we propose to examine the effects of SGK-1 co-expression with the R-domain deletion ΔNEG2. As described in section(s) 3 &4, the NEG2 region of CFTR is essential for the channels regulated trafficking following cAMP/PKA stimulation. In Lewarchik *et al.,* [228], we proposed that when CFTR is unphosphorylated, the NEG2 region may interact with proteins that regulate trafficking, such as a SNARE protein, preventing its forward trafficking to the plasma membrane. Since forward trafficking is stimulated by phosphorylation, it is possible that SGK-1 is regulating CFTR trafficking by phosphorylating the channel, preventing its interaction with trafficking proteins (ex. S1A) allowing for its delivery to the plasma membrane independent of cAMP/PKA stimulation.

To determine if myosin V is involved in the mechanism of SGK-1 regulation of CFTR trafficking, we will examine the effects of co-expression of the myosinVb-tail region we will perform a series of co-injection experiments in *Xenopus* oocytes to measure changes in C_m and measure cell surface expression using methods described in sections 2.6 & 2.7. In these experiments we will co-express WT-CFTR with S422D with and without myosin Vb-tail. This construct contains the SGK-1 consensus phosphorylation site and is able to interact with cargo. However, the myosin Vb-tail is not able to interact with the actin cytoskeleton which prevents forward trafficking of bound cargo [245]. Thus if SGK-1 regulates CFTR trafficking, via a myosin Vb dependent mechanism, co-expression of only the tail region should eliminate the effect of SGK-1 on CFTR stimulated I_m as well as non-stimulated cell surface expression.

6.0 BIBLIOGRAPHY

1. Riordan, J.R., et al., *Identification of the cystic fibrosis gene: cloning and characterization of complementary DNA.* Science, 1989. **245**(4922): p. 1066-73.
2. Welsh, M., et al., *Cystic fibrosis: The Metabolic and Molecular Basis of Inherited diseases*, C. Scriver, et al., Editors. 1995, McGraw-Hill: New York. p. 3799-3876.
3. Ashcroft, F.M., *Ion Channels and Disease*. 2000, New York: Academic Press.
4. Bertrand, C.A. and R.A. Frizzell, *The role of regulated CFTR trafficking in epithelial secretion.* Am J Physiol Cell Physiol, 2003. **285**(1): p. C1-18.
5. Ma, J., *Stimulatory and Inhibitory Functions of the R Domain on CFTR Chloride Channel.* News Physiol Sci, 2000. **15**: p. 154-158.
6. Xie, J., et al., *A short segment of the R domain of cystic fibrosis transmembrane conductance regulator contains channel stimulatory and inhibitory activities that are separable by sequence modification.* J Biol Chem, 2002. **277**(25): p. 23019-27.
7. Byrne, J.H. and S.G. Schultz, *An Introduction to Membrane Transport and Bioelectricity*, ed. W.G. Ganong. 1988, New York: Raven Press.
8. W.Pfeffer, W., *Osmotische Untersuchungen*, W. Engelmann, Editor. 1875: Leipzig.
9. Gorter, E. and F. Grendel, *On bimolecular layers of lipoids on the chromocytes of the blood.* . Journal of Experimental Medicine, 1925. **41**: p. 439–443.
10. Danielli, J.F. and D. H., J. Cell. Comp. Physiol., 1935. **5**: p. 495.
11. Singer, S.J. and G.L. Nicolson, *The fluid mosaic model of the structure of cell membranes.* Science, 1972. **175**: p. 720-731.
12. Overton, E., *Beiträge zur allgemeinin Muskel-und Nervenphysiologic.* Pflug Arch Physiol, 1902. **92**: p. 115–280, .
13. Collander, R., *On lipid solubility.* . Acta Physiol Scand, 1947. **13**: p. 363–381.
14. Davson, H. and J.F. Danielli, *The permibility of natural membranes.* . 1943, New York: Cambridge University Press.
15. Matteucci, C., *Annales de chimie et de physique*. 1858, Rome.
16. Nernst, W., *Die elektromotorische Wirksamkeit der Ionen.* . Z Phys Chem 4:129–181 1889. **4**
p. 129–181

17. Ostwald, W., *'Studien zur Energetik'*. Zeitschrift für physikalische Chemie, 1892. **9**: p. 563-578.
18. Bernstein, J., *Untersuchungen zur Thermodynamik der bioelektrischen Ströme.* . Pflügers Arch, 1902. **92**(521-562).
19. Webb, D. and J. Young, *Electrolyte content and action potential of the giant nerve fibres of loligo.* J Physiol., 1940. **98**: p. 299-313.

20. Hodgkin, A.L. and A.F. Huxley, *Movement of sodium and potassium ions during nervous activity.* Cold Spring Harb Symp Quant Biol, 1952. **17**: p. 43-52.
21. Ling, G. and R.W. Gerard, *The membrane potential and metabolism of muscle fibers.* J Cell Physiol, 1949. **34**(3): p. 413-38.
22. Cole, K.S., *Dynamic electrical characteristics of the squi axon membrane.* Arch. Sci. physiol, 1949. **3**: p. 253-258.
23. Hodgkin, A.L., A.F. Huxley, and B. Katz, *Measurement of current-voltage relations in the membrane of the giant axon of Loligo.* J Physiol, 1952. **116**(4): p. 424-48.
24. Marmont, G., *Studies on the axon membrane.* J. cell. comp. Physiol., 1949. **34**: p. 351-382.
25. Hodgkin, A.L. and A.F. Huxley, *Movement of radioactive potassium and membrane current in a giant axon.* J Physiol, 1953. **121**(2): p. 403-14.
26. Neher, E. and B. Sakmann, *Single-channel currents recorded from membrane of denervated frog muscle fibres.* Nature, 1976. **260**(5554): p. 799-802.
27. Hille, B., *Ion channels of excitable membranes*. 3rd ed. 2001, Sunderland ,MA: Sinauer Associates.
28. Ussing, H., *The active ion transport through the isolated frog skin in the light of tracer studies.* Acta Physiol Scand., 1949. **17**: p. 1-37.
29. Ussing, H. and K. Zerhan, *Active transport of sodium as the source of electric current in the short-circuited isolated frog skin.* Acta Physiol Scand. , 1951. **23**: p. 110-27.
30. Koefoed-Johnsen, V. and H. Ussing, *The nature of the frog skin potential.* Acta Physiol Scand., 1958. **42**: p. 298-308.
31. Lindemann, B., *Hans Ussing, Experiments and Models.* J. Membrane Biol., 2001. **184**: p. 203-210.
32. Frizzell, R.A., M.C. Dugas, and S.G. Schultz, *Sodium Chloride Transport by Rabbit Gallbladder: Direct evidence for a Coupled NaCl Influx Process.* Journal of General Physiology, 1975. **65**: p. 769-795.
33. Boucher, R., et al., *Na+ transport in cystic fibrosis respiratory epithelia. Abnormal basal rate and response to adenylate cyclase activation.* J Clin Invest. , 1986. **78**: p. 1245-52.
34. Jiang, C., et al., *Altered fluid transport across airway epithelium in cystic fibrosis.Science.* Science, 1993. **262**: p. 427-427.
35. Knowles, M., et al., *Abnormal ion permeation through cystic fibrosis respiratory epithelium.* Science, 1983. **221**: p. 1067-1070.
36. Canessa, C., et al., *Amiloride-sensitive epithelial Na+ channel is made of three homologous subunits.* Nature, 1994. **367**: p. 463-467.
37. Stutts, M., et al., *Oxygen consumption and ouabain binding sites in cystic fibrosis nasal epithelium.* Pediatr Res., 1986. **20**: p. 1316-1320.
38. Welsh, M., et al., *Crypts are the site of intestinal fluid and electrolyte secretion.* Science, 1982. **218**: p. 1219-1221.
39. Willumsen, N., C. Davis, and R. Boucher, *Cellular Cl- transport in cultured cystic fibrosis airway epithelium.* Am J Physiol., 1989. **256**: p. 1045-53.
40. Smith, P., et al., *Chloride secretion by canine tracheal epithelium: I. Role of intracellular c AMP levels.* J Membr Biol., 1982. **70**: p. 217-226.
41. Geck, P., et al., *Electrically silent cotransport on Na+, K+ and Cl- in Ehrlich cells.* Biochim Biophys Acta., 1980. **600**: p. 432-447.

42. Frizzell, R., M. Welsh, and P. Smith, *Hormonal control of chloride secretion by canine tracheal epithelium: an electrophysiologic analysis.* Ann N Y Acad Sci., 1981. **372**: p. 558-570.
43. Kunzelmann, K., et al., *Characterization of potassium channels in respiratory cells. I. General properties.* Pflugers Arch., 1989. **414**: p. 291-6.
44. Kunzelmann, K., H. Pavenstädt, and R. Greger, *Characterization of potassium channels in respiratory cells. II. Inhibitors and regulation.* Pflugers Arch., 1989. **414**: p. 297-303.
45. McCann, J. and M. Welsh, *Basolateral K+ channels in airway epithelia. II. Role in Cl- secretion and evidence for two types of K+ channel.* Am J Physiol., 1990. **258**: p. 343-8.
46. Smith, P. and R. Frizzell, *Chloride secretion by canine tracheal epithelium: IV. Basolateral membrane K permeability parallels secretion rate.* J Membr Biol., 1984. **77**: p. 187-99.
47. Pilewski, J. and R. Frizzell, *Role of CFTR in airway disease.* Physiol Rev., 1999. **79 (1 Suppl)**: p. S215-55.
48. Knowles, M., et al., *Abnormal respiratory epithelial ion transport in cystic fibrosis.* Clin Chest Med., 1986 **7**: p. 285-297.
49. Quinton, P., *Chloride impermeability in cystic fibrosis.* Nature, 1983. **301**: p. 421-422.
50. Knowles, M., J. Gatzy, and R. Boucher, *Relative ion permeability of normal and cystic fibrosis nasal epithelium.* .J Clin Invest., 1983. **71**: p. 1410-1417.
51. Knowles, M., J. Gatzy, and R. Boucher, *Increased bioelectric potential difference across respiratory epithelia in cystic fibrosis.* N Engl J Med., 1981. **305**: p. 1489-1495.
52. Wood, R., T. Boat, and C. Doershuk, *Cystic fibrosis.* Am Rev Respir Dis., 1976. **113**: p. 833-878.
53. Widdicombe, J., M. Welsh, and W. Finkbeiner, *Cystic fibrosis decreases the apical membrane chloride permeability of monolayers cultured from cells of tracheal epithelium.* Proc Natl Acad Sci, 1985. **82**: p. 6167-6171.
54. Coleman, D., I. Tuet, and J. Widdicombe, *Electrical properties of dog tracheal epithelial cells grown in monolayer culture.* Am J Physiol., 1984. **246**: p. 355-359.
55. Widdicombe, J., et al., *Electrical properties of monolayers cultured from cells of human tracheal mucosa.* J Appl Physiol., 1985. **58**: p. 1729-1735.
56. Halm, D., et al., *Apical membrane chloride channels in a colonic cell line activated by secretory agonists.* Am J Physiol. , 1988. **254**: p. 505-511.
57. Welsh, M., *An apical-membrane chloride channel in human tracheal epithelium.* Science, 1986. **27**: p. 1648-1650.
58. Rommens, J., et al., *Identification of the cystic fibrosis gene: chromosome walking and jumping.* Science, 1989. **245**: p. 1059-1065.
59. Farrall, M., et al., *Recombinations between IRP and cystic fibrosis.* Am J Hum Genet., 1988. **43**: p. 471-475.
60. Kerem, B., et al., *Identification of the cystic fibrosis gene: genetic analysis.* 1989. **245**: p. 1073-1080.
61. Bodian, M., *Fibrocystic Disease of the Pancreas: a Congenital Disorder of Mucus Production Mucosis.* 1953, New York: Grune & Stratton.
62. Farber, S., *Some organic digestive disturbances in early life.* J. Mich. State. Med. Soc, 1945. **44**: p. 587-594.
63. Quinton, P., *Exocrine Glands*, in *Exocrine Glands*, L. Taussig, Editor. 1984, Thieme-Stratton: New York. p. 338-375.

64. Zeuler, W. and W. Newton, *The pathogenisis of fibrocystic disease of the pancreas. A study of 36 cases with special reference to the pulmonary lesions.* Pediatrics, 1949. **4**: p. 53-69.
65. Davis, P., M. Drumm, and M. Konstan, *Cystic fibrosis.* Am. J. Respir. Crit. Care Med., 1996. **154**: p. 1229-1256.
66. Dimagno, E., M. JR., and V. Go, *Fate of orally ingested enzymes in pancreatic insufficiency: comparison of two dosage schedules.* N. Engl. J. Med., 1977. **296**: p. 1318-1322.
67. Forstner, G., G. Gall, and M. Corey, *Digestion and absorption of nutrients in cystic fibrosis.*, in *Perspectives in Cystic Fibrosis*, Sturgess, Editor. 1980, Impereal: Toronto. p. 137-148.
68. Mastella, G., G. Barbato, and C. Trabucchi, *Il pancreas esocrino nella fibrosi cistica: indagine funzionale su 169 pazienti e 118 controlli.* Riv. Ital. Pediatr., 1975. **1**: p. 109-130.
69. Holsclaw, D., et al., *Genital abnormalities in males with cystic fibrosis: an emerging problem.* J. Urol., 1971. **106**: p. 568-574.
70. Kaplan, et al., *Reproductive failure in males with cystic fibrosis.* N. Engl. J. Med., 1968. **279**: p. 65-69.
71. Landing, B., T. Wells, and C. Wang, *Abnormality of the edipidymus and vas deferens in cystic fibrosis.* Arch. Pathol., 1969. **88**: p. 239-247.
72. Leung, A., et al., *cAMP- but not Ca2+-regulated Cl conductance is lacking in cystic fibrosis mice epididymides and seminal vesicles.* Am. J. Physiol., 1996. **271**: p. 188-193.
73. Oppenheimer, E. and J. Esterly, *Observations on cystic fibrosis of the pancreas. V. Developmental changes in the male genital system.* J. Pediatr., 1969. **75**: p. 806-811.
74. Zielenski, J., A. O'Brien, and L. Tsui. *Cystic Fibrosis Mutation Database*. 2007 Mar 02, 2007 [cited; Available from: http://www.genet.sickkids.on.ca/cftr/app.
75. Denning, G., et al., *Processing of mutant cystic fibrosis transmembrane conductance regulator is temperature-sensitive.* Nature, 1992. **358**: p. 761-764.
76. Thomas, P., Y. Ko, and P. Pedersen, *Altered protein folding may be the molecular basis of most cases of cystic fibrosis.* Thomas PJ, Ko YH, Pedersen PL.Altered protein folding may be the molecular basis of most cases of cystic fibrosis.FEBS Lett. 1992 Nov 2;312(1):7-9. Review. , 1992. **FEBS Lett.** : p. 7-9.
77. Logan, J., et al., *Cystic fibrosis transmembrane conductance regulator mutations that disrupt nucleotide binding.* J Clin Invest., 1994. **94**: p. 228-236.
78. Dean, M., et al., *Multiple mutations in highly conserved residues are found in mildly affected cystic fibrosis patients.* Cell, 1990. **61**: p. 863-870.
79. Sheppard, D., et al., *Mutations in CFTR associated with mild-disease-form Cl- channels with altered pore properties.* Nature, 1993. **362**: p. 160-164.
80. Bronsveld, I., et al., *Chloride conductance and genetic background modulate the cystic fibrosis phenotype of Delta F508 homozygous twins and siblings.* J Clin Invest., 2001. **108**: p. 1705-1715.
81. Bronsveld, I., et al., *Residual chloride secretion in intestinal tissue of deltaF508 homozygous twins and siblings with cystic fibrosis. The European CF Twin and Sibling Study Consortium.* Gastroenterology, 2000. **119**: p. 32-40.

82. Carvalho-Oliveira, I., et al., *CFTR localization in native airway cells and cell lines expressing wild-type or F508del-CFTR by a panel of different antibodies.* J Histochem Cytochem., 2004. **52**: p. 193-203.
83. Cheng, S., et al., *Defective intracellular transport and processing of CFTR is the molecular basis of most cystic fibrosis.* Cell, 1990. **63**: p. 827-834.
84. Dalemans, W., et al., *Altered chloride ion channel kinetics associated with the delta F508 cystic fibrosis mutation.* Nature, 1991. **354**: p. 526-528.
85. Drumm, M., et al., *Chloride conductance expressed by delta F508 and other mutant CFTRs in Xenopus oocytes.* Science, 1991. **254**: p. 1797-1799.
86. Haws, C., et al., *CFTR in Calu-3 human airway cells: channel properties and role in cAMP-activated Cl- conductance.* Am J Physiol., 1994. **266**: p. L502-12.
87. Kälin, N., et al., *DeltaF508 CFTR protein expression in tissues from patients with cystic fibrosis.* J Clin Invest., 1999. **103**: p. 1379-1389.
88. Lukacs, G.L., et al., *The delta F508 mutation decreases the stability of cystic fibrosis transmembrane conductance regulator in the plasma membrane. Determination of functional half-lives on transfected cells.* J Biol Chem, 1993. **268**(29): p. 21592-8.
89. Welsh, M. and A. Smith, *Molecular mechanisms of CFTR chloride channel dysfunction in cystic fibrosis.* Cell, 1993. **73**: p. 1251-1254.
90. Drumm, et al., *Correction of the cystic fibrosis defect in vitro by retrovirus-mediated gene transfer.* Cell, 1990. **62**: p. 1227-1233.
91. Rich, et al., *Expression of cystic fibrosis transmembrane conductance regulator corrects defective chloride channel regulation in cystic fibrosis airway epithelial cells.* Nature, 1990. **347**: p. 358-363.
92. Lodish, *Anion transport. Revelations of a chloride channel.* Nature, 1990. **348**: p. 489-490.
93. Ringe and Petsko, *Cystic fibrosis. A transport problem?* Nature, 1990. **346**: p. 312-313.
94. Gray, M.A., et al., *Two types of chloride channel on duct cells cultured from human fetal pancreas.* Am J Physiol, 1989. **257**(2 Pt 1): p. C240-51.
95. Kartner, N., et al., *Expression of the cystic fibrosis gene in non-epithelial invertebrate cells produces a regulated anion conductance.* Cell, 1991. **64**(4): p. 681-91.
96. Tabcharani, J.A., et al., *Phosphorylation-regulated Cl- channel in CHO cells stably expressing the cystic fibrosis gene.* Nature, 1991. **352**(6336): p. 628-31.
97. Anderson, M.P., et al., *Nucleoside triphosphates are required to open the CFTR chloride channel.* Cell, 1991. **67**(4): p. 775-84.
98. Bear, C.E., et al., *Purification and functional reconstitution of the cystic fibrosis transmembrane conductance regulator (CFTR).* Cell, 1992. **68**(4): p. 809-18.
99. O'Riordan, et al., *Purification and functional reconstitution of the cystic fibrosis transmembrane conductance regulator (CFTR).* Cell, 1995. **68**: p. 809-818.
100. Anderson, M., et al., *Demonstration that CFTR is a chloride channel by alteration of its anion selectivity.* Science 1991. **253**: p. 202-205.
101. Linsdell, P., et al., *Permeability of wild-type and mutant cystic fibrosis transmembrane conductance regulator chloride channels to polyatomic anions.* J Gen Physiol., 1997. **110**: p. 355-364.
102. Cotten, J.F. and M. Welsh, *Covalent modification of the regulatory domain irreversibly stimulates cystic fibrosis transmembrane conductance regulator.* J Biol Chem., 1997. **272**: p. 25617-25622.

103. Ishihara, H. and M. Welsh, *Block by MOPS reveals a conformation change in the CFTR pore produced by ATP hydrolysis.* Am J Physiol., 1997. **273**: p. 1278-1289.
104. Carson, M.R., S.M. Travis, and M.J. Welsh, *The two nucleotide-binding domains of cystic fibrosis transmembrane conductance regulator (CFTR) have distinct functions in controlling channel activity.*
. J. Biol. Chem., 1995. **270**: p. 1711–1717
105. Gunderson, K.L. and R.R. Kopito, *Conformational states of CFTR associated with channel gating: the role of ATP binding and hydrylysis.* Cell 1995. **82**: p. 231–239.
106. Gunderson, K. and R. Kopito, *Effects of pyrophosphate and nucleotide analogs suggest a role for ATP hydrolysis in cystic fibrosis transmembrane regulator* J Biol Chem., 1994. **269**: p. 19349-19353.
107. Linsdell, P., et al., *Permeability of wild-type and mutant cystic fibrosis transmembrane conductance regulator chloride channels to polyatomic anions.* J Gen Physiol. , 1997. **110**: p. 355-364.
108. Tilly, B., et al., *Cyclic AMP-dependent protein kinase activation of cystic fibrosis transmembrane conductance regulator chloride channels in planar lipid bilayers.* J Biol Chem., 1992. **267**: p. 9470-9473.
109. Venglarik, C., et al., *ATP alters current fluctuations of cystic fibrosis transmembrane conductance regulator: evidence for a three-state activation mechanism.* J Gen Physiol., 1994. **104**: p. 123-146.
110. Vergani, P., et al., *CFTR channel opening by ATP-driven tight dimerization of its nucleotide-binding domains.* Nature, 2005. **433**(7028): p. 876-80.
111. Csanady, L., et al., *Severed channels probe regulation of gating of cystic fibrosis transmembrane conductance regulator by its cytoplasmic domains.* J Gen Physiol, 2000. **116**(3): p. 477-500.
112. Ostedgaard, L., O. Baldursson, and M. Welsh, *Regulation of the cystic fibrosis transmembrane conductance regulator Cl- channel by its R domain.* J Biol Chem., 2001. **276**: p. 7689-7692.
113. Gadsby, D.C. and A.C. Nairn, *Control of CFTR channel gating by phosphorylation and nucleotide hydrolysis.* Physiol Rev, 1999. **79**(1 Suppl): p. S77-S107.
114. Cheng, S.H., et al., *Phosphorylation of the R domain by cAMP-dependent protein kinase regulates the CFTR chloride channel.* Cell, 1991. **66**(5): p. 1027-36.
115. Picciotto, M.R., et al., *Phosphorylation of the cystic fibrosis transmembrane conductance regulator.* J Biol Chem, 1992. **267**(18): p. 12742-52.
116. Neville, D.C., et al., *Evidence for phosphorylation of serine 753 in CFTR using a novel metal-ion affinity resin and matrix-assisted laser desorption mass spectrometry.* Protein Sci, 1997. **6**(11): p. 2436-45.
117. Seibert, F.S., et al., *cAMP-dependent protein kinase-mediated phosphorylation of cystic fibrosis transmembrane conductance regulator residue Ser-753 and its role in channel activation.* J Biol Chem, 1995. **270**(5): p. 2158-62.
118. Townsend, R.R., et al., *Identification of protein kinase A phosphorylation sites on NBD1 and R domains of CFTR using electrospray mass spectrometry with selective phosphate ion monitoring.* Protein Sci, 1996. **5**(9): p. 1865-73.
119. Rich, D.P., et al., *Regulation of the cystic fibrosis transmembrane conductance regulator Cl- channel by negative charge in the R domain.* J Biol Chem, 1993. **268**(27): p. 20259-67.

120. Chang, X.B., et al., *Protein kinase A (PKA) still activates CFTR chloride channel after mutagenesis of all 10 PKA consensus phosphorylation sites.* J Biol Chem, 1993. **268**(15): p. 11304-11.
121. Hoshi, T., W.N. Zagotta, and R.W. Aldrich, *Biophysical and molecular mechanisms of Shaker potassium channel inactivation.* Science, 1990. **250**(4980): p. 533-8.
122. Kukuljan, M., P. Labarca, and R. Latorre, *Molecular determinants of ion conduction and inactivation in K+ channels.* Am J Physiol, 1995. **268**(3 Pt 1): p. C535-56.
123. Ma, J., et al., *Function of the R domain in the cystic fibrosis transmembrane conductance regulator chloride channel.* J Biol Chem, 1997. **272**(44): p. 28133-41.
124. Winter, M.C. and M.J. Welsh, *Stimulation of CFTR activity by its phosphorylated R domain.* Nature, 1997. **389**(6648): p. 294-6.
125. Baldursson, O., et al., *Cystic fibrosis transmembrane conductance regulator Cl- channels with R domain deletions and translocations show phosphorylation-dependent and -independent activity.* J Biol Chem, 2001. **276**(3): p. 1904-10.
126. Chappe, V., et al., *Phosphorylation of CFTR by PKA promotes binding of the regulatory domain.* Embo J, 2005. **24**(15): p. 2730-40.
127. Lehrich, R.W., et al., *Vasoactive intestinal peptide, forskolin, and genistein increase apical CFTR trafficking in the rectal gland of the spiny dogfish, Squalus acanthias. Acute regulation of CFTR trafficking in an intact epithelium.* J Clin Invest, 1998. **101**(4): p. 737-45.
128. Ameen, N., J. Alexis, and P. Salas, *Cellular localization of the cystic fibrosis transmembrane conductance regulator in mouse intestinal tract.* Histochem Cell Biol, 2000. **114**(1): p. 69-75.
129. Ameen, N.M.B., Bourguinon L, Marino C, Isenberg J, McLaughlin GE., *CFTR channel insertion to the apical surface in rat duodenal villus epithelial cells is upregulated by VIP in vivo.* J Cell Sci., 1999. **112**(March): p. 887-94.
130. Prince, L.S., R.B. Workman, Jr., and R.B. Marchase, *Rapid endocytosis of the cystic fibrosis transmembrane conductance regulator chloride channel.* Proc Natl Acad Sci U S A, 1994. **91**(11): p. 5192-6.
131. Lukacs, G.L., et al., *Constitutive internalization of cystic fibrosis transmembrane conductance regulator occurs via clathrin-dependent endocytosis and is regulated by protein phosphorylation.* Biochem J, 1997. **328 (Pt 2)**: p. 353-61.
132. Bradbury, N.A., et al., *Regulation of plasma membrane recycling by CFTR.* Science, 1992. **256**(5056): p. 530-2.
133. Schwiebert, E.M., et al., *Heterotrimeric G proteins, vesicle trafficking, and CFTR Cl- channels.* Am J Physiol, 1994. **267**(1 Pt 1): p. C272-81.
134. Webe, W.M., et al., *Different activation mechanisms of cystic fibrosis transmembrane conductance regulator expressed in Xenopus laevis oocytes.* Comp Biochem Physiol A Mol Integr Physiol, 2001. **130**(3): p. 521-31.
135. Weber, W.M., et al., *Capacitance measurements reveal different pathways for the activation of CFTR.* Pflugers Arch, 1999. **438**(4): p. 561-9.
136. Takahashi, A., et al., *CFTR-dependent membrane insertion is linked to stimulation of the CFTR chloride conductance.* Am J Physiol, 1996. **271**(6 Pt 1): p. C1887-94.
137. Peters, K.W., et al., *Syntaxin 1A inhibits regulated CFTR trafficking in xenopus oocytes.* Am J Physiol, 1999. **277**(1 Pt 1): p. C174-80.

138. Almers, W., *Gating currents and charge movements in excitable membranes.* Rev Physiol Biochem Pharmacol, 1978. **82**: p. 96-190.
139. Atia, F., W. Zeiske, and W. van Driessche, *Secretory apical Cl- channels in A6 cells: possible control by cell Ca2+ and cAMP.* Pflugers Arch., 1999. **438**: p. 344-353.
140. Chang, S., et al., *Mechanisms of CFTR regulation by syntaxin 1A and PKA.* J Cell Sci., 2002. **115**: p. 783-791.
141. Chen, P., T. Hwang, and K. Gillis, *The relationship between cAMP, Ca(2)+, and transport of CFTR to the plasma membrane.* J Gen Physiol., 2001. **118**: p. 135-144.
142. Greger, R., et al., *Does stimulation of NaCl secretion in in vitro perfused rectal gland tubules of squalus acanthias increase membrane capacitance?* Pflugers Arch., 1998. **436**: p. 538-544.
143. Hug MJ, Thiele IE, and G. R., *The role of exocytosis in the activation of the chloride conductance in Chinese hamster ovary cells (CHO) stably expressing CFTR.* Pflugers Arch., 1997. **434**: p. 779-784.
144. Sherman-Gold, R., ed. *The Axon Guide for Electrophysiology & Biophysical Laboratory Techniques*. 1993, Axon Instruments: Foster City, CA.
145. Cunningham, S.A., et al., *cAMP-stimulated ion currents in Xenopus oocytes expressing CFTR cRNA.* Am J Physiol, 1992. **262**(3 Pt 1): p. C783-8.
146. Gurdon, J.B. and M.P. Wickens, *The use of Xenopus oocytes for the expression of cloned genes.* Methods Enzymol, 1983. **101**: p. 370-86.
147. Lang, J., et al., *The first C2 domain of synaptotagmin is required for exocytosis of insulin from pancreatic beta-cells: action of synaptotagmin at low micromolar calcium.* Embo J, 1997. **16**(19): p. 5837-46.
148. Gentzsch, M., et al., *Endocytic trafficking routes of wild type and DeltaF508 cystic fibrosis transmembrane conductance regulator.* Mol Biol Cell, 2004. **15**(6): p. 2684-96.
149. Qi, J., *Regulation of CFTR and ENaC Channel Densities.*, in *Cell Biology and Molecular Physiology*. 2001, University of Pittsburgh: Pittsburgh. p. 139.
150. Kay, B. and B. Peng, eds. *Methods In Cell Biology*. *Xenopus* laevis: Preacical uses in Cell and Molecular Biology. Vol. 36. 1991, Academic Press Inc.: New York.
151. Liu, X., et al., *CFTR: covalent modification of cysteine-substituted channels expressed in Xenopus oocytes shows that activation is due to the opening of channels resident in the plasma membrane.* J Gen Physiol, 2001. **118**(4): p. 433-46.
152. Uezono, Y., et al., *Receptors that couple to 2 classes of G proteins increase cAMP and activate CFTR expressed in Xenopus oocytes.* Receptors Channels, 1993. **1**(3): p. 233-41.
153. Chappe, V., et al., *Structural basis for specificity and potency of xanthine derivatives as activators of the CFTR chloride channel. .* Br. J. Pharmacol., 1998. **123**: p. 683-693.
154. Jones, H.M., et al., *Role of the NH2 terminus in the assembly and trafficking of the intermediate conductance Ca2+-activated K+ channel hIK1.* J Biol Chem, 2004. **279**(15): p. 15531-40.
155. Ma, D., et al., *Diverse trafficking patterns due to multiple traffic motifs in G protein-activated inwardly rectifying potassium channels from brain and heart.* Neuron, 2002. **33**(5): p. 715-29.
156. Butterworth, M.B., et al., *Acute ENaC stimulation by cAMP in a kidney cell line is mediated by exocytic insertion from a recycling channel pool.* J Gen Physiol, 2005. **125**(1): p. 81-101.

157. Sargeant, R.J. and M.R. Paquet, *Effect of insulin on the rates of synthesis and degradation of GLUT1 and GLUT4 glucose transporters in 3T3-L1 adipocytes.* Biochem J, 1993. **290 (Pt 3)**: p. 913-9.
158. Shimkets, R.A., R.P. Lifton, and C.M. Canessa, *The activity of the epithelial sodium channel is regulated by clathrin-mediated endocytosis.* J Biol Chem, 1997. **272**(41): p. 25537-41.
159. Devidas, S., H. Yue, and W.B. Guggino, *The second half of the cystic fibrosis transmembrane conductance regulator forms a functional chloride channel.* J Biol Chem, 1998. **273**(45): p. 29373-80.
160. Condliffe, S.B., H. Zhang, and R.A. Frizzell, *Syntaxin 1A regulates ENaC channel activity.* J Biol Chem, 2004. **279**(11): p. 10085-92.
161. Naren, A., et al., *Regulation of CFTR chloride channels by syntaxin and Munc18 isoforms.* Nature, 1997. **390**: p. 302-305.
162. Naren, A.P., et al., *Syntaxin 1A inhibits CFTR chloride channels by means of domain-specific protein-protein interactions.* Proc Natl Acad Sci U S A, 1998. **95**(18): p. 10972-7.
163. Condliffe, S.B., et al., *Syntaxin 1A regulates ENaC via domain-specific interactions.* J Biol Chem, 2003. **278**(15): p. 12796-804.
164. Firsov, D., et al., *Mutational analysis of cysteine-rich domains of the epithelium sodium channel (ENaC). Identification of cysteines essential for channel expression at the cell surface.* J Biol Chem, 1999. **274**(5): p. 2743-9.
165. Dubel, S.J., et al., *Plasma membrane expression of T-type calcium channel alpha(1) subunits is modulated by high voltage-activated auxiliary subunits.* J Biol Chem, 2004. **279**(28): p. 29263-9.
166. Rich, D.P., et al., *Effect of deleting the R domain on CFTR-generated chloride channels.* Science, 1991. **253**(5016): p. 205-7.
167. Rich, D.P., et al., *Effect of deletion mutations on the function of CFTR chloride channels.* Receptors Channels, 1993. **1**(3): p. 221-32.
168. Prince, L.S., et al., *Efficient endocytosis of the cystic fibrosis transmembrane conductance regulator requires a tyrosine-based signal.* J Biol Chem, 1999. **274**(6): p. 3602-9.
169. Swiatecka-Urban, A., et al., *The short apical membrane half-life of rescued {Delta}F508-cystic fibrosis transmembrane conductance regulator (CFTR) results from accelerated endocytosis of {Delta}F508-CFTR in polarized human airway epithelial cells.* J Biol Chem, 2005. **280**(44): p. 36762-72.
170. Naren, A., et al., *CFTR chloride channel regulation by an interdomain interaction.Science.* Science, 1999. **286**: p. 544-548.
171. Webster, M.K., L. Goya, and G.L. Firestone, *Immediate-early transcriptional regulation and rapid mRNA turnover of a putative serine/threonine protein kinase.* J Biol Chem, 1993. **268**(16): p. 11482-5.
172. Webster, M.K., et al., *Characterization of sgk, a novel member of the serine/threonine protein kinase gene family which is transcriptionally induced by glucocorticoids and serum.* Mol Cell Biol, 1993. **13**(4): p. 2031-40.
173. Loffing, J., S.Y. Flores, and O. Staub, *Sgk kinases and their role in epithelial transport.* Annu Rev Physiol, 2006. **68**: p. 461-90.

174. Dai, F., et al., *Cloning and mapping of a novel human serum/glucocorticoid regulated kinase-like gene, SGKL, to chromosome 8q12.3-q13.1.* Genomics, 1999. **62**(1): p. 95-7.
175. Liu, D., X. Yang, and Z. Songyang, *Identification of CISK, a new member of the SGK kinase family that promotes IL-3-dependent survival.* Curr Biol, 2000. **10**(19): p. 1233-6.
176. Xu, B.E., et al., *WNK1 activates SGK1 to regulate the epithelial sodium channel.* Proc Natl Acad Sci U S A, 2005. **102**(29): p. 10315-20.
177. Kobayashi, T. and P. Cohen, *Activation of serum- and glucocorticoid-regulated protein kinase by agonists that activate phosphatidylinositide 3-kinase is mediated by 3-phosphoinositide-dependent protein kinase-1 (PDK1) and PDK2.* Biochem J, 1999. **339 (Pt 2)**: p. 319-28.
178. Kobayashi, T., et al., *Characterization of the structure and regulation of two novel isoforms of serum- and glucocorticoid-induced protein kinase.* Biochem J, 1999. **344 Pt 1**: p. 189-97.
179. Park, J., et al., *Serum and glucocorticoid-inducible kinase (SGK) is a target of the PI 3-kinase-stimulated signaling pathway.* Embo J, 1999. **18**(11): p. 3024-33.
180. Alessi, D.R., et al., *3-Phosphoinositide-dependent protein kinase-1 (PDK1): structural and functional homology with the Drosophila DSTPK61 kinase.* Curr Biol, 1997. **7**(10): p. 776-89.
181. Stokoe, D., et al., *Dual role of phosphatidylinositol-3,4,5-trisphosphate in the activation of protein kinase B.* Science, 1997. **277**(5325): p. 567-70.
182. Kobayashi, T. and P. Cohen, *Activation of serum- and glucocorticoid-regulated protein kinase by agonists that activate phosphatidylinositide 3-kinase is mediated by 3-phosphoinositide-dependent protein kinase-1 (PDK1) and PDK2.* Biochem J., 1999. **339**: p. 319-328.
183. Shelly, C. and R. Herrera, *Activation of SGK1 by HGF, Rac1 and integrin-mediated cell adhesion in MDCK cells: PI-3K-dependent and -independent pathways.* J Cell Sci, 2002. **115**(Pt 9): p. 1985-93.
184. Hayashi, M., et al., *BMK1 mediates growth factor-induced cell proliferation through direct cellular activation of serum and glucocorticoid-inducible kinase.* J Biol Chem, 2001. **276**(12): p. 8631-4.
185. Meng, F., et al., *IL-6 activates serum and glucocorticoid kinase via p38alpha mitogen-activated protein kinase pathway.* Am J Physiol Cell Physiol, 2005. **289**(4): p. C971-81.
186. Frödin, M., et al., *A phosphoserine/threonine-binding pocket in AGC kinases and PDK1 mediates activation by hydrophobic motif phosphorylation.* Embo J, 2002. **21**: p. 5396–5407.
187. Brickley, D.R., et al., *Ubiquitin modification of serum and glucocorticoid-induced protein kinase-1 (SGK-1).* J Biol Chem, 2002. **277**(45): p. 43064-70.
188. Zhou, R. and P.M. Snyder, *Nedd4-2 phosphorylation induces serum and glucocorticoid-regulated kinase (SGK) ubiquitination and degradation.* J Biol Chem, 2005. **280**(6): p. 4518-23.
189. Bogusz, A., et al., *A novel N-terminal hydrophobic motif mediates constitutive degradation of serum- and glucocorticoid-induced kinase-1 by the ubiquitin-proteasome pathway.* FEBS J., 2006. **273**: p. 2913-2928.
190. Loffing, J., et al., *Aldosterone induces rapid apical translocation of ENaC in early portion of renal collecting system: possible role of SGK.* Am J Physiol Renal Physiol, 2001. **280**(4): p. F675-82.

191. Chen, H.I. and M. Sudol, *The WW domain of Yes-associated protein binds a proline-rich ligand that differs from the consensus established for Src homology 3-binding modules.* Proc Natl Acad Sci U S A, 1995. **92**(17): p. 7819-23.
192. Staub, O., et al., *WW domains of Nedd4 bind to the proline-rich PY motifs in the epithelial Na+ channel deleted in Liddle's syndrome.* Embo J, 1996. **15**(10): p. 2371-80.
193. Abriel, H., et al., *Defective regulation of the epithelial Na+ channel by Nedd4 in Liddle's syndrome.* J Clin Invest, 1999. **103**(5): p. 667-73.
194. Dinudom, A., et al., *Nedd4 mediates control of an epithelial Na+ channel in salivary duct cells by cytosolic Na+.* Proc Natl Acad Sci U S A, 1998. **95**(12): p. 7169-73.
195. Goulet, C.C., et al., *Inhibition of the epithelial Na+ channel by interaction of Nedd4 with a PY motif deleted in Liddle's syndrome.* J Biol Chem, 1998. **273**(45): p. 30012-7.
196. Harvey, K.F., et al., *The Nedd4-like protein KIAA0439 is a potential regulator of the epithelial sodium channel.* J Biol Chem, 2001. **276**(11): p. 8597-601.
197. Kamynina, E., et al., *A novel mouse Nedd4 protein suppresses the activity of the epithelial Na+ channel.* Faseb J, 2001. **15**(1): p. 204-214.
198. Kamynina, E., C. Tauxe, and O. Staub, *Distinct characteristics of two human Nedd4 proteins with respect to epithelial Na(+) channel regulation.* Am J Physiol Renal Physiol, 2001. **281**(3): p. F469-77.
199. Kanelis, V., D. Rotin, and J.D. Forman-Kay, *Solution structure of a Nedd4 WW domain-ENaC peptide complex.* Nat Struct Biol, 2001. **8**(5): p. 407-12.
200. Alvarez de la Rosa, D., et al., *The serum and glucocorticoid kinase sgk increases the abundance of epithelial sodium channels in the plasma membrane of Xenopus oocytes.* J Biol Chem, 1999. **274**(53): p. 37834-9.
201. Chen, S.Y., et al., *Epithelial sodium channel regulated by aldosterone-induced protein sgk.* Proc Natl Acad Sci U S A, 1999. **96**(5): p. 2514-9.
202. Debonneville, C., et al., *Phosphorylation of Nedd4-2 by Sgk1 regulates epithelial Na(+) channel cell surface expression.* Embo J, 2001. **20**(24): p. 7052-9.
203. Lang, F., et al., *Deranged transcriptional regulation of cell-volume-sensitive kinase hSGK in diabetic nephropathy.* Proc Natl Acad Sci U S A, 2000. **97**(14): p. 8157-62.
204. Naray-Fejes-Toth, A., et al., *sgk is an aldosterone-induced kinase in the renal collecting duct. Effects on epithelial na+ channels.* J Biol Chem, 1999. **274**(24): p. 16973-8.
205. Setiawan, I., et al., *Stimulation of Xenopus oocyte Na(+),K(+)ATPase by the serum and glucocorticoid-dependent kinase sgk1.* Pflugers Arch, 2002. **444**(3): p. 426-31.
206. Vuagniaux, G., et al., *Synergistic activation of ENaC by three membrane-bound channel-activating serine proteases (mCAP1, mCAP2, and mCAP3) and serum- and glucocorticoid-regulated kinase (Sgk1) in Xenopus Oocytes.* J Gen Physiol, 2002. **120**(2): p. 191-201.
207. Zecevic, M., et al., *SGK1 increases Na,K-ATP cell-surface expression and function in Xenopus laevis oocytes.* Pflugers Arch, 2004. **448**(1): p. 29-35.
208. Ichimura, T., et al., *14-3-3 proteins modulate the expression of epithelial Na+ channels by phosphorylation-dependent interaction with Nedd4-2 ubiquitin ligase.* J Biol Chem, 2005. **280**(13): p. 13187-94.
209. Bhalla, V., et al., *Serum- and glucocorticoid-regulated kinase 1 regulates ubiquitin ligase neural precursor cell-expressed, developmentally down-regulated protein 4-2 by inducing interaction with 14-3-3.* Mol Endocrinol, 2005. **19**(12): p. 3073-84.

210. Snyder, P.M., D.R. Olson, and B.C. Thomas, *Serum and glucocorticoid-regulated kinase modulates Nedd4-2-mediated inhibition of the epithelial Na+ channel.* J Biol Chem, 2002. **277**(1): p. 5-8.
211. Diakov, A. and C. Korbmacher, *A novel pathway of epithelial sodium channel activation involves a serum- and glucocorticoid-inducible kinase consensus motif in the C terminus of the channel's alpha-subunit.* J Biol Chem, 2004. **279**(37): p. 38134-42.
212. Wang, J., et al., *SGK integrates insulin and mineralocorticoid regulation of epithelial sodium transport.* Am J Physiol Renal Physiol, 2001. **280**(2): p. F303-13.
213. Alvarez de la Rosa, D., et al., *Mechanisms of regulation of epithelial sodium channel by SGK1 in A6 cells.* J Gen Physiol, 2004. **124**(4): p. 395-407.
214. Fillon, S., et al., *Serum- and glucocorticoid-dependent kinase, cell volume, and the regulation of epithelial transport.* Comp Biochem Physiol A Mol Integr Physiol, 2001. **130**(3): p. 367-76.
215. Gamper, N., et al., *IGF-1 up-regulates K+ channels via PI3-kinase, PDK1 and SGK1.* Pflugers Arch, 2002. **443**(4): p. 625-34.
216. Yun, C.C., Y. Chen, and F. Lang, *Glucocorticoid activation of Na(+)/H(+) exchanger isoform 3 revisited. The roles of SGK1 and NHERF2.* J Biol Chem, 2002. **277**(10): p. 7676-83.
217. Marshall, W.S., et al., *Time course of salinity adaptation in a strongly euryhaline estuarine teleost, fundulus heteroclitus: a multivariable approach.* J Exp Biol, 1999. **202 (Pt 11)**: p. 1535-44.
218. Shaw, J.R., et al., *Role of glucocorticoid receptor in acclimation of killifish (Fundulus heteroclitus) to seawater and effects of arsenic.* Am J Physiol Regul Integr Comp Physiol, 2007. **292**(2): p. R1052-60.
219. Stanton, C.R., et al., *Arsenic inhibits CFTR-mediated chloride secretion by killifish (Fundulus heteroclitus) opercular membrane.* Cell Physiol Biochem, 2006. **17**(5-6): p. 269-78.
220. Marshall, W., *Rapid regulation of NaCl secretion by estuarine teleost fish: coping strategies for short-duration freshwater exposures.* Biochim Biophys Acta, 2003. **1618**: p. 95-105.
221. Wood, C. and P. Laurent, *Na+ versus Cl- transport in the intact killifish after rapid salinity transfer.* Biochim Biophys Acta, 2003. **1618**(106-119).
222. Marshall, W., E. Lynch, and R. Cozzi, *Redistribution of immunofluorescence of CFTR anion channel and NKCC cotransporter in chloride cells during adaptation of the killifish Fundulus heteroclitus to sea water.* J Exp Biol., 2002. **205**: p. 1265-73.
223. Singer, T., et al., *A divergent CFTR homologue: highly regulated salt transport in the euryhaline teleost F. heteroclitus.* Am J Physiol., 1998. **274**: p. 715-723.
224. Wagner, C.A., et al., *Effects of the serine/threonine kinase SGK1 on the epithelial Na(+) channel (ENaC) and CFTR: implications for cystic fibrosis.* Cell Physiol Biochem, 2001. **11**(4): p. 209-18.
225. Sato, J.D., et al., *Regulation of human cystic fibrosis transmembrane conductance regulator (CFTR) by serum- and glucocorticoid-inducible kinase (SGK1).* Cell Physiol Biochem, 2007. **20**(1-4): p. 91-8.
226. Singer, et al., *A divergent CFTR homologue: highly regulated salt transport in the euryhaline teleost Fundulus heteroclitus.* . Am. J. Physiol., 1998. **274**: p. C715–C723. .

227. Obenauer, J., L. Cantley, and M. Yaffe, *Scansite 2.0: Proteome-wide prediction of cell signaling interactions using short sequence motifs.* Nucleic Acids Res., 2003. **31**: p. 3635-3641.
228. Lewarchik, C., et al., *Regulation of CFTR trafficking by its R domain.* .J Biol Chem., 2008. **Epub ahead of print**: p. Epub ahead of print.
229. Boehmer, C., et al., *Serum and glucocorticoid inducible kinases in the regulation of the cardiac sodium channel SCN5A.* Cardiovasc Res., 2003. **57**: p. 1079-1084.
230. Embark, H., et al., *Regulation of KCNE1-dependent K(+) current by the serum and glucocorticoid-inducible kinase (SGK) isoforms.* Pflugers Arch., 2002. **445**: p. 601-606.
231. Henke, G., et al., *Regulation of the voltage gated K+ channel Kv1.3 by the ubiquitin ligase Nedd4-2 and the serum and glucocorticoid inducible kinase SGK1.* J Cell Physiol., 2004. **199**: p. 194-199.
232. Yun, C., et al., *The serum and glucocorticoid-inducible kinase SGK1 and the Na+/H+ exchange regulating factor NHERF2 synergize to stimulate the renal outer medullary K+ channel ROMK1.* J Am Soc Nephrol., 2002. **13**: p. 2823-2830.
233. Martel, J.A., et al., *Melanophilin, a novel aldosterone-induced gene in mouse cortical collecting duct cells.* Am J Physiol Renal Physiol, 2007. **293**: p. F904–F913.
234. Fukud, M., T. Kuroda, and K. Mikoshiba, *Slac2-a/melanophilin, the missing link between Rab27 and myosin Va: implications of a tripartite protein complex for melanosome transport.* J Biol Chem. , 2002. **277**: p. 12432-1246.
235. Hume, A., et al., *Rab27a regulates the peripheral distribution of melanosomes in melanocytes.* J Cell Biol., 2001. **152**: p. 795-808.
236. Matesic, L., et al., *Mutations in Mlph, encoding a member of the Rab effector family, cause the melanosome transport defects observed in leaden mice.* Proc Natl Acad Sci, 2001. **98**: p. 10238-10243.
237. Ménasché, G., et al., *Mutations in RAB27A cause Griscelli syndrome associated with haemophagocytic syndrome.* Nat Genet., 2000. **25**: p. 173-176.
238. Mercer, J., et al., *Novel myosin heavy chain encoded by murine dilute coat colour locus.* Nature, 1991. **349**: p. 709-713.
239. Moore, K., et al., *Dilute suppressor dsu acts semidominantly to suppress the coat color phenotype of a deletion mutation, dl20J, of the murine dilute locus.* Proc Natl Acad Sci, 1988. **85**: p. 8131-8135.
240. Pashkova, N., et al., *Structural basis for myosin V discrimination between distinct cargoes.* Embo J, 2006. **25**: p. 693-700.
241. Rogers, S., et al., *Regulation of melanosome movement in the cell cycle by reversible association with myosin V.* J Cell Biol., 1999. **146**: p. 1265-1276.
242. Wilson, S., et al., *A mutation in Rab27a causes the vesicle transport defects observed in ashen mice.* Proc Natl Acad Sci, 2000. **97**: p. 7933-7938.
243. Zerial M, M.H., *Rab proteins as membrane organizers.* Nat Rev Mol Cell Biol., 2001. **2**: p. 107-117.
244. Karcher, R., et al., *Cell cycle regulation of myosin-V by calcium/calmodulin-dependent protein kinase II.* Science, 2001. **293**: p. 1317-1320.
245. Swiatecka-Urban, et al., *Myosin Vb Is Required for Trafficking of the Cystic Fibrosis Transmembrane Conductance Regulator in Rab11a-specific Apical Recycling Endosomes in Polarized Human Airway Epithelial Cells.* J. Biol. Chem, 2007. **Vol. 282**(32): p. 23725-23736.